August 8, 1983

SECY-83-267B

POLICY ISSUE
(Information)

FOR: The Commissioners

FROM: William J. Dircks
Executive Director for Operations

SUBJECT: UPDATE OF STATUS REPORT ON OBSERVATION OF PIPE CRACKING AT BWRS (SECY 83-267 AND 267A)

PURPOSE: To provide the Commission with recent results of BWR piping inspections.

DISCUSSION: A status report covering results of recent inspections of BWR piping was furnished to the Commission by SECY 83-267 dated July 1, 1983, and updated by SECY 83-267A. The enclosed tables summarize all data received to date. The most recent inspection results are as follows:

FitzPatrick - A total of 54 welds have been examined; no IGSCC has been reported.

Peach Bottom 2 - Preliminary information indicates that 15 out of 38 welds examined showed indication of cracking (eight 12" riser welds, one 28" weld, and six 20" RHR welds).

On August 4 the staff met with the BWR Owners Group, EPRI and General Electric on results of the EPRI-sponsored ultrasonic sizing round robin. The EPRI report on this program is enclosed.

XA Copy Has Been Sent to PDR

William J. Dircks for
Executive Director for Operations

Enclosures:
1. BWR Inspection Results
2. EPRI Report

CONTACT: R. VOLLMER, NRR
X27207

XA

8308230648

DISTRIBUTION:
Commissioners
OGC
OPE
OCA
OIA
OPA
REGIONAL OFFICES
EDO
ELD
ACRS
ASLBP
ASLAP
SECY

BWR INSPECTION RESULTS

			12" RISER WELDS					≥ 20" RECIRC. WELDS					RHR WELDS				
8302 PLANTS	DATE OF INSPECTION	INSPECTION TEAM	NUMBER OF WELDS	NUMBER EXAMINED	NUMBER DEFECTIVE	WORST CIRCUM CRACK/LOCATION	WORST AXIAL CRACK/LOCATION	NUMBER OF WELDS	NUMBER EXAMINED	NUMBER DEFECTIVE	WORST CIRCUM CRACK/LOCATION	WORST AXIAL CRACK/LOCATION	NUMBER OF WELDS	NUMBER EXAMINED	NUMBER DEFECTIVE	WORST CIRCUM CRACK/LOCATION	WORST AXIAL CRACK/LOCATION
PEACH BOTTOM 3	MAY 1982	GE (RDP) & SONICS INTL	40	38	40	—	0.75" X 92% PIPE TO ELBOW	62	42	0	—	—	38	35	5	20" X 48% 20" PIPE TO ELBOW	0.75" X 75% 20" PIPE TO ELBOW
VERMONT YANKEE	APRIL 1983	MAGNAFLUX	40	40	22	360° INTERMITTANT X 40% PIPE TO ELBOW	—	63	18	11	28" X 15% or 360° X 10% PIPE TO ELBOW	—	30	2	1	3.0" X 5% 24" TEE TO ELBOW	—
BROWNS FERRY 1	JAN 1983	TVA & LMI	40	40	6	360° INTERMITTANT X 35% PIPE TO ELBOW	—	94	51	27	360° INTERMITTANT X 45% PIPE TO ELBOW	—	32	32	14	360° INTERMITTANT X 44% ELBOW TO ELBOW	—
COOPER	MAY 1983	GE (CHICAGO) & GE (SAN JOSE)	58	58	14	3" X 51% PIPE TO ELBOW	SPOTTY, 24% PIPE TO ELBOW	59	58	6	8.2" X 41% PIPE TO PIPE	—	7	7	0	—	—
HATCH 2	APRIL 1983	SCC & LMI	51	40	23	360° INTERMITTANT X 30% PIPE TO ELBOW	—	52	51	8	360° INTERMITTANT X 37% or 60.5" X 42% MANIFOLD END CAP	—	8	8	3	360° INTERMITTANT X 14% PIPE TO ELBOW	—
BIG ROCK POINT	MAY 1983	MAGNAFLUX & NDE TECH	THE INSPECTION WAS COMPLETED AND NO CRACK WAS FOUND					DETAILED INFORMATION IS NOT AVAILABLE AT THIS TIME.									
FITZPATRICK	MAY 1983	EBASCO	RESULTS UNDER EVALUATION														
QUAD CITIES 2	AUG 1983	CECO & LMI															
BROWNS FERRY 3	SEPT 1983																
BRUNSWICK 2	SEPT 1983																
LACROSSE	OCT 1983																
PEACH BOTTOM 2	JULY 1983	GE (RDP) & SONICS INTL	UT EXAMINATION CONTINUING PRELIMINARY DATA INDICATES THAT IS OUT OF 38 WELDS EXAMINED SHOWED INDICATIONS (8 RISER WELDS & 28" RHR WELDS AND 1 28" RECIRC WELD)														
ORESDEN 3	OCT 1983																
PILGRIM 1	JAN 1984																

BWR INSPECTION RESULTS

			12" RISER WELDS					≥ 20" RECIRC. WELDS					RHR WELDS				
8293 PLANTS	DATE OF INSPECTION	INSPECTION TEAM	NUMBER OF WELDS	NUMBER EXAMINED	NUMBER DEFECTIVE	WORST CIRCUM CRACK/LOCATION	WORST AXIAL CRACK/LOCATION	NUMBER OF WELDS	NUMBER EXAMINED	NUMBER DEFECTIVE	WORST CIRCUM CRACK/LOCATION	WORST AXIAL CRACK/LOCATION	NUMBER OF WELDS	NUMBER EXAMINED	NUMBER DEFECTIVE	WORST CIRCUM CRACK/LOCATION	WORST AXIAL CRACK/LOCATION
MONTICELLO	OCT 1982	LMI	50	50	5	1.0" X 9% PIPE TO SAFE END	3 LEAKS (2) RISER TO SAFE END & (1) ELBOW TO PIPE	46	46	1	—	1.0" X 8% 22" MANIFOLD END CAP	18	18	0	—	—
BROWNS FERRY 2	NOV 1982	TVA & LMI	40	13	0	—	—	62	12	2	1.25" X 20% PARALLEL TO WELD MANIFOLD TO SWEEPOLET	—	30	0	0	—	—
QUAD CITIES 1	FALL 1982	CECO & U.S. TESTING	≈40	4	0	—	—	≈50	5	0	—	—	≈42	9	0	—	—
DRESDEN 2	JAN 1981	COMMON WEALTH EDISON (CECO)	40	35	9	1.5" X 38% PIPE TO ELBOW	1.2" X 27% PIPE TO ELBOW	51	10	1	1" X 6% FURNACE SENSITIZED SAFE END	—	≈12	4	0	—	—
MILESTONE 1	OCT 1982	EBASCO & NUSCO	≈40	6	0	—	—	≈50	5	0	—	—		0	0	—	—
HATCH 1	NOV 1982	SSC, SW RES INST & LMI	≈50	22	0	—	—	≈50	33	5	—	0.5" X 22% 22" MANIFOLD END CAP	≈8	8	2	1.5" X 33% 20" PIPE TO ELBOW	0.37" X 94% 20" PIPE TO ELBOW
BRUNSWICK 1	JAN 1983	LMI & SW RES INST	≈40	20	2	—	2 LEAKS PIPE TO SAFE END	≈60	9	1	—	0.5" X 8% PIPE TO ELBOW	4	3	0	—	—
OYSTER CREEK	1983	MAGNAFLUX				RESULTS UNDER EVALUATION											
DUANE ARNOLD	1982	LMI	48 (10" RISER)	24	0	—	—	45	25	0	—	—	5	0	0	—	—

EPRI

ULTRASONIC SIZING CAPABILITY OF IGSCC AND ITS RELATION TO FLAW EVALUATION PROCEDURES

AUGUST 4, 1983

PRESENTED SIMULTANEOUSLY TO:

-- USNRC
BETHESDA, MD

-- UTILITY INDUSTRY
CHARLOTTE, NC

ELECTRIC POWER RESEARCH INSTITUTE

ULTRASONIC SIZING CAPABILITY OF IGSCC AND ITS RELATION TO FLAW EVALUATION PROCEDURES

Research Project 1570-2

Interim Report, August 4, 1983

Prepared by

EPRI NDE CENTER
Operated by
J.A. Jones Applied Research Company
1300 Harris Boulevard
Charlotte, NC 28213

and

EPRI Staff

Prepared for

Electric Power Research Institute
3412 Hillview Avenue
Palo Alto, California 94304

EPRI Project Manager
Gary J. Dau

System Integrity Program
Nuclear Power Division

ACKNOWLEDGEMENTS

This round robin exercise was organized, conducted and documented in an amazingly short time period, two months. Several programs with similar goals have been underway for several years on both a national and international basis. This significant achievement was due to many factors, the most significant is the dedication and cooperation given by all people who participated in the exercise.

The very professional, dedicated efforts of Dr. Monamad Behravesh set the tone throughout the organization and conduct of the program. His staff of Ms. Janet Wade, Mr. John Hunt and Mr. Y.H. Jeong were responsible for the large amount of high quality documentation of the ultrasonic and destructive data.

The high priority service given by the metallography laboratories at both Battelle Northwest and Battelle Columbus are noted. Without their extra efforts the completion deadline could not have been met. Special thanks and appreciation are due to all the teams who willingly agreed to participate on very short notice while realizing that some risk was involved. My colleagues at EPRI, particularly Dr. Douglas Norris, Dr. Ted Marston and Ms. Joey Johnson made timely and needed contributions. Finally, special thanks are due to Mr. Robert Stone for his many contributions to the preparation of the report and Ms. April Hinson for her excellent typing and word processing skill. Without these latter efforts this report would not have been completed.

Gary Dau

TABLE OF CONTENTS

I. INTRODUCTION

The owners and operators of nuclear power plants in the U.S. are required by law to perform periodic inservice inspection of components of the primary pressure boundary (1)*. Basic inspection requirements in terms of specific components, frequency of inspection, coverage, etc. are contained in the American Society of Mechanical Engineers (ASME) Boiler and Pressure Vessel Code Section XI "Rules for Inservice Inspection of Nuclear Power Plant Components." The basic code requirements can also be augmented by the NRC through the issuance of Regulatory Guides, Inspection and Enforcement (IE) Bulletins, and other documents such as NUREG Reports.

Generally these documents treat the inspection process of detection, signal discrimination, and flaw sizing as a composite function. In reality, each step is a distinct function. Detection consists of using the appropriate gear to detect signals that could be indicative of the presence of flaws. The discrimination process consists of analyzing the signal identified in the detection process and making a decision of whether the signal either indicates the presence of a flaw or originates from benign sources that are peculiar to the weld geometry. Once the signal indicates presence of a flaw, the third step of the inspection process, sizing, must be completed. For the remainder of this report only ultrasonic inspection methods will be considered.

In piping, sizing consists of determining the length of the flaw, e.g. its circumferential extent, plus its depth, i.e. the through-wall penetration. Schematically this is shown in Figure 1-1. For circumferentially oriented cracks the normally applied ultrasonic inspection procedure for detection and discrimination also determines the flaw length.

* ( ) Indicates article listed in Reference Section.

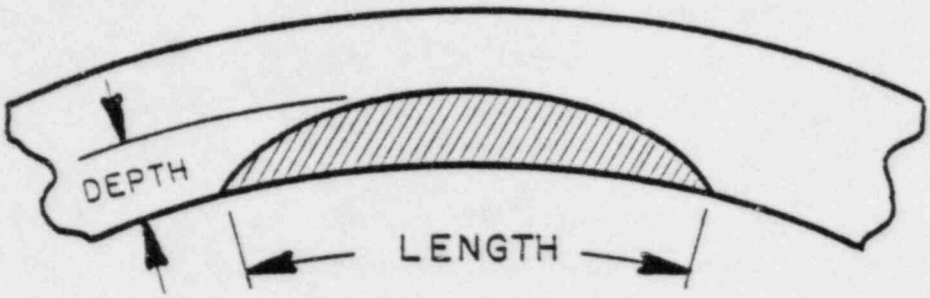

Figure 1-1. Cross Sectional Representation Of An IGSCC Flaw In A Pipe Wall.

With this background, it is appropriate to review prior events regarding the detection, discrimination and sizing of intergranular stress corrosion cracks (IGSCC) in BWR power plants.

Stress Corrosion cracking of piping in BWR's first received attention in the U.S. in January 1975 when all BWR's were shut down for inspection of the by-pass and core spray piping welds. Numerous indications were observed and the industry took immediate steps to deal with the problem. Subsequently the NRC issued a report (NUREG 0313) (2) that identified "service sensitive" lines requiring augmented inservice inspection (ISI) beyond that required by the ASME Section XI Code. Service sensitive lines were identified as those that field experience indicated were susceptible to IGSCC.

While preparing for the replacement of furnace sensitized safe ends at Nine Mile Point Unit 1 Power Plant (NMP-1) in early 1982, Niagara Mohawk Power Company personnel reported finding IGSCC in the large diameter piping being inspected under the normal Code rules. This large diameter piping was not covered by the augmented ISI requirements. More extensive inspections revealed additional

cracking in the pipe to the point that the owner made a decision to replace the entire main recirculation piping system. Removal and subsequent testing provided positive information that IGSCC was present in the large diameter piping.

As a result of the NMP-1 experience, the NRC became concerned that the inspection techniques and procedures being used on large diameter piping might not be sensitive enough to detect presence of IGSCC. As a consequence, IE Bulletin 82-03 (3) was issued on October 15, 1982 requiring that inspection teams demonstrate their ability to detect IGSCC before the nine plants identified in the bulletin could return to operation. EPRI on behalf of the Industry, working through its Nondestructive Evaluation (NDE) Center, coordinated closely with the NRC to provide samples, laboratory space, sample documentation, and other logistical support necessary to conduct the demonstration process. The samples used were actual segments of piping removed from NMP-1 with the interior concealed from the inspection groups. Personnel from the NRC witnessed all performance capability demonstrations (PCD) and made the final Pass/Fail determination. After this round of capability demonstrations was completed, it was obvious that the process had generated more uniform results throughout the industry and also seemed to upgrade overall performance for both detection and discrimination. Based on these improvements, a second bulletin IEB 83-02 (4) was issued to address the remaining BWR's. This second bulletin built on the lessons learned from the first bulletin and defined the performance capability demonstration in more formal terms. EPRI, on behalf of the industry, responded by providing a special facility at the EPRI NDE Center to handle radioactive samples used in this continuation of the performance demonstration process. Again, the NRC monitored the demonstration process and rendered the Pass/Fail decision. A preliminary analysis of the results indicate continuing improvement in the detection and discrimination process.

A review of the procedures used by the utilities and their inspection vendors plus observation of the qualification process indicated that a specific course was needed to either refine existing inspection personnel skills or train new people for detection and discrimination of IGSCC in large diameter piping. Accordingly EPRI NDE Center staff members, aided by a group of utility personnel, initiated development of such a training course in December 1982. The first session was

held tne week of June 27, 1983. The course, now being offered twice a month, is completely subscribed through October.

Thus, since the concern about detection of IGSCC in large diameter piping developed in September 1982, the industry working in close coordination with the NRC has made several efforts to assure a high quality reliable inspection of BWR piping. As a result the detection and identification of IGSCC is no longer a major concern.

In mid-May some utilities evidenced growing concern about the status of sizing the depth of IGSCC with the ultrasonic testing (UT) method. This concern was generated by individual utilities experience in conducting their own performance capability demonstrations to select both contractors and techniques for IGSCC sizing. As a result, all available information on ultrasonic sizing methods actually used on power plants that had been positively correlated with actual crack depth measurements by destructive evaluation were assembled. The number was small and did not cover a large range of flaw depths. Recognizing the sparseness of the data and its importance to the flaw evaluation process, these utilities requested EPRI to conduct an accelerated effort to determine the adequacy of the UT sizing methods being used in the field. This exercise, called a round robin, was initiated on June 1 with a targeted completion date of July 31, and a report to the industry on August 4, 1983. This schedule was met.

It should be emphasized that the round robin was initiated and conducted at the industry's request to generate information necessary to assess the current state of practice in the industry. Where performance gaps are identified the information is useful to indicate the corrective action needed. The effort was not designed to serve as a qualification program. Any attempt to do so is an incorrect use of the results.

Sections of the report that follow address the following subjects, summary of results, relation of flaw measurement to flaw evaluation procedure, description of round robin process, presentation of conventional results, results obtained with advanced approaches, training programs, suggested qualification process for

sizing, consideration of radiation exposure limits and available trained people and the possible deployment of advanced equipment.

II. SUMMARY AND CONCLUSIONS

At the request of the utility industry, the Electric Power Research Institute (EPRI), working through its Nondestructive Evaluation (NDE) Center conducted a round robin exercise on ultrasonic flaw depth measurements. The objective of the exercise was to generate information necessary to assess the current state of practice of ultrasonic depth measurements of intergranular stress corrosion cracks (IGSCC) found in the piping of some boiling water reactors (BWRs). The exercise consisted of having all inservice inspection vendor and utility teams who have worked on BWR's measure the depths of 16 preselected flawed specimens. A permanent record of each flaw signal as a function of position was also obtained. After all data were recorded, the samples were subjected to a destructive evaluation process to establish the true depth of the flaws. This true depth was then compared to the nondestructive ultrasonic measurements.

A total of seventeen teams participated, 13 of them are active in the inspection of US BWR's, one represented a foreign BWR utility owner and one was from a regional US Nuclear Regulatory Commission (NRC) office. The final two teams were evaluating advanced approaches.

The data from all teams was subjected to a statistical analysis whereby a linear regression line was generated to represent the performance of each team. Figure 2-1 presents these curves for all teams. Teams 15 and 17 represent the advanced systems.

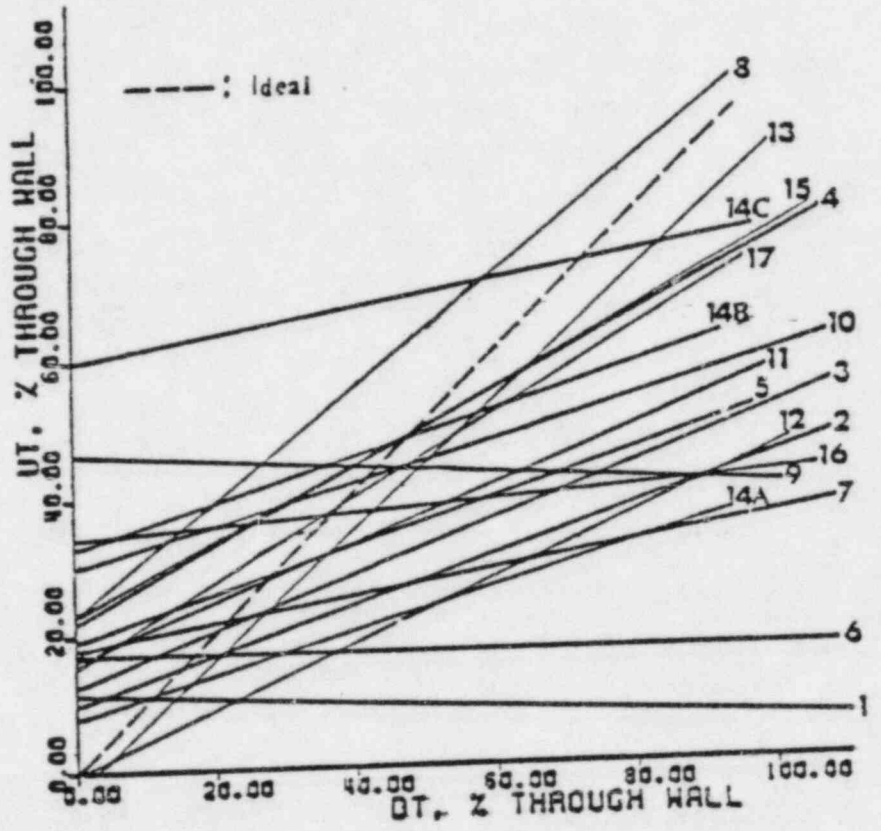

FIGURE 2-1. Linear Regression Line For All Teams.

The results show the following:

- The number of teams doing an adequate job is much lower than anticipated
- The range of performance from best to worst is very large
- The advanced techniques provide verification that the crack-tip diffraction sizing approach is the most viable method
- The influence of the ultrasonic measurement uncertainty to the flaw evaluation results must be assessed on case-by-case basis.
- Corrective actions are needed.

The recommended corrective actions are:

- Develop and implement a training program for people who size IGSCC
- Implement a qualification program that requires all people who perform sizing operations demonstrate their capability prior to making field measurements
- Accelerate completion, evaluation, and deployment of advanced systems.

The planning required to implement these recommendations is presently underway.

III. RELATIONSHIP OF FLAW SIZING TO THE FLAW EVALUATION PROCEDURE

Introduction

Intergranular stress corrosion cracks (IGSCC) in BWR piping pose no threat to the health and safety of the public. The inherent toughness of the stainless steel insures that IGSCC will not precipitate pipe rupture even during extreme accident conditions. There is some small probability that susceptible pipes may leak due to IGSCC, but even the leaking pipes will not rupture during these postulated accident conditions.

Acceptance of a flawed pipe for continued service using the evaluation procedures of Code Section XI IWB 3640 and Appendix X requires initial flaw size determination using UT. Because of the uncertainty associated with current UT sizing techniques, the procedure may lead to erroneous conclusions for flaws exceeding about 30% of pipe circumference. In the following, we discuss how these uncertainties affect the safety margins inherent in these procedures and propose a sizing criteria based on crack area that reduces this uncertainty. We focus here only on circumferential flaws since axial flaws pose no safety issue.

Flaw Evaluation Procedure

Evaluation procedures and acceptance criteria for flaws in austenitic steel piping have recently been approved for incorporation into ASME Section XI (Article IWB-3640 and Appendix X). Appendix C provides a detailed description of the technical basis for these procedures and criteria. The elements of the procedure are as follows:

1. Determination of maximum allowable flaw size at the end of a defined period of operation based on a net-section collapse theory of structural failure. This ensures that the presence of a flaw does not reduce the margin-to-failure below that implicit in the original design code for construction of the piping.

2. Subcritical flaw-growth analysis to determine the size flaw that would grow to the allowable flaw size during the defined operating period.

These elements are illustrated graphically in Figure 3-1. In this figure, a flaw of given depth (defined as a fraction of pipe wall thickness, $^{d}/_{t}$) and length (defined as a fraction of the pipe circumference, $^{\theta}/_{\pi}$) is predicted to cause failure if the length and depth exceed the net-section collapse line. The collapse line is a function of load, chosen here to be equal to the Code allowable design stress. Imposing the design code safety factor on this collapse line results in the code allowable curve which has been truncated at a depth of $^{d}/_{t}$ of 0.75 to preclude acceptance of a leaking flaw. These data are presented as tables in IWB-3640.

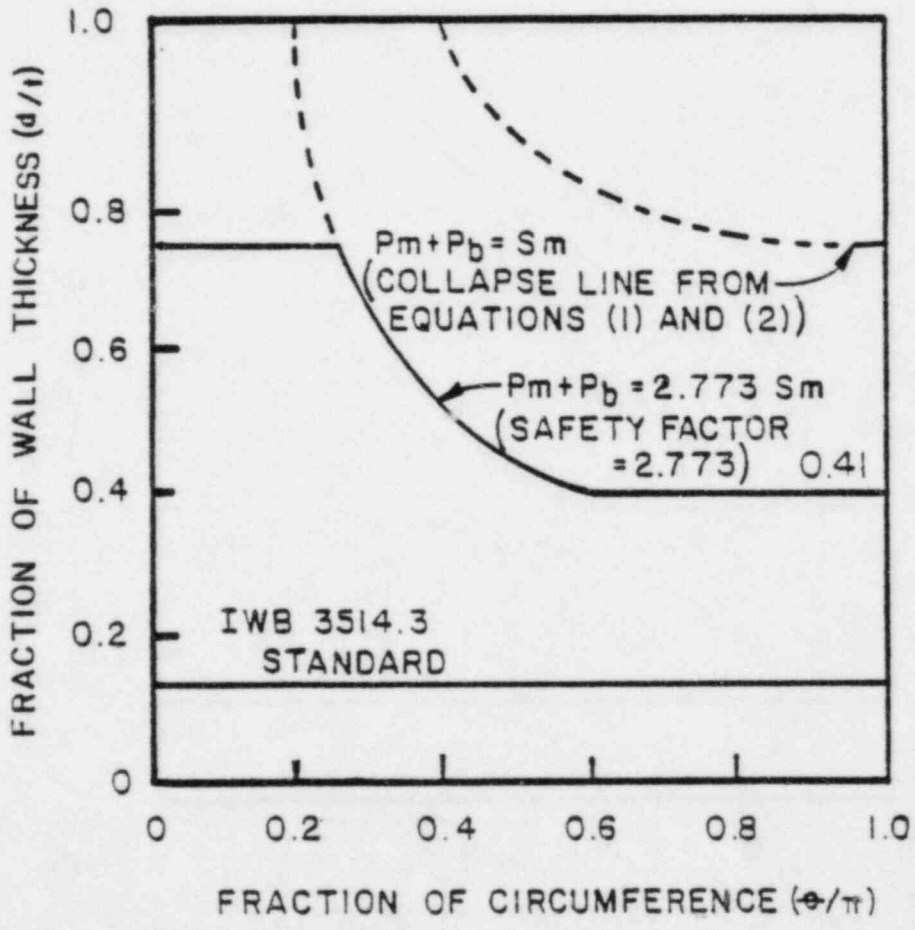

Figure 3-1. Flaw Evaluation Diagram (IWB-3640) For Normal Conditions And A Stress Ratio = 1.0

While the published flaw evaluation procedure is presented in terms of permissible crack length and depths, the underlying position is based upon remaining (uncracked) area. The notch insensitivity of wrought stainless steel, resulting from its extreme fracture toughness and ductility, is conservatively assessed using a simple strength of materials approach and sophisticated fracture mechanics is not required. In fact, the flaw acceptance criteria developed by the ASME Task Group were based on area, but it was felt that in-service inspectors need a length measurement for evaluation. One can easily convert Figure 3-1 to a permissible crack area diagram by multiplying the permissible length by the permissible depth and plotting the product versus normalized crack length. The permissible crack area curve is illustrated as Figure 3-2.

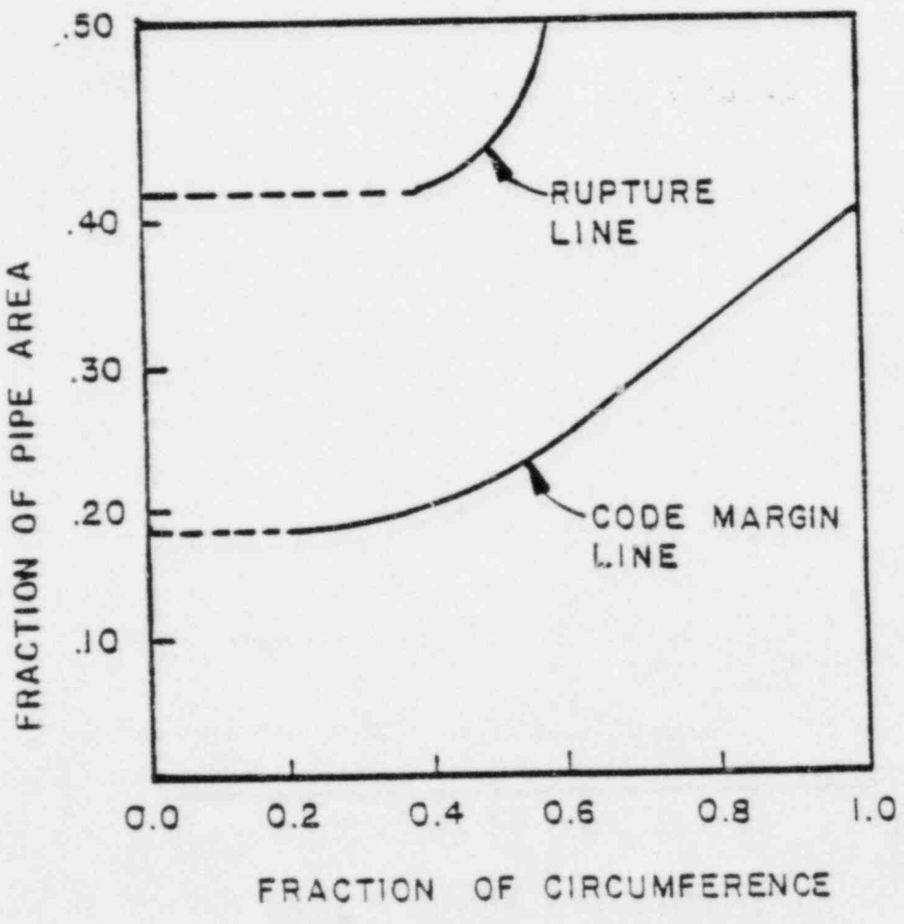

Figure 3-2. Permissible Crack Area Diagram Developed From Figure 3-1, Stress Ratio Equal To One

Flaw Characterization Based on Area

A simple method to evaluate flaw size that accounts for length and depth uncertainty can be achieved through the use of cracked area as a single flaw characterizing parameter, a direct measure of the load carrying capability of the structure. For example, on a 20-inch diameter pipe the maximum possible crack depth-to-length ratio is one to 66 and therefore it is less important how accurately a UT inspection characterizes crack depth than how accurately it characterizes crack area.

Consider, for example, a 20-inch diameter schedule 80 pipe with a crack 8 inches long and 0.30 inches deep. It is assumed for this example that crack depth can be determined to within ± 0.25-inch. This is a ± 83% uncertainty in crack depth sizing. Although crack lengths can be measured with greater accuracy than crack depth we assume a ± 0.25 inch uncertainty for both length and depth. This example is plotted in Figure 3-3 on the standard flaw evaluation diagram. The diagram is prepared for normal conditions that are generally limiting for pipe flaws, and assumes axial stress equal to the Code allowable design stress. The sizing uncertainty is clearly illustrated.

This evaluation curve is translated into crack area in Figure 3-4. The plot goes from 18% of pipe area for short through-wall flaws to 41% crack area for fully circumferential flaws. The uncertainty based on area is plotted for this example crack. It becomes obvious that even an ± 83% origin uncertainty when properly perceived does not pose a structural integrity concern. The sizing round robin illustrates that this ± 0.25-inch sizing ability is achieveable.

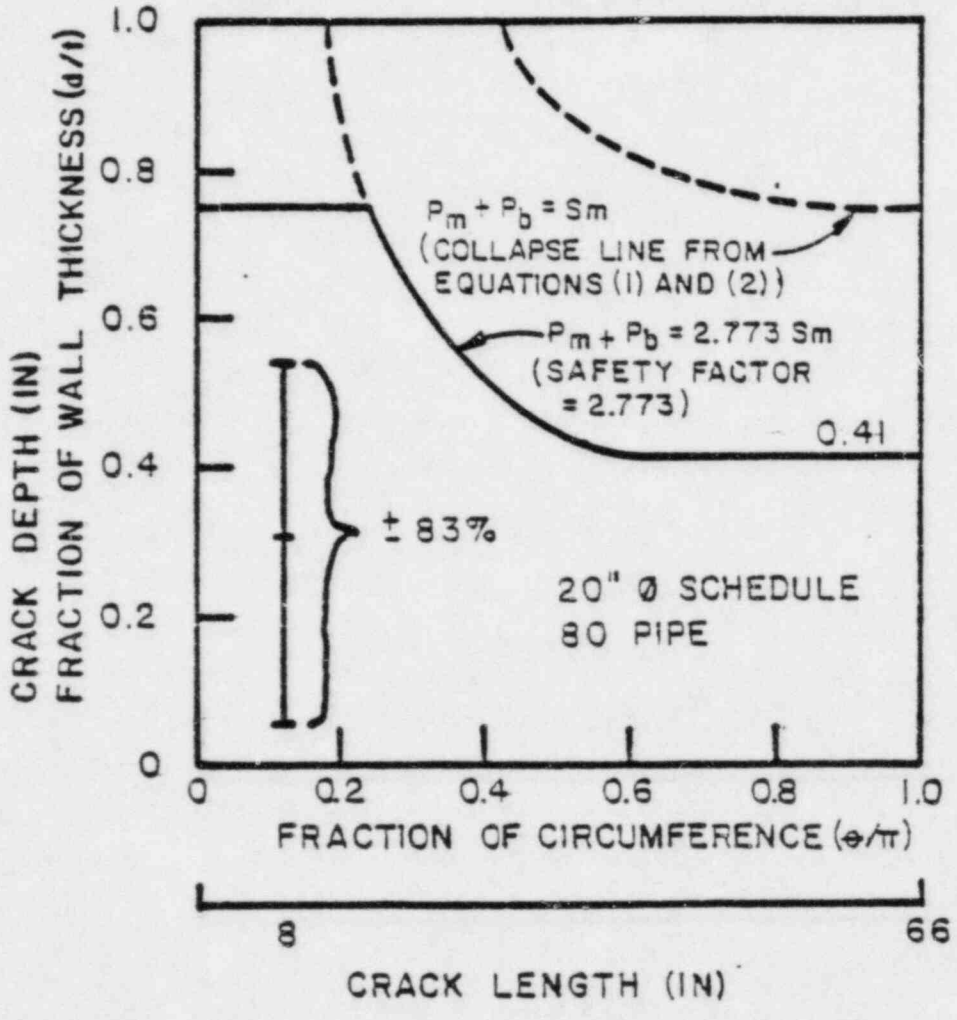

Figure 3-3. Example Crack Plotted On Flaw Evaluation Diagram IWB 3640. Crack Depth = 0.3 Inch, Crack Length = 8 Inches, Measurement Uncertainty = ± 0.25 Inch

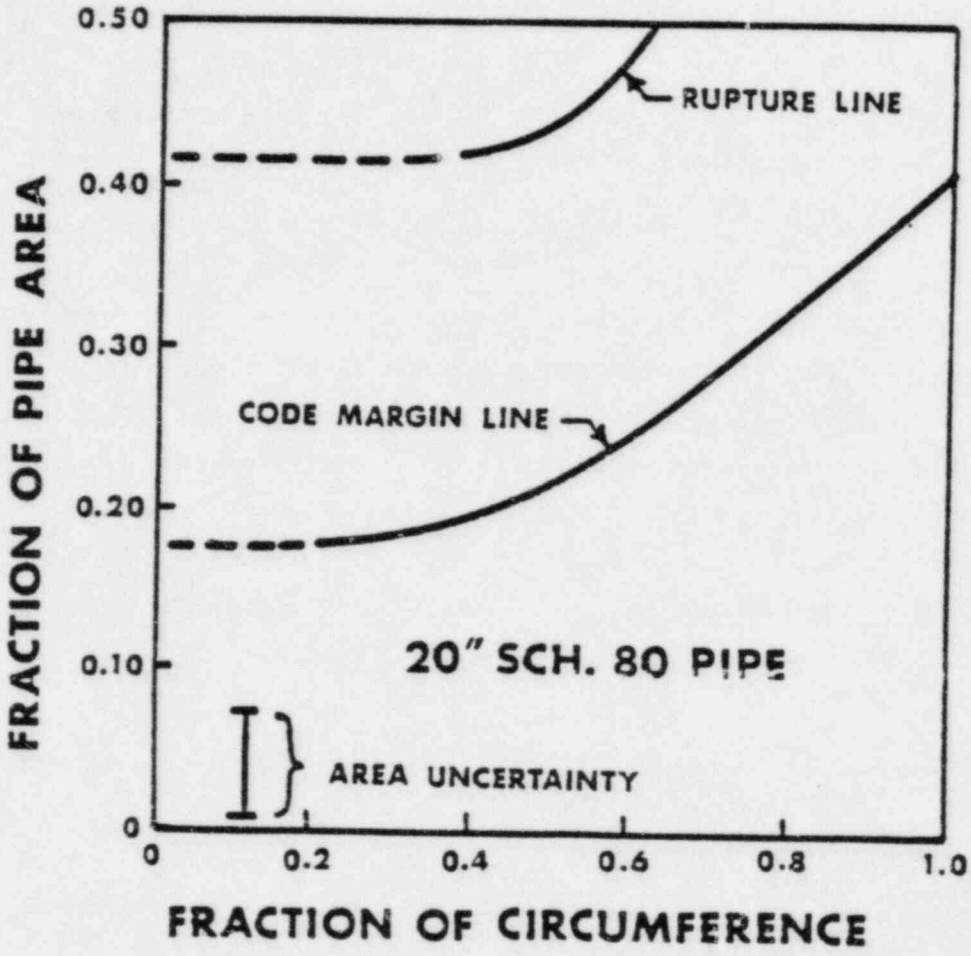

Figure 3-4. Example Crack Plotted On Permissible Area Diagram. Crack Depth = 0.3 Inch, Crack Length = 8.0 Inches, Measurement Uncertainty = 0.25 Inch, Normal Conditions Stress Ratio of 1.0

Discussion

There are a number of piping conditions that may be different from those assumed in the previous example. These include pipe size, design stress ratio for various design conditions, crack growth characteristics, and real versus idealized crack geometries. The impact of some of these different situations are briefly summarized in the following section.

Nuclear pipes are designed for varying stress ratios depending upon the specific application. The ASME Code presents methods for calculating stress levels and maximum acceptable levels for the design conditions. In BWR primary piping, the actual design stress levels are substantially below the maximum levels. For normal conditions, the maximum stress ratio, the summation of bending load (P_b) and the membrane load (P_m) divided the design stress level (S_m), is 1.5 while most pipes are designed to a level less than 0.6. The previous example uses a very conservative stress level of 1.0.

The impact of design stress level on permissible crack area is illustrated in Figure 3-5. A similar figure can easily be developed for accident conditions from the table included in Appendix C. It is obvious from Figure 3-5 that the tolerable uncertainty in crack measurement increases with decreasing stress level.

The crack growth characteristic in BWR pipe is bimodal in nature: either the cracks are short and deep or they are long and shallow. This bimodal behavior can be explained from the morphology of the residual stress and sensitization expected in these pipes.

The welded joints in a BWR can be normally placed into two categories. The first category, type A, is characterized as having asymmetric residual stresses and welding induced sensitization. These asymmetrics manifest themselves in cracks that are deep (sometimes through wall) but short in circumferential extent. The second category, type B, has symmetrical residual stresses and nearly uniform sensitization. Type B joints, if cracked, have a strong tendency towards shallow, fully circumferential cracks. Type A joints typically occur in smaller diameter

lines 4-12 inches in diameter. Type B joints occur in large diameter lines (18 inches and greater) because of their large heat dissipation capacity. Joints in the range 12-18 inches can be of either variety depending upon the specific welding conditions of the joint. Type A joints can leak but will not rupture because of the limited circumferential extent of the crack. Type B joints have a symmetric residual stress field and have a large compressive stress region beginning about 20% through the wall and IGSCC will not continue far into this compressive region. Consequently, type B joints will neither leak nor break.

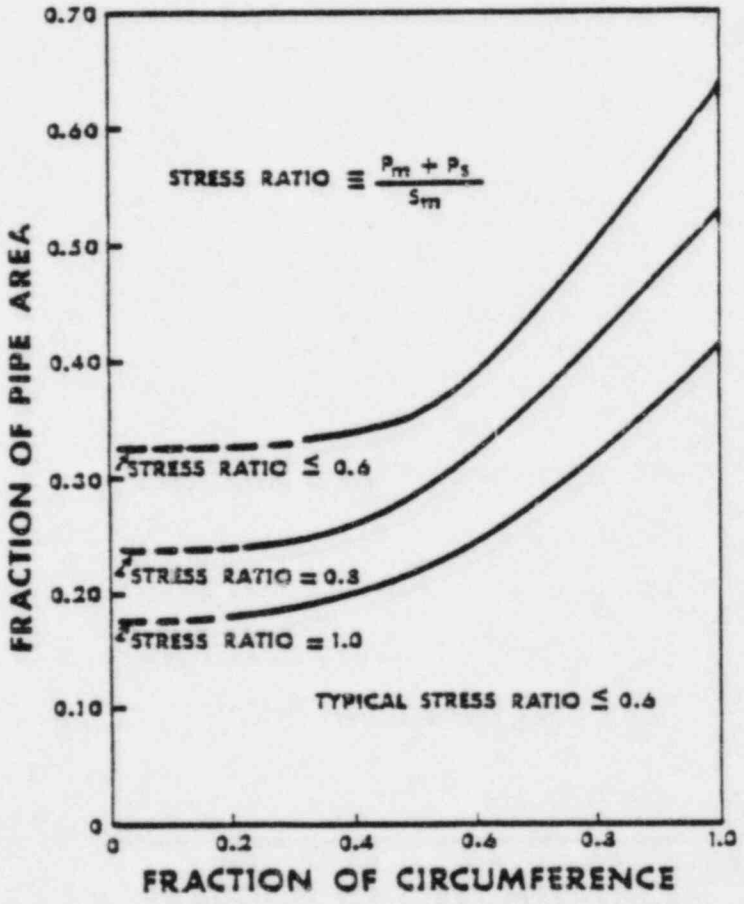

Figure 3-5. Permissible Crack Areas Developed For Normal Conditions And Various Stress Ratios

The crack growth characteristics of the two types of joints are illustrated in Figure 3-6. Although one can generalize that small joints are type A and large joints are type B, there are some circumstances that might cause this generalization to fail. For example, if an automatic weld procedure were used on a small diameter joint, the residual stress pattern would tend toward symmetry and the uniform compressive stress field would develop. In this case, a small diameter line may become a type B joint. Conversely, if some event, possible a major weld repair perturbed the symmetry of the stress field, a large diameter joint might become a type A joint. These apparent anomalies do not refute the leak before break postulate. More details are given in Appendix C.

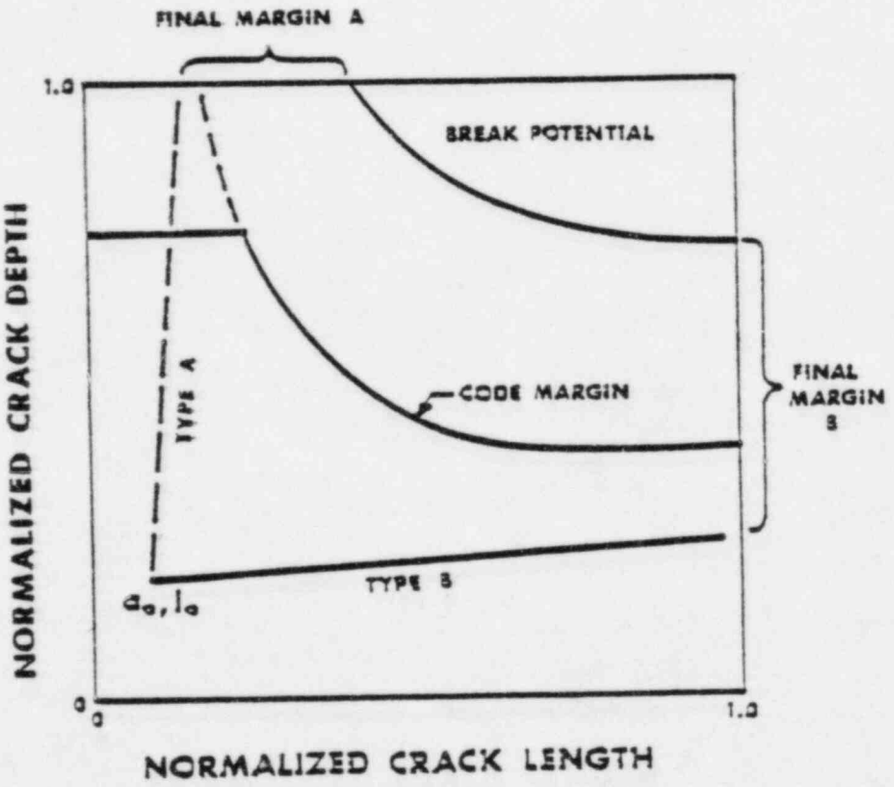

Figure 3-6. Crack Growth Characteristics For Type A And Type B Weld Joints

The flaw evaluation procedure requires the bounding of the IGSCC in a rectangle that is the maximum crack depth in width and the maximum crack length in length. IGSCC tends to be much less uniform. Figure 3-7 illustrates this idealized versus real situation. The evaluation rectangle is shown along with the actual crack geometry. The difference between these cracks is unrealized margin.

Conclusions

Ultimate safety relies on the strong leak-before-break arguments made in Appendix C that show for the steady intergranular stress corrosion crack growth from normal loads or the tearing growth from postulated accident conditions, leak, not break is the failure mechanism. These leak rates are readily detectable before the crack reaches a critical size. Crack sizing uncertainty may be placed in a more favorable aspect when viewed from an allowable crack area perspective that shows the large safety margins available in stainless steel piping.

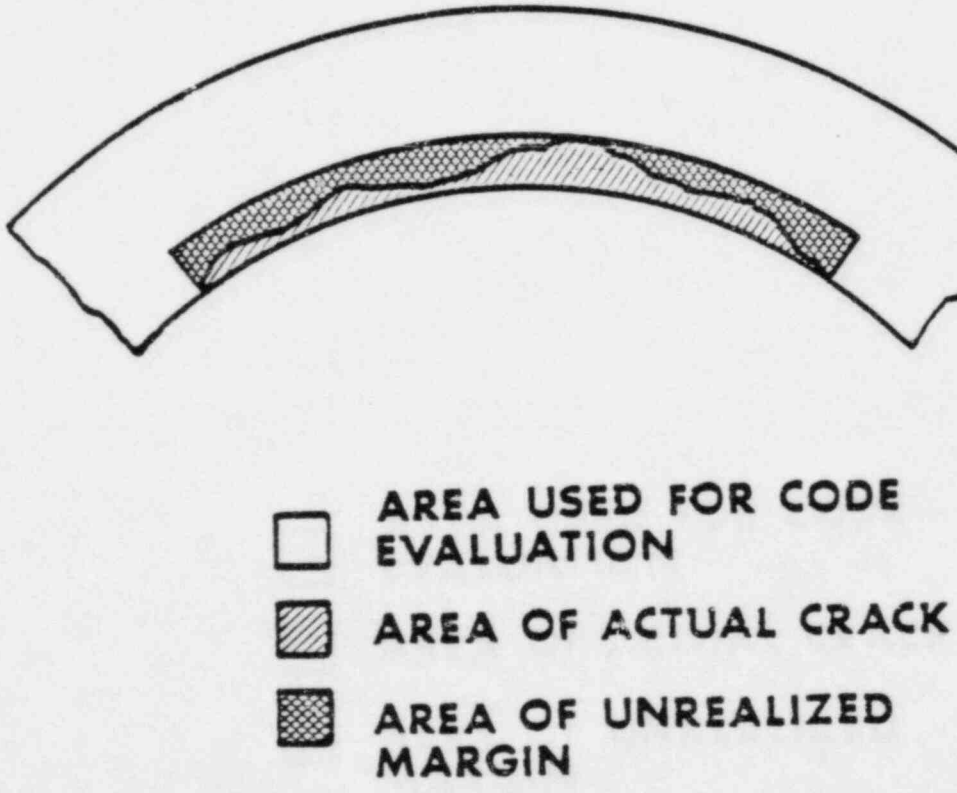

Figure 3-7. Schematic Of Idealized And Actual IGSCC Crack

IV. ROUND ROBIN PROCESS

The round robin process consists of gathering a group of representative samples and having teams inspect them as if they were in a field environment. It is an imperfect process but often is the most efficient method of quickly generating information about the current state of practice. The major product of any round robin is information. Additional work is needed to analyze this information to generate a smaller body of knowledge. The latter then becomes the basis on which decisions are made regarding the future actions needed to resolve any performance gaps noted. This round robin was conceived on May 18, 1983 initiated on June 1, and completed on August 4, 1983.

The material that follows describes the samples, participants, instructions to participants, role of data acquisition for advanced approaches, advanced signal processing, and destructive evaluation.

Samples

Sixteen sections of welded 304 stainless steel pipe were chosen for this exercise. The original pipe diameters ranged from 10-inch to 28-inch. In order to conserve time, the round robin was structured so that sizing the depth of a flaw was the only point of issue. Accordingly, 1.5 inch long circumferential zones were identified on each sample and all measurements were made within this region. Where flaws exist on both sides of a selected weld region, the flaw on the side near the stamped identification number is called "near" and the flaw on the opposite side of the identification number is called "far". This is illustrated in Figure 4-1 which shows a sample with two measurement regions in which both have flaws on the "near" and "far" side of the weld. The four flaws in the figure are identified as 9N, 9F, 10N and 10F.

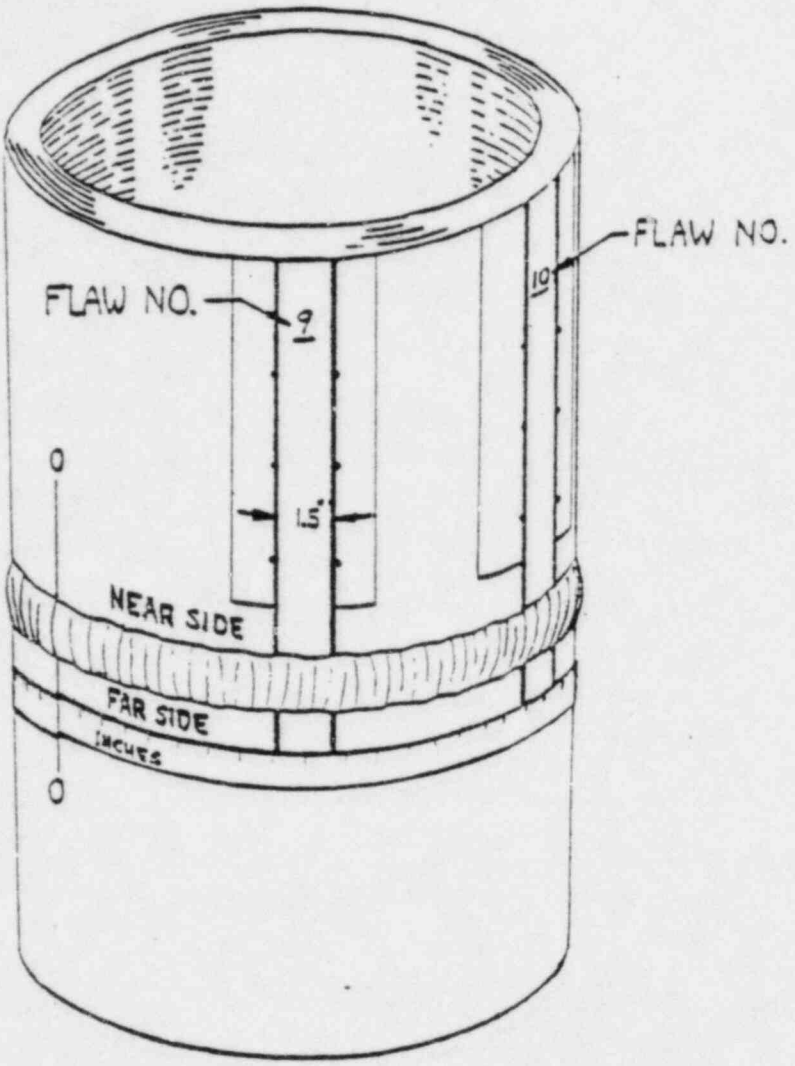

Figure 4-1. Typical Areas Of Inspection On Pipe Sample

Table 4-1 describes the specifics of each flaw region selected. In some cases flaws existed on both sides of the weld or there were more than one flaw per sample. It should be noted that although UT data were collected from all of the 16 regions listed, it was decided not to perform destructive tests of regions 13-16. This may occur at a later time. This is not believed to be a serious loss as these samples should be very similar to the four flaws contained in samples 11 and 12. A maximum of 16 flaws were examined by any team.

TABLE 4-1

Flaw Samples Used in Round Robin on UT Sizing of IGSCC

Sample No.	Flaw Type	Configuration	Flaw Side(s)	Nominal Diameter, Inches	Schedule/ Nominal Wall, Inches	Manufacturer, Origin	Current Location
1	IGSCC	Pipe-Pipe	One	12	100/0.90	IHI	NDEC (2)
2	IGSCC	Pipe-Pipe	One	12	100/0.88	IHI	NDEC
3	EDM Notch (1)	Pipe-Pipe	One	12	80/0.70	IHI	NDEC
4	EDM Notch	Pipe-Pipe	One	12	80/0.70	IHI	NDEC
5	EDM Notch	Pipe-Pipe	One	12	80/0.70	IHI	NDEC
6	IGSCC	Pipe-Pipe	One	10	80/0.55	BNWL (3)	NDEC
7	IGSCC	Safe end-Elbow	Safe end	28	80/1.0	Nine Mile Point	NDEC
8	IGSCC	Elbow-Riser	Elbow	28	80/1.3	Nine Mile Point	NDEC
9	IGSCC	Pipe-Pipe	Both	12	100/0.9	IHI	BNWL/NDEC
10	IGSCC	Pipe-Pipe	Both	12	100/0.9	IHI	BNWL/NDEC
11	IGSCC	Pipe-Pipe	Both	24	80/1.3	BNWL	BNWL
12	IGSCC	Pipe-Pipe	Both	24	80/1.3	BNWL	BNWL
13	IGSCC	Pipe-Pipe	Both	24	80/1.3	BNWL	BNWL
14	IGSCC	Pipe-Pipe	Both	24	80/1.3	BNWL	BNWL
15	IGSCC	Pipe-Pipe	Both	24	80/1.3	BNWL	BNWL
16	IGSCC	Pipe-Pipe	Both	24	80/1.3	BNWL	BNWL

Footnotes:

(1) EDM = Electro discharge machined
(2) NDEC = EPRI NDE Center, Charlotte, North Carolina
(3) BNWL = Battelle Pacific Northwest Laboratories, Richland, Washington

Participants

This activity was organized, implemented and completed in a very short time. As a consequence, priority was given to assuring that personnel from companies active in pipe examinations of BWR's were involved. This goal was achieved as all teams who had conducted recent examinations on US BWR's were involved as well as one team representing a foreign BWR owner. Thus, a total of fourteen teams from the ISI vendors and utilities participated in all or portions of the round robin activities at the NDE Center and Battelle Northwest. In addition, an NRC Inspector from Region II in Atlanta also took part in the Round Robin at the NDE Center. The unusual opportunity to have access to this large a sample selection and a definite commitment to confirmation by destructive testing was also used to evaluate some advanced concepts at various stages of development. Two series of results are included. Table 4-2 lists the teams and the specific samples that they examined.

Table 2

Participating Teams in Round Robin
on UT Sizing of IGSCC

TEAM	Flaws Examined at NDEC	Flaws Examined at BNWL
SWRI	1-8	9-16
Magnaflux	1-8	9-16
Ebasco	1-8	
NES	1-8	9-16
LMT	1-8	9-16
GE/San Jose	1-8	9-16
GE/King of Prussia	1-8	
CECO	1-8	9-16
NUSCO	1-8	9-16
TVA	1-8	9-16
GPU	1-8	
KKM (Switzerland)	1-10	
SCS I	1-3	9-16
SCS II	6,9,&10	
NRC Region II	1-10	
General Research Corp. (Adaptronics)	3-6 (Data on tape)	9-12 (Data on tape)
Amdata (Axicon transducer)	3-5, 7, 8	

Instructions to Participants

Upon arrival at the NDE Center each participant was given the sheet of instructions shown in Figure 4-2. Similar instructions were given for the exercise at Battelle Northwest. As the exercise progressed each team was required to fill out a data sheet reproduced on Figure 4-3. The information from this sheet was then transferred to the data sheets contained in Appendix A. During this transformation the team corporate identities were removed.

ROUND ROBIN ON UT SIZING OF IGSCC
EPRI NDE Center
Charlotte, NC

INFORMATION FOR PARTICIPANTS

1. There are eight (8) cracks to be sized at the NDE Center. All cracks are circumferential and their locations as well as the region of interest (1.5 inches wide) in which they must be sized are clearly marked on each of the eight specimens. We only want the maximum crack depth in the specified region. Clear all questions before you proceed.

2. Use your own equipment and procedure(s) and report the results for each crack on the forms that are provided to you.

3. Size each crack from the near side and far side (through the weld) if possible.

4. You are strongly encouraged to size each crack with more than one technique to allow yourself the chance of evaluating the applicability of your different techniques to the same crack once the destructive results are out.

5. Given below are the list of cracks and information on the specimens.

Crack No.	Configuration	Nominal Dia. (in.)	Schedule/Nominal Wall Thickness
1	Pipe-pipe	12	100/0.90"
2	Pipe-pipe	12	100/0.88"
3	Pipe-pipe	12	80/0.70"
4	Pipe-pipe	12	80/0.72"
5	Pipe-pipe	12	80/0.71"
6	Pipe-pipe	10	80/0.55"
7	Safe end-elbow	28	80/1.06" Safe end 80/1.32" Elbow
8	Elbow-riser	28	80/1.29" Elbow 80/ -- Riser

The cracks No. 7 and No. 8 are in specimens that are radioactive and should be examined in the controlled area under HP supervision. The other six cracks will be examined in the ultrasonic laboratory.

Figure 4-2. Instructions Given To Round Robin Participants.

ROUND ROBIN ON UT SIZING OF IGSCC
EPRI NDE Center
Charlotte, NC

Crack No. _____

Inspector/Level _____
ISI Company _____
Utility _____

Date _____

UT Instrument, Make & Model _____

Transducer: Single ( ) Dual ( )

Make & Model _____
Size _____
Frequency _____
Band width, if known _____
Angle _____°
Mode: shear ( ), longitudinal ( )

Method of Sizing:

( ) Amplitude drop, at _____% of Peak ( ) DAC ( )
( ) Crack tip diffraction
( ) Others, describe briefly

_____
_____

Measurements from: Near Side ( ) Far Side ( )
Sound Path: 1/2V ( ), 3/2V ( ), other _____
Beam Spread: Accounted for ( ) Not accounted for ( )

Measured crack depth: _____ inch

Figure 4-3. Data Sheet Completed For Each Flaw.

Data Acquisition for Advanced Approaches

The integrated EPRI-BWROG nondestructive R&D effort has pursued development of the necessary hardware and software to automate the IGSCC inspection process. The hardware for the system control and data recording electronics, transducer housing, and mechanical scanner have all been developed and are undergoing evaluation and eventual qualification under the auspices of the NDE Center. See Figure 4-4 for a schematic representation of the system. The system has thus far been evaluated in the data acquisition mode. This permitted an appraisal of all the electronic and mechanical functions of the system independent of the automatic decision software, which is in the final development stage.

In this mode of operation the system records the complete ultrasonic waveform with position coordinates for each point in a predetermined scan plan. System calibration is done in accordance with ASME Section XI requirements. The system had successfully completed it's first field test in a nuclear power plant just prior to the start of the round robin. Thus it was decided to use it to obtain magnetic tape records of UT signals and position information for all samples. All of this information was recorded by a team of NDE Center personnel on a non-interference basis while the teams performed crack sizing by conventional means. In addition, the NDE Center staff also collected some data with a BNWL supplied probe for their processing by the synthetic aperture focusing technique (SAFT) under their NRC funded program. As a result it will be possible to compare on a very detailed basis the ultrasonic reflection properties of IGSCC with the destructive evaluation results.

A schematic representation of the data acquisition system is shown in Figure 4-4 while additional details on the components can be found in References 5 and 6.

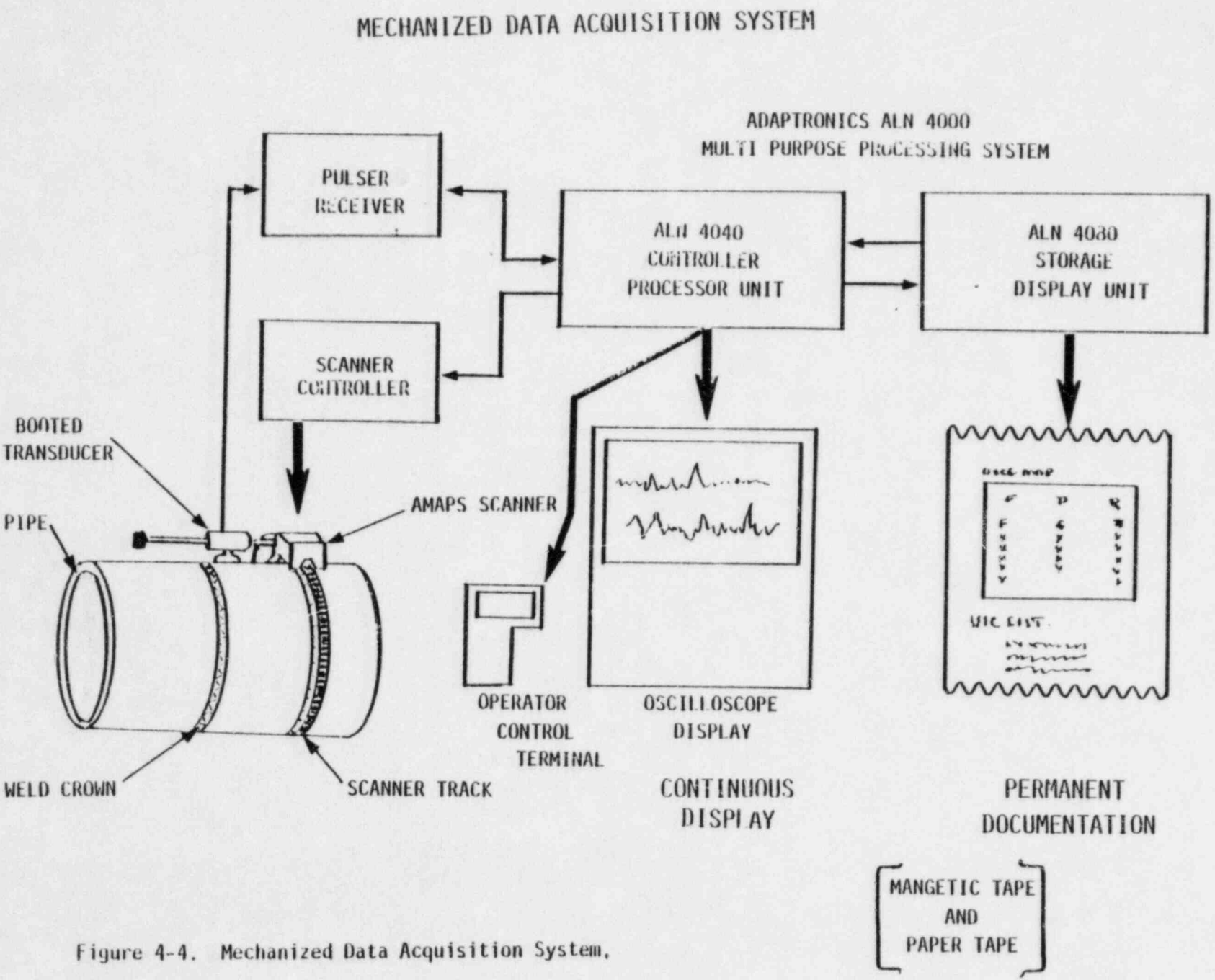

Figure 4-4. Mechanized Data Acquisition System.

Advanced Signal Processing

Some of the digital UT data recorded on magnetic tape by the NDE Center has already been sent to R&D firms to be analyzed by advanced signal processing techniques. The data is also being reformatted to be sent to several other research groups for analysis and development of reliable algorithms for crack sizing. These groups include Ultrasonics International, General Research Corp. (formerly Adaptronics, Inc.), Southwest Research Institute, and Battelle's Pacific Northwest Laboratories. In addition to the Data Acquisition System data that will be supplied to Ultrasonics International, a team of their engineers also collected their own digital data from the round robin samples to assess the applicability of echo dynamics characteristics of the IGSCC signals to the crack depth.

Destructive Evaluation

The only way to obtain absolute information about flaw depths to correlate with UT measurements is to do destructive analysis. Only a small amount of this type analysis has been performed before because by definition it destroys the sample's usefulness for other activities such as training and equipment development. However, the importance of the issue dictated that these samples undergo a destructive analysis to confirm actual crack depth.

Samples 1, 2, 6, 7, 8, 9 and 10 were sectioned at Battelle Columbus and samples 11 and 12 were sectioned at Battelle Northwest. Samples 3, 4 and 5 contained EDM notches and hence no destructive sectioning was necessary. Samples 13, 14, 15 and 16 were not sectioned. This will not have a significant effect on the round robin data since they are very similar to samples 11 and 12.

The seven samples that were sent to Battelle Columbus for destructive assay were sectioned in the following manner. Noting that each region of interest for flaw sizing was 1.5 inches wide, each sample was cut at the scribed center line and, then at distances of 0.375 and 0.750 inch on either side of that center line as shown in Figure 4-5 for a total of 5 cuts per sample. The sections were then ground, polished, and lightly etched to reveal the crack and the weld structure. Photomicrographs were taken and a scale was incorporated in each photograph to aid

in direct measurement of the crack depth. Detailed information from the destructive evaluation for each flaw is contained in Appendix B. A similar process was followed by Battelle Northwest.

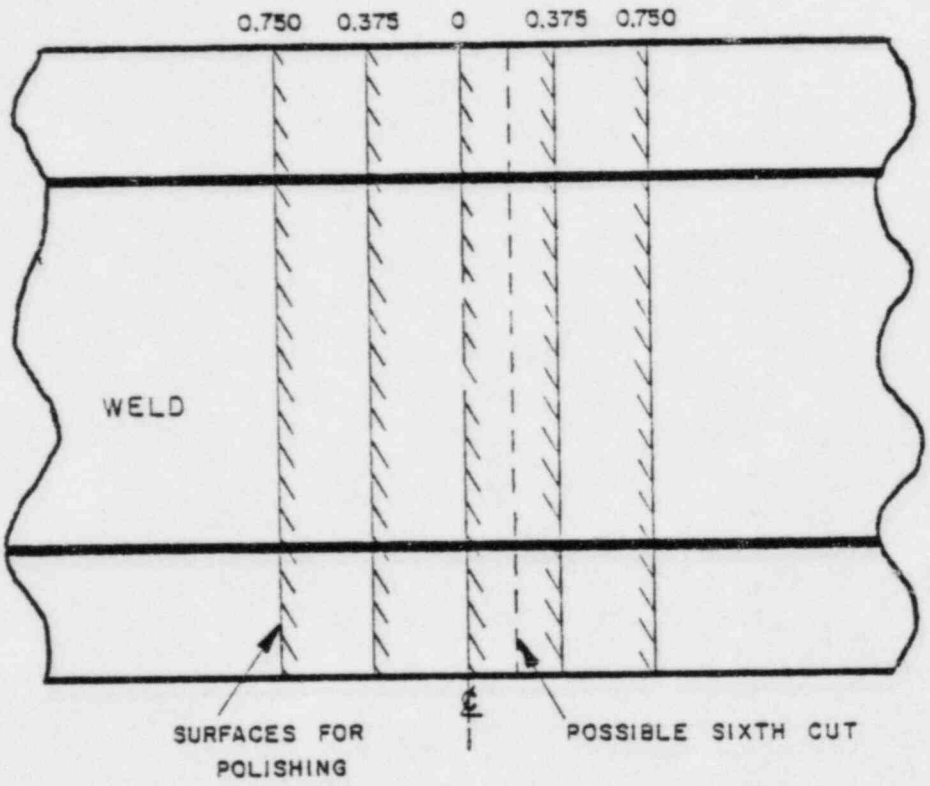

Figure 4-5. Schematic Showing Cutting Diagram For Samples.

V. CONVENTIONAL RESULTS

Results are presented in this section for the fifteen teams which performed UT flaw depth sizing by conventional methods. The basic mode of data presentation is through the use of plots which compare the depth predicted by UT versus the depth determined from destructive sectioning. Both depths are presented as a percentage of wall in order to normalize the data. Each plot has a thin 45° line which represents perfact sizing. The closer a data point lies to the 45° line the better the sizing performance is for that flaw. Figures 5-1 through 5-15 present the data by teams.

The data of each team has been analyzed by performing a linear regression. Significant parameters calculated include the slope of the best fit regression line, the vertical axis intercept, the standard deviation, and the correlation coefficient. The correlation coefficient provides the best global measure of performance with 1.0 being perfect correlation between the predicted and actual depths and values near 0.0 representing no correlation. Table 5-1 provides a summary of these parameters by team as well as listing the number of data points used in the analysis process. On each of Figures 5-1 through 5-15 the linear regression line is shown with a thick line and the slope, number of data points used in the analysis, standard deviation and correlation coefficient are listed.

It is important to keep in mind that the purpose of this round robin was to generate information about the current state of practice in the industry. The exercise was initiated and conducted at the industry's request. Where performance shortcomings are identified this information is useful to indicate corrective action needed. The round robin should not be considered as a qualification program.

Table 5-1

STATISTICAL PARAMETERS CALCULATED FROM
UT FLAW SIZING ROUND ROBIN DATA

Team Number	Linear Regression Analysis Parameters				
	Number of Data Points	Regression Line Slope	Regression Line Intercept (% of wall)	Correlation Coefficient	Standard Deviation (% wall)
1	16	-0.05	11	-0.24	5
2	14	0.35	10	0.33	23
3	16	0.39	12	0.56	20
4	8	0.54	23	0.79	14
5	14	0.33	19	0.61	12
6	16	0.00	17	-0.02	3
7	14	0.19	18	0.49	8
8	14	0.82	23	0.70	25
9	14	-0.05	46	0.06	16
10	8	0.31	29	0.41	16
11	14	0.42	16	0.71	16
12	5	0.46	-1	0.52	27
13	12	0.92	-3	0.80	34
14	12	0.29	33	0.45	19
15	5	0.55	22	0.70	20
16	12	0.09	34	0.28	10
17	8	0.60	15	0.82	22

TEAM NO. 1
TRUE VS. MEASURED DEPTH

EPRI NDE CENTER

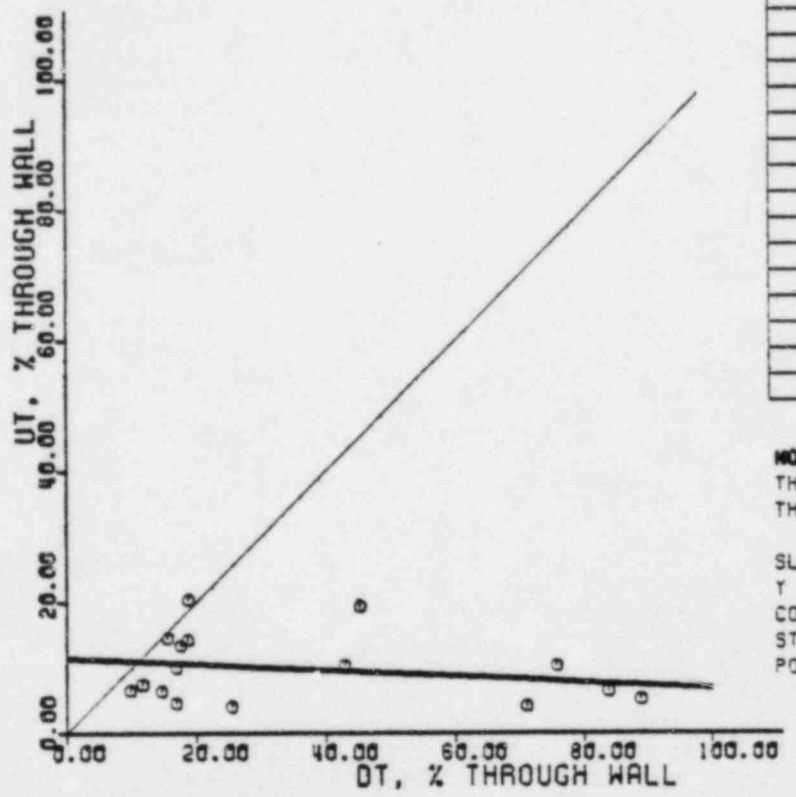

PIPE THK. (IN)	DEPTH (IN)	
	DT	UT
0.785	0.147	0.160
0.812	0.094	0.060
0.620	0.280	0.120
0.620	0.440	0.045
0.620	0.060	0.040
0.565	0.105	0.080
1.050	0.184	0.140
1.253	0.318	0.050
0.780	0.590	0.080
0.780	0.653	0.050
0.780	0.334	0.080
0.780	0.892	0.040
1.100	0.160	0.070
1.100	0.170	0.160
1.100	0.185	0.050
1.100	0.185	0.110

NOTES:
THIN LINE: IDEAL CASE
THICK LINE: LINEAR REGRESSION
Y = AX + B
SLOPE (A) = -0.05
Y INTERCEPT (B) = 11.4
CORRELATION COEFF. = -0.24
STANDARD DEVIATION = 5.3
POPULATION (N) = 16

FIGURE 5-1.

TEAM NO. 2
TRUE VS. MEASURED DEPTH

EPRI NDE CENTER

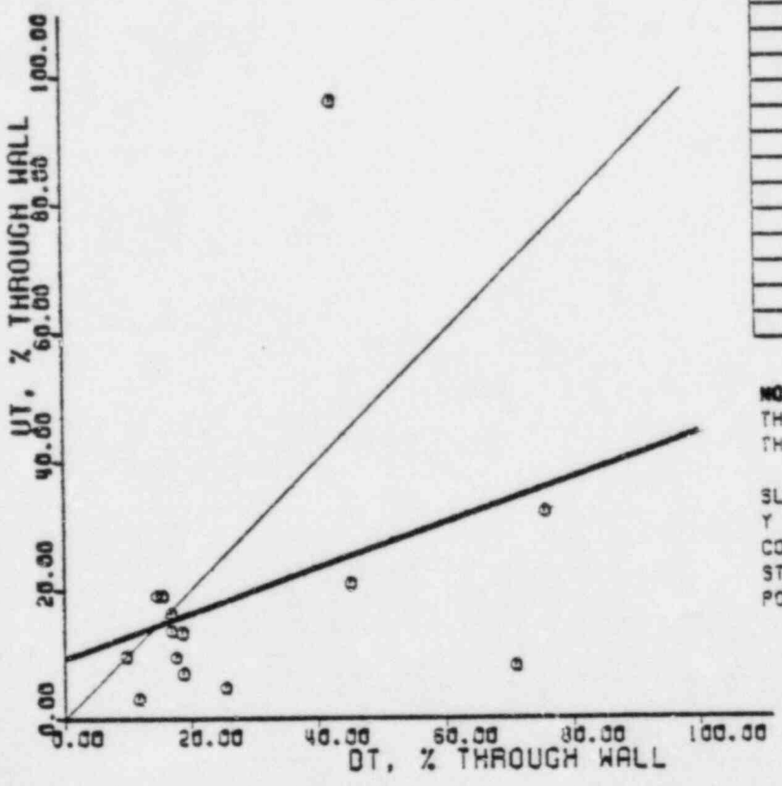

PIPE THK. (IN)	DEPTH (IN)	
	DT	UT
0.785	0.147	0.055
0.812	0.094	0.025
0.620	0.280	0.130
0.620	0.440	0.050
0.620	0.060	0.060
0.565	0.105	0.075
1.050	0.184	0.100
1.253	0.318	0.060
0.780	0.590	0.250
0.780	0.334	0.750
1.100	0.160	0.210
1.100	0.170	0.210
1.100	0.185	0.190
1.100	0.185	0.150

NOTES:
THIN LINE: IDEAL CASE
THICK LINE: LINEAR REGRESSION
$Y = AX + B$
SLOPE (A) = 0.35
Y INTERCEPT (B) = 9.5
CORRELATION COEFF. = 0.33
STANDARD DEVIATION = 23.3
POPULATION (N) = 14

FIGURE 5-2.

TEAM NO. 3
TRUE VS. MEASURED DEPTH

EPRI NDE CENTER

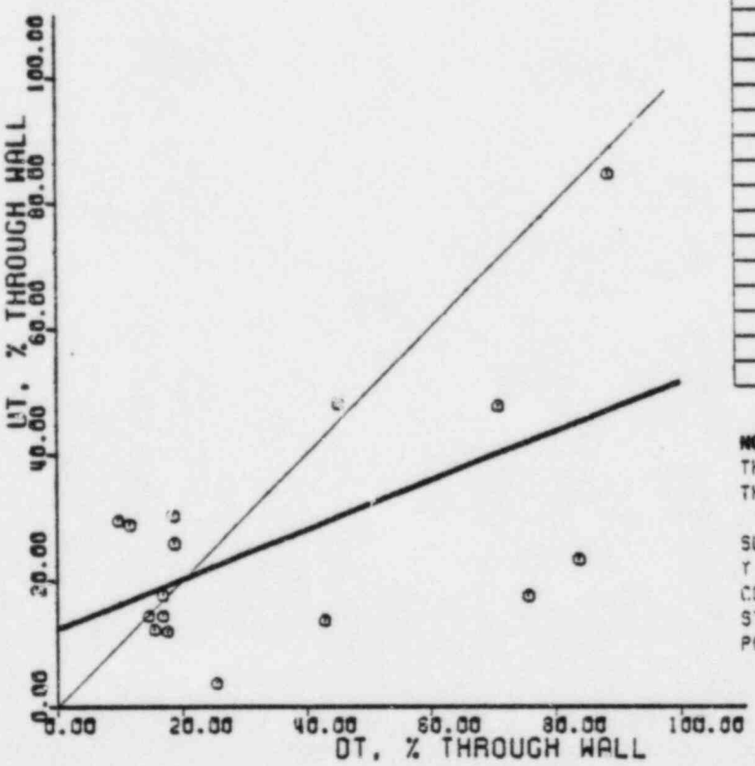

PIPE THK. (IN)	DEPTH (IN)	
	DT	UT
0.785	0.147	0.203
0.812	0.094	0.234
0.620	0.280	0.298
0.620	0.440	0.296
0.620	0.060	0.183
0.555	0.105	0.171
1.050	0.184	0.125
1.253	0.318	0.046
0.780	0.590	0.137
0.780	0.653	0.182
0.780	0.334	0.106
0.780	0.692	0.661
1.100	0.160	0.158
1.100	0.170	0.134
1.100	0.185	0.195
1.100	0.185	0.158

NOTES:
THIN LINE: IDEAL CASE
THICK LINE: LINEAR REGRESSION
$Y = AX + B$
SLOPE (A) = 0.39
Y INTERCEPT (B) = 12.4
CORRELATION COEFF. = 0.56
STANDARD DEVIATION = 19.8
POPULATION (N) = 16

FIGURE 5-3.

TEAM NO. 4
TRUE VS. MEASURED DEPTH

EPRI NDE CENTER

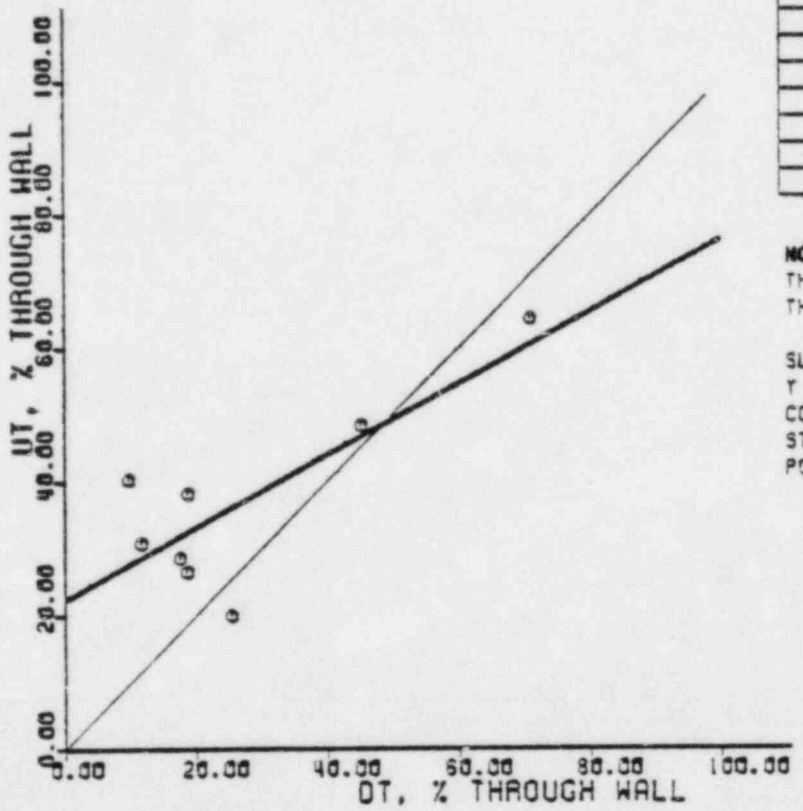

PIPE THK. (IN)	DEPTH (IN)	
	DT	UT
0.785	0.147	0.300
0.812	0.094	0.250
0.620	0.280	0.300
0.620	0.440	0.400
0.620	0.060	0.250
0.565	0.105	0.150
1.050	0.184	0.300
1.253	0.318	0.250

NOTES:
THIN LINE: IDEAL CASE
THICK LINE: LINEAR REGRESSION
$Y = AX + B$
SLOPE (A) = 0.54
Y INTERCEPT (B) = 22.5
CORRELATION COEFF. = 0.79
STANDARD DEVIATION = 14.2
POPULATION (N) = 8

FIGURE 5-4.

TEAM NO. 5
TRUE VS. MEASURED DEPTH

EPRI NDE CENTER

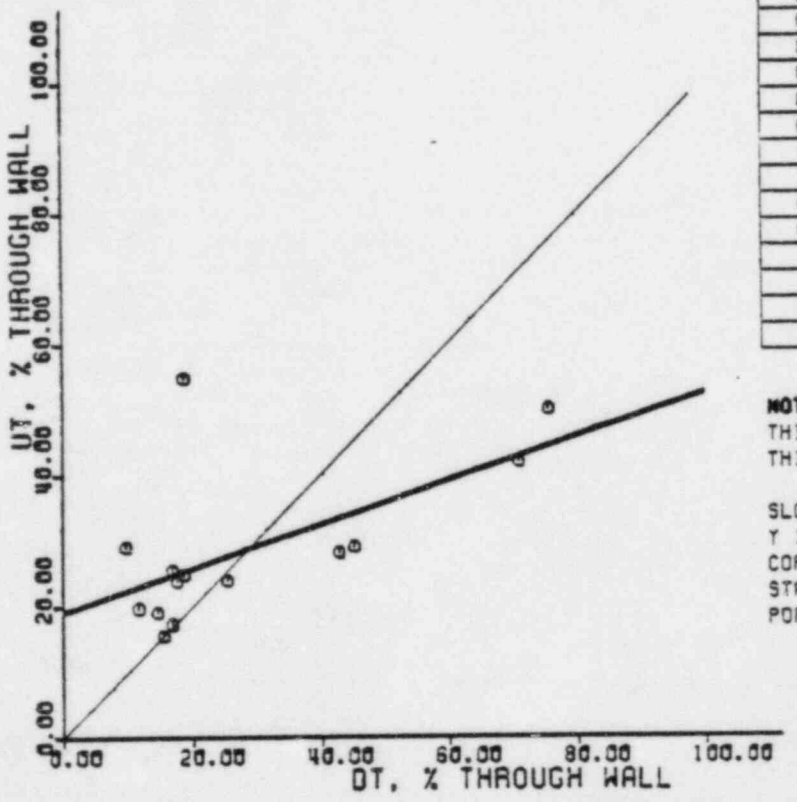

PIPE THK. (IN)	DEPTH (IN)	
	DT	UT
0.785	0.147	0.430
0.812	0.094	0.160
0.620	0.280	0.180
0.620	0.440	0.260
0.620	0.060	0.180
0.565	0.105	0.140
1.050	0.184	0.250
1.253	0.318	0.300
0.780	0.590	0.390
0.780	0.334	0.220
1.100	0.160	0.210
1.100	0.170	0.170
1.100	0.185	0.280
1.100	0.185	0.190

NOTES:
THIN LINE: IDEAL CASE
THICK LINE: LINEAR REGRESSION
$Y = AX + B$
SLOPE (A) = 0.33
Y INTERCEPT (B) = 19.2
CORRELATION COEFF. = 0.61
STANDARD DEVIATION = 12.0
POPULATION (N) = 14

FIGURE 5-5.

TEAM NO. 6
TRUE VS. MEASURED DEPTH

EPRI NDE CENTER

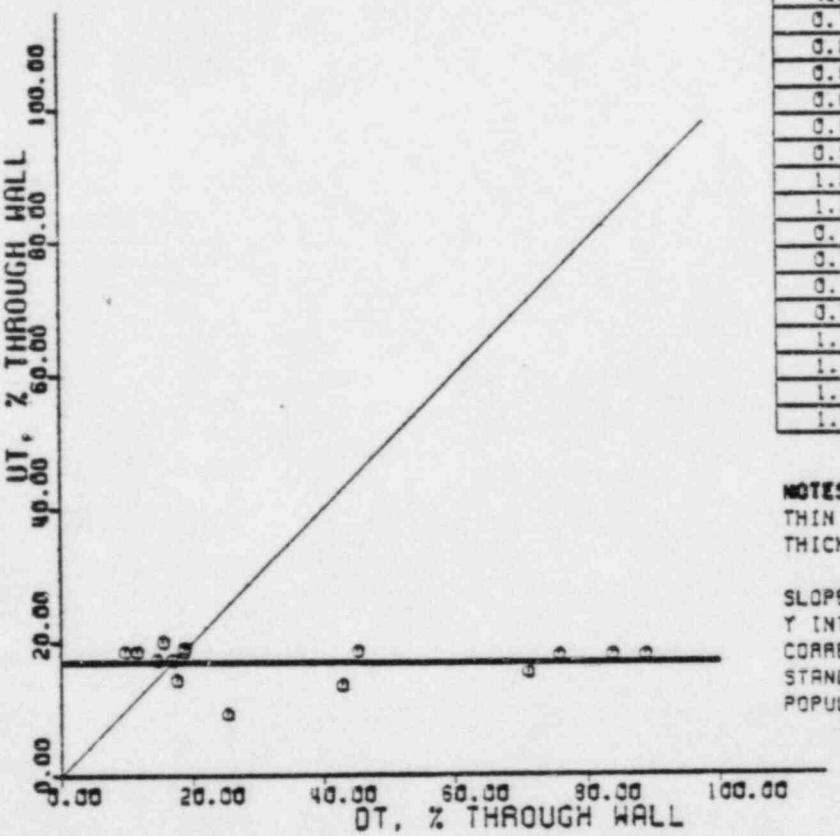

PIPE THK. (IN)	DEPTH (IN)	
	DT	UT
0.785	0.147	0.150
0.812	0.094	0.150
0.620	0.280	0.115
0.620	0.440	0.095
0.620	0.050	0.115
0.565	0.105	0.105
1.050	0.184	0.150
1.253	0.318	0.115
0.780	0.590	0.140
0.780	0.553	0.140
0.780	0.334	0.105
0.780	0.392	0.140
1.100	0.160	0.190
1.100	0.170	0.220
1.100	0.185	0.190
1.100	0.185	0.190

NOTES:
THIN LINE: IDEAL CASE
THICK LINE: LINEAR REGRESSION
$Y = AX + B$
SLOPE (A) = -0.00
Y INTERCEPT (B) = 17.0
CORRELATION COEFF. = -0.02
STANDARD DEVIATION = 2.7
POPULATION (N) = 16

FIGURE 5-6.

TEAM NO. 7
TRUE VS. MEASURED DEPTH

EPRI NDE CENTER

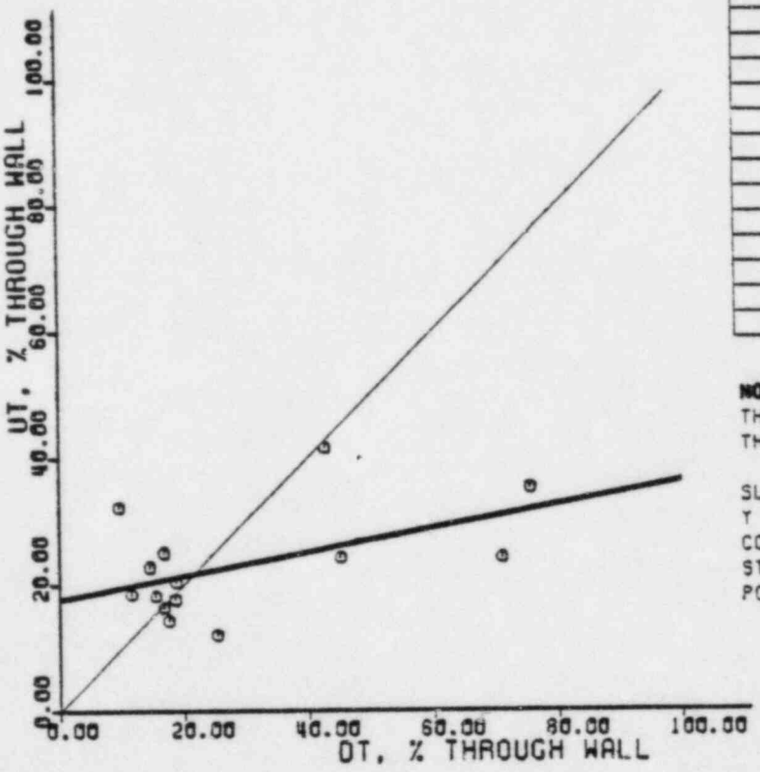

PIPE THK. (IN)	DEPTH (IN)	
	DT	UT
0.785	0.147	0.160
0.812	0.094	0.150
0.620	0.280	0.150
0.620	0.440	0.150
0.820	0.060	0.200
0.565	0.105	0.100
1.050	0.184	0.150
1.253	0.318	0.150
0.780	0.590	0.275
0.780	0.334	0.325
1.100	0.160	0.250
1.100	0.170	0.200
1.100	0.185	0.275
1.100	0.185	0.180

NOTES:
THIN LINE: IDEAL CASE
THICK LINE: LINEAR REGRESSION
Y = AX + B
SLOPE (A) = 0.19
Y INTERCEPT (B) = 17.7
CORRELATION COEFF. = 0.49
STANDARD DEVIATION = 8.4
POPULATION (N) = 14

FIGURE 5-7.

TEAM NO. 8
TRUE VS. MEASURED DEPTH

EPRI NDE CENTER

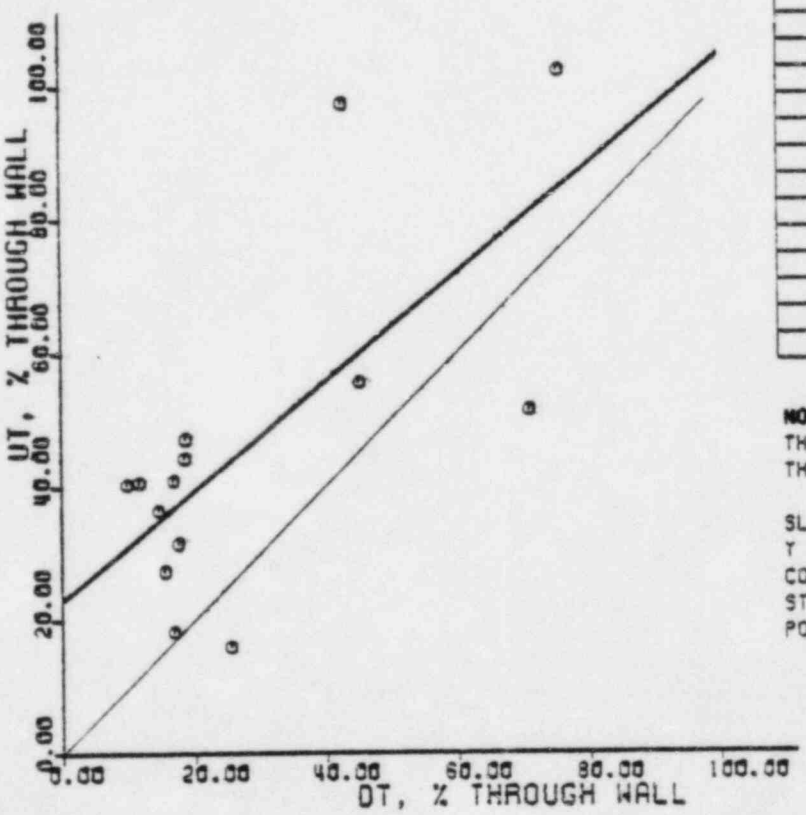

PIPE THK. (IN)	DEPTH (IN)	
	DT	UT
0.785	0.147	0.370
0.812	0.094	0.330
0.620	0.280	0.345
0.620	0.440	0.319
0.620	0.060	0.250
0.565	0.105	0.250
1.050	0.184	0.330
1.253	0.318	0.200
0.780	0.590	0.800
0.760	0.334	0.760
1.100	0.160	0.400
1.100	0.170	0.300
1.100	0.185	0.200
1.100	0.185	0.450

NOTES:
THIN LINE: IDEAL CASE
THICK LINE: LINEAR REGRESSION
$Y = AX + B$
SLOPE (A) = 0.82
Y INTERCEPT (B) = 23.0
CORRELATION COEFF. = 0.70
STANDARD DEVIATION = 25.4
POPULATION (N) = 14

FIGURE 5-8.

TEAM NO. 9
TRUE VS. MEASURED DEPTH

EPRI NDE CENTER

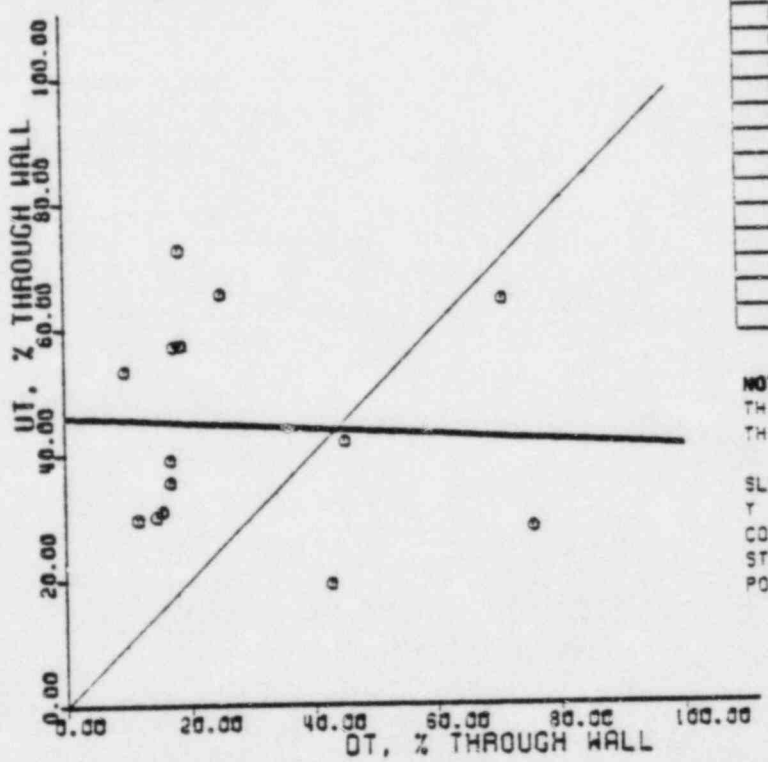

PIPE THK. (IN)	DEPTH (IN)	
	DT	UT
0.785	0.147	0.450
0.812	0.094	0.240
0.820	0.280	0.260
0.820	0.440	0.400
0.820	0.350	0.330
0.885	0.105	0.410
1.050	0.134	0.800
1.253	0.318	0.920
0.790	0.590	0.220
0.780	0.334	0.150
1.100	0.160	0.330
1.100	0.170	0.340
1.100	0.185	0.430
1.100	0.185	0.390

NOTES:
THIN LINE: IDEAL CASE
THICK LINE: LINEAR REGRESSION
$Y = AX + B$
SLOPE (A) = -0.05
Y (INTERCEPT B) = 46.0
CORRELATION COEFF. = -0.06
STANDARD DEVIATION = 16.8
POPULATION (N) = 14

FIGURE 5-9.

TEAM NO. 10
TRUE VS. MEASURED DEPTH

EPRI NDE CENTER

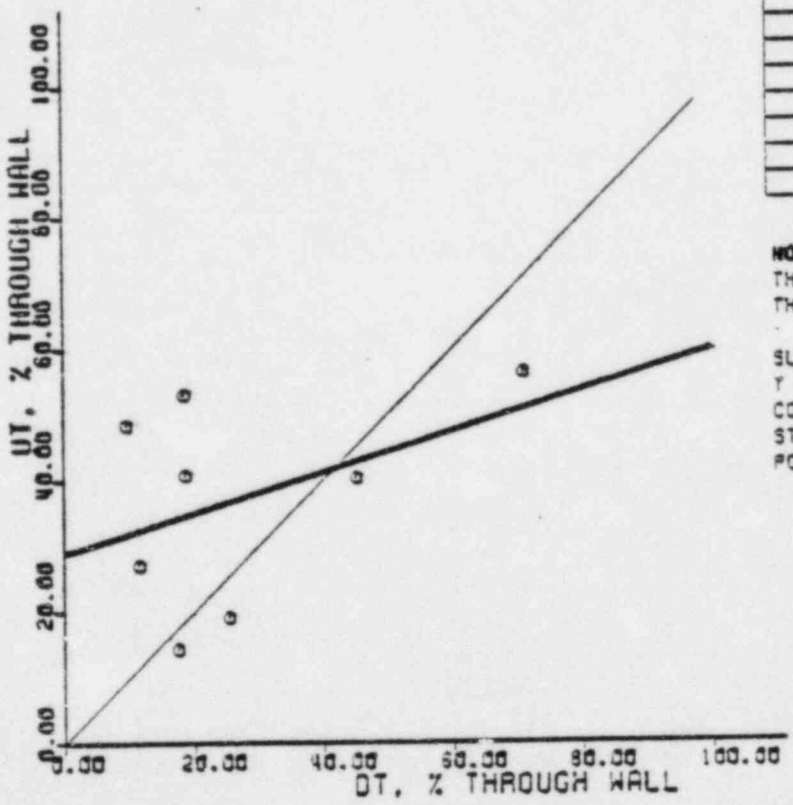

PIPE THK. (IN)	DEPTH (IN)	
	DT	UT
0.785	0.147	0.320
0.812	0.394	0.220
0.620	0.280	0.250
0.620	0.440	0.350
0.620	0.060	0.300
0.585	0.105	0.300
1.050	0.184	0.150
1.253	0.318	0.240

NOTES:
THIN LINE: IDEAL CASE
THICK LINE: LINEAR REGRESSION
$Y = AX + B$
SLOPE (A) = 0.31
Y INTERCEPT (B) = 28.9
CORRELATION COEFF. = 0.41
STANDARD DEVIATION = 15.7
POPULATION (N) = 8

FIGURE 5-10.

TEAM NO. 11
TRUE VS. MEASURED DEPTH

EPRI NDE CENTER

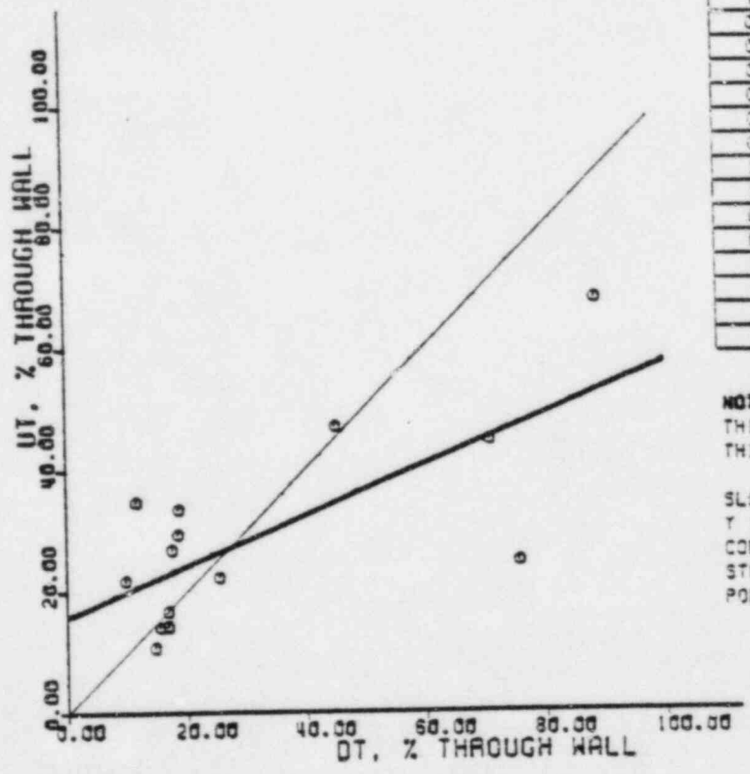

PIPE THK. (IN)	DEPTH (IN)	
	DT	UT
0.785	0.147	0.263
0.812	0.394	0.282
0.620	0.280	0.292
0.620	0.440	0.279
0.620	0.050	0.135
0.585	0.105	0.166
1.050	0.184	0.282
1.253	0.319	0.279
0.780	0.550	0.139
0.780	0.692	0.531
1.100	0.160	0.118
1.100	0.170	0.155
1.100	0.195	0.157
1.100	0.185	0.184

NOTES:
THIN LINE: IDEAL CASE
THICK LINE: LINEAR REGRESSION
$Y = AX + B$
SLOPE (A) = 0.42
Y INTERCEPT (B) = 15.9
CORRELATION COEFF. = 0.71
STANDARD DEVIATION = 15.7
POPULATION (N) = 14

FIGURE 5-11.

TEAM NO. 12
TRUE VS. MEASURED DEPTH

EPRI NDE CENTER

PIPE THK. (IN)	DEPTH (IN)	
	OT	UT
0.565	0.105	0.073
0.780	0.390	0.104
0.780	0.663	0.139
0.780	0.234	0.160
0.780	0.692	0.589

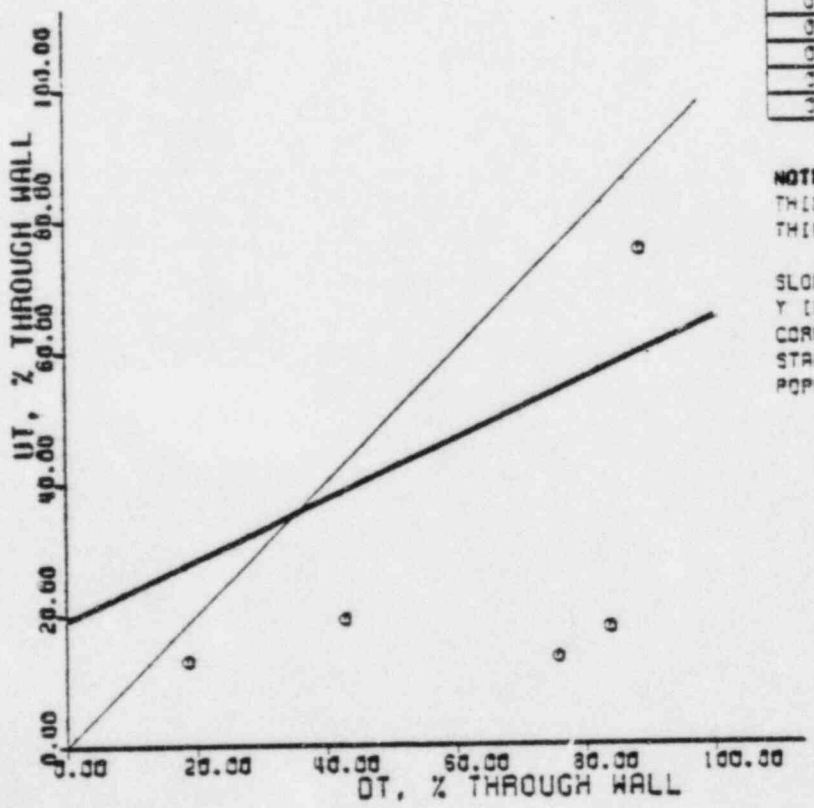

NOTES:
THIN LINE: IDEAL CASE
THICK LINE: LINEAR REGRESSION
Y = AX + B
SLOPE (A) = 0.46
Y INTERCEPT (B) = -0.8
CORRELATION COEFF. = 0.52
STANDARD DEVIATION = 26.8
POPULATION (N) = 5

FIGURE 5-12.

TEAM NO. 13
TRUE VS. MEASURED DEPTH

EPRI NDE CENTER

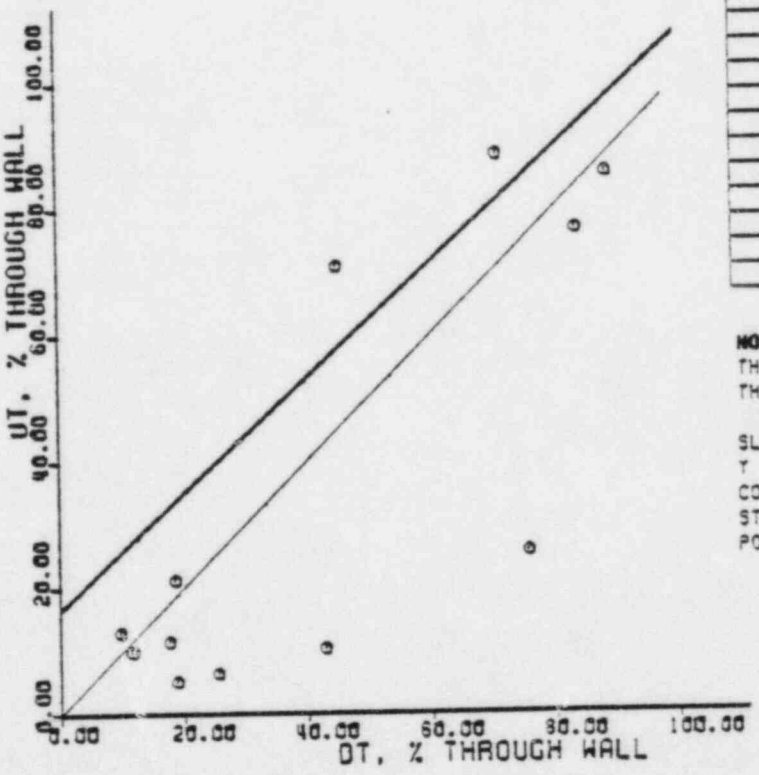

PIPE THK. (IN)	DEPTH (IN)	
	DT	UT
0.785	0.147	0.040
0.812	0.394	0.080
0.620	0.280	0.440
0.820	0.440	0.550
0.820	0.050	0.290
0.565	0.105	0.120
1.050	0.184	0.120
1.253	0.318	0.080
0.780	0.590	0.200
0.780	0.653	0.600
0.780	0.334	0.080
0.780	0.682	0.570

NOTES:
THIN LINE: IDEAL CASE
THICK LINE: LINEAR REGRESSION
Y = AX + B
SLOPE (A) = 0.92
Y INTERCEPT (B) = -3.4
CORRELATION COEFF. = 0.80
STANDARD DEVIATION = 34.1
POPULATION (N) = 12

FIGURE 5-13.

NOTE: This team used three approaches per flaw to generate three estimates, but would not identify a single result on each flaw. This Figure uses an average of the ultrasonic prediction at each flaw depth. Figures 14A, 14B, and 14C present the results individually for each of the approaches.

AVERAGED, TEAMS : 14A,14B,14C
TRUE VS. MEASURED DEPTH

EPRI NDE CENTER

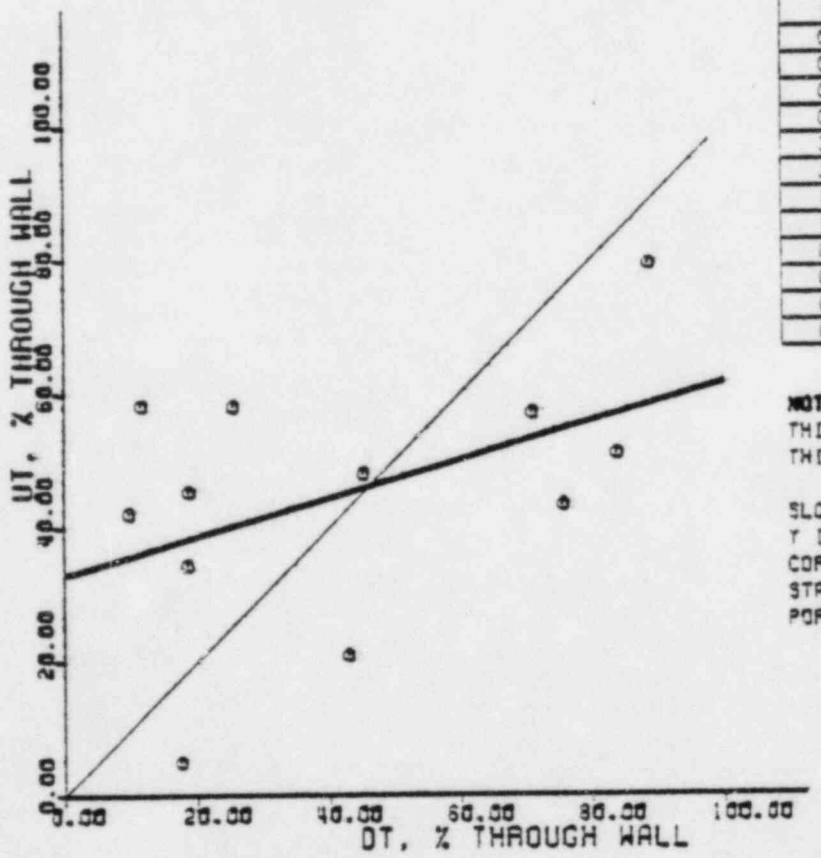

PIPE THK. (IN)	DEPTH (IN)	
	DT	UT
0.785	0.147	0.358
0.812	0.394	0.473
0.820	0.280	0.298
0.820	0.440	0.354
0.820	0.080	0.261
0.865	0.105	0.194
1.050	0.184	0.052
1.253	0.318	0.729
0.780	0.590	0.338
0.780	0.553	0.398
0.780	0.334	0.183
0.780	0.692	0.820

NOTES:
THIN LINE: IDEAL CASE
THICK LINE: LINEAR REGRESSION
Y = AX + B
SLOPE (A) = 0.29
Y INTERCEPT (B) = 33.0
CORRELATION COEFF. = 0.45
STANDARD DEVIATION = 19.2
POPULATION (N) = 12

FIGURE 5-14.

TEAM NO.14A
TRUE VS. MEASURED DEPTH

EPRI NDE CENTER

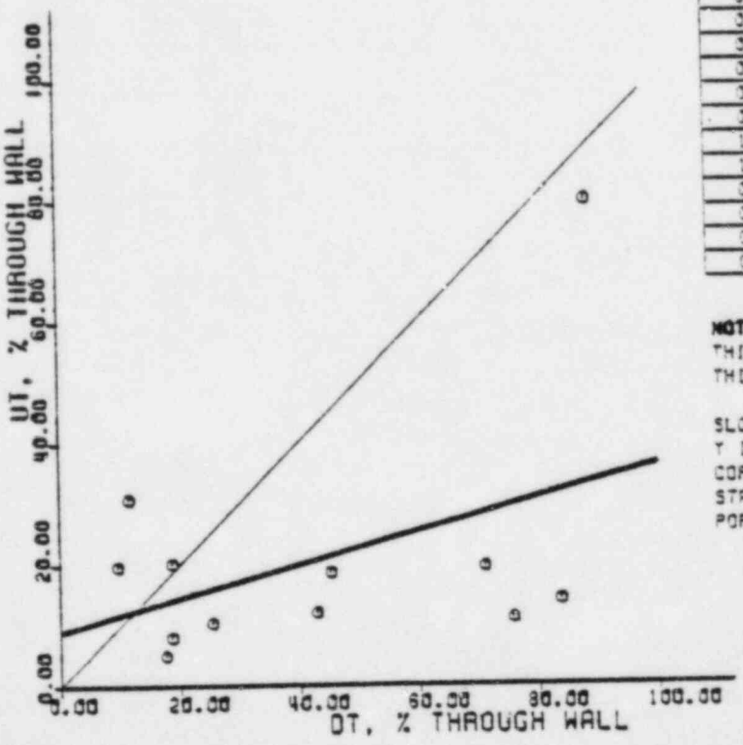

PIPE THK. (IN)	DEPTH (IN)	
	DT	UT
0.785	0.147	0.158
0.812	0.094	0.250
0.820	0.280	0.115
0.827	0.440	0.121
0.820	0.060	0.122
0.585	0.105	0.045
1.050	0.184	0.052
1.253	0.319	0.129
0.780	0.580	0.095
0.790	0.563	0.109
0.780	0.334	0.093
0.780	0.692	0.624

NOTES:
THIN LINE: IDEAL CASE
THICK LINE: LINEAR REGRESSION
Y = AX + B
SLOPE(A) = 0.28
Y INTERCEPT(B) = 9.1
CORRELATION COEFF. = 0.41
STANDARD DEVIATION = 19.9
POPULATION(N) = 12

FIGURE 5-14A.

TEAM NO.14B
TRUE VS. MEASURED DEPTH

EPRI NDE CENTER

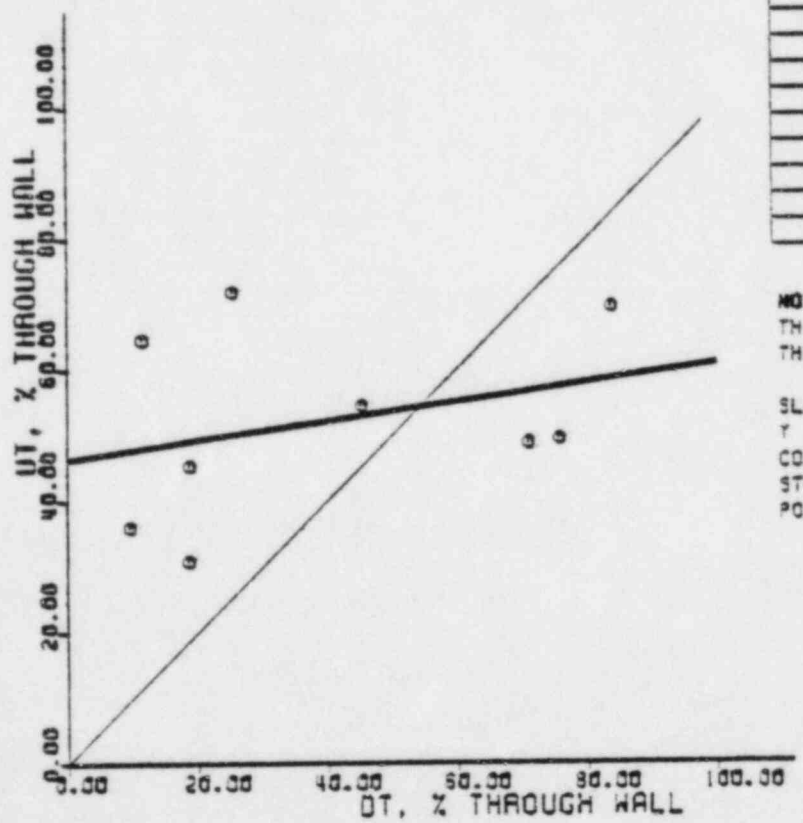

PIPE THK. (IN)	DEPTH (IN)	
	DT	UT
0.785	0.147	0.358
0.812	0.094	0.524
0.820	0.280	0.338
0.820	0.440	0.303
0.820	0.080	0.223
0.585	0.105	0.174
1.253	0.318	0.900
0.790	0.590	0.386
0.780	0.593	0.343

NOTES:
THIN LINE: IDEAL CASE
THICK LINE: LINEAR REGRESSION
Y = AX + B
SLOPE (A) = 0.15
Y INTERCEPT (B) = 46.5
CORRELATION COEFF. = 0.30
STANDARD DEVIATION = 14.3
POPULATION (N) = 9

FIGURE 5-148

TEAM NO.14C
TRUE VS. MEASURED DEPTH

EPRI NDE CENTER

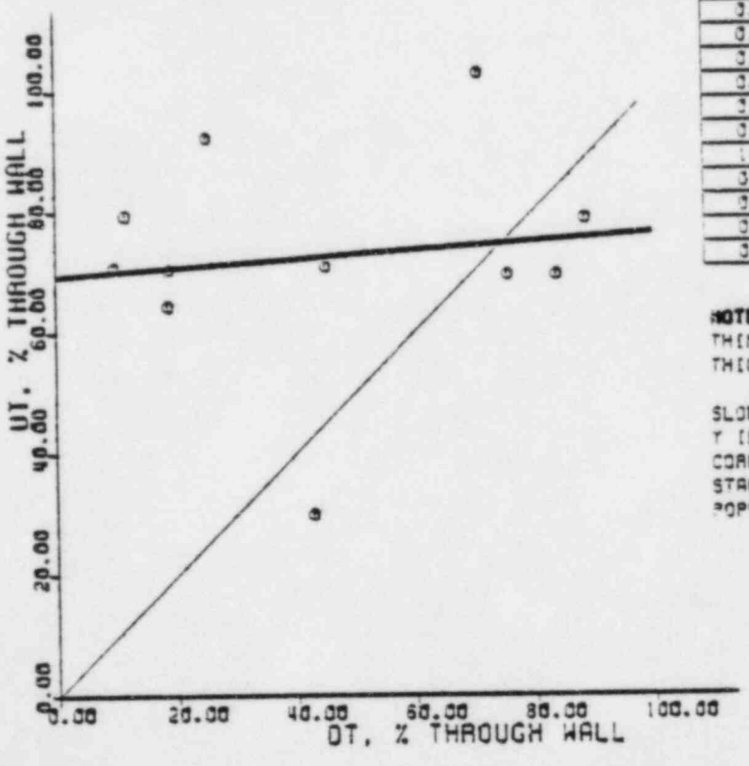

PIPE THK. (IN)	DEPTH (IN)	
	DT	UT
0.785	0.147	0.583
0.812	0.394	0.645
0.820	0.280	0.440
0.820	0.440	0.639
0.820	0.260	0.439
0.585	0.105	0.384
1.253	0.319	1.157
0.780	0.380	0.543
0.780	0.653	0.543
0.780	0.334	0.283
0.780	0.692	0.616

NOTES:
THIN LINE: IDEAL CASE
THICK LINE: LINEAR REGRESSION
Y = AX + B
SLOPE (A) = 0.37
Y INTERCEPT (B) = 59.4
CORRELATION COEFF. = 0.12
STANDARD DEVIATION = 18.2
POPULATION (N) = 11

FIGURE 5-14C

TEAM NO. 16
TRUE VS. MEASURED DEPTH

EPRI NDE CENTER

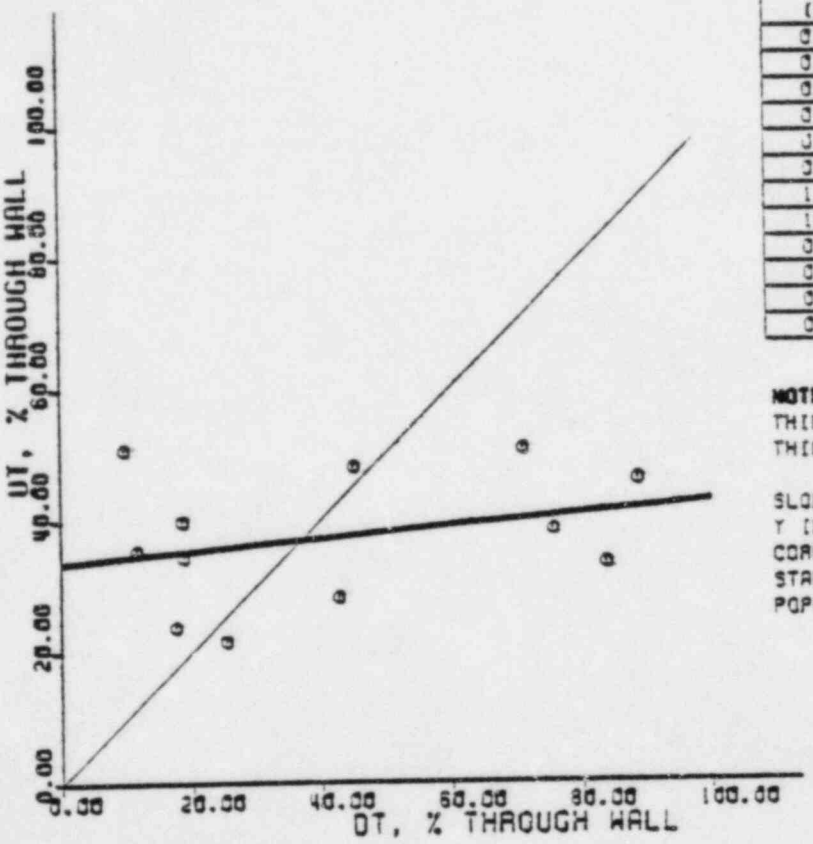

PIPE THK. (IN)	DEPTH (IN)	
	DT	UT
0.785	0.147	0.270
0.812	0.094	0.287
0.620	0.280	0.298
0.620	0.440	0.315
0.620	0.360	0.315
0.565	0.105	0.225
1.050	0.184	0.250
1.253	0.318	0.270
0.780	0.390	0.300
0.780	0.353	0.260
0.780	0.334	0.220
0.780	0.592	0.360

NOTES:
THIN LINE: IDEAL CASE
THICK LINE: LINEAR REGRESSION
Y = AX + B
SLOPE (A) = 0.09
Y INTERCEPT (B) = 33.6
CORRELATION COEFF. = 0.28
STANDARD DEVIATION = 10.3
POPULATION (N) = 12

FIGURE 5-15.

VI. ADVANCED RESULTS

As mentioned in Section IV data was recorded on magnetic cassettes to provide a complete permanent record for later analysis. Because the data acquisition effort was the last sequential item of round robin work little time was left to attempt computer processing. However, General Research Corp. (Adaptronics) agreed to make an attempt at crack sizing based on similar work done for EPRI on BWR feedwater nozzle studies (7). The approach consisted of identifying the signal from the crack-ID surface intersection, the signal caused by the crack tip diffraction effect, measuring the time difference and calculating crack depth. A typical record that was used is shown in Figure 6-1. The actual process was complicated by the fact that the person analyzing the data had no previous experience with IGSCC, was denied information available to the manual inspector such as pipe wall thickness, ID contour, contour of weld crown; etc. In spite of these obstacles the contractor was able to take the data for nine flaws received on July 12, analyze it and provide his final estimates on July 30. This result is displayed on Figure 6-2. The same presentation format and analysis parameters are provided that were presented for the conventional results. The results are quite good by themselves. There is good reason to believe they could be improved by providing greater interaction between the analyst and the data acquisition team.

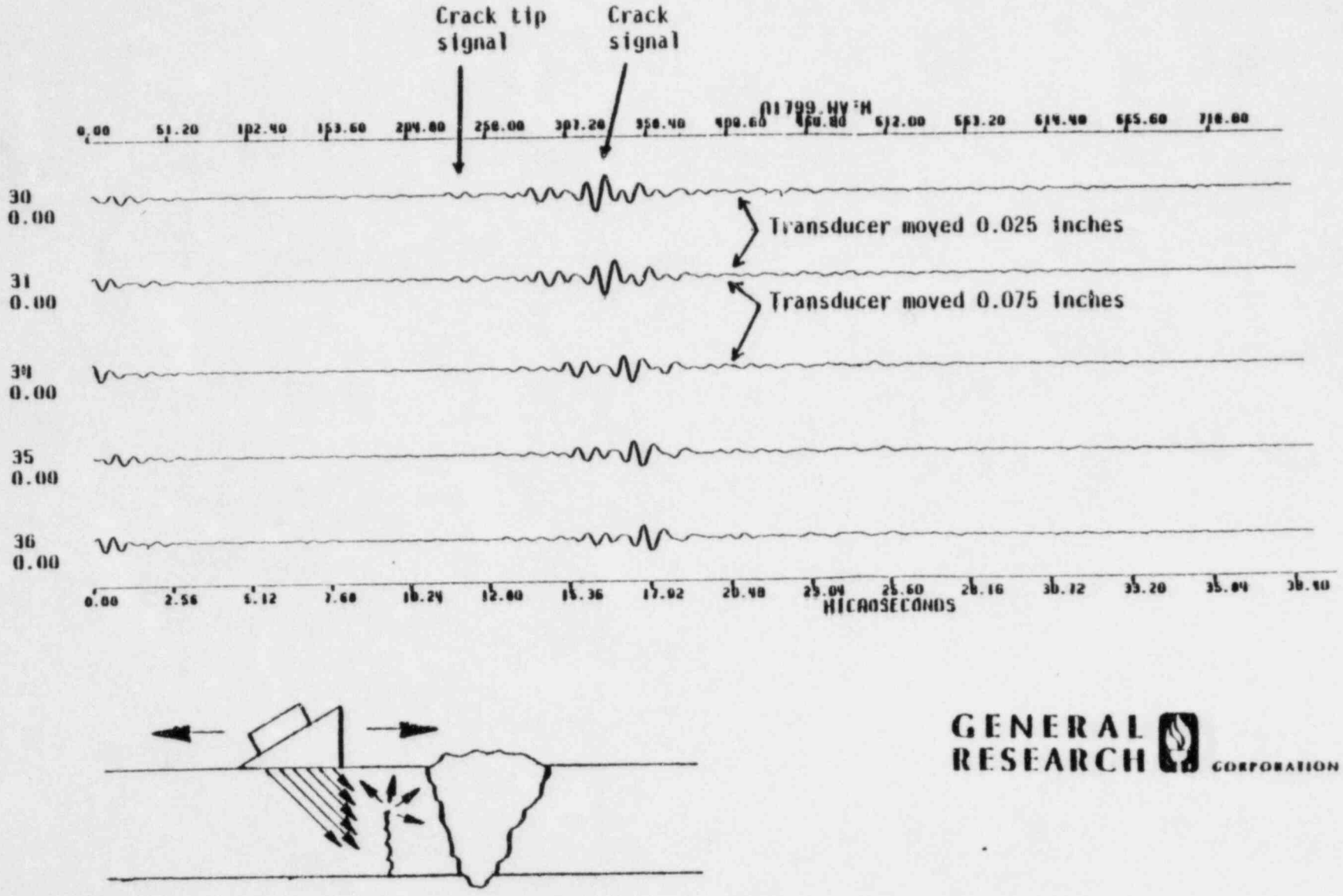

GENERAL RESEARCH CORPORATION

Figure 6-1. Data Record For Advanced Method Crack Tip Diffraction Sizing Approach

TEAM NO. 17
TRUE VS. MEASURED DEPTH

EPRI NDE CENTER

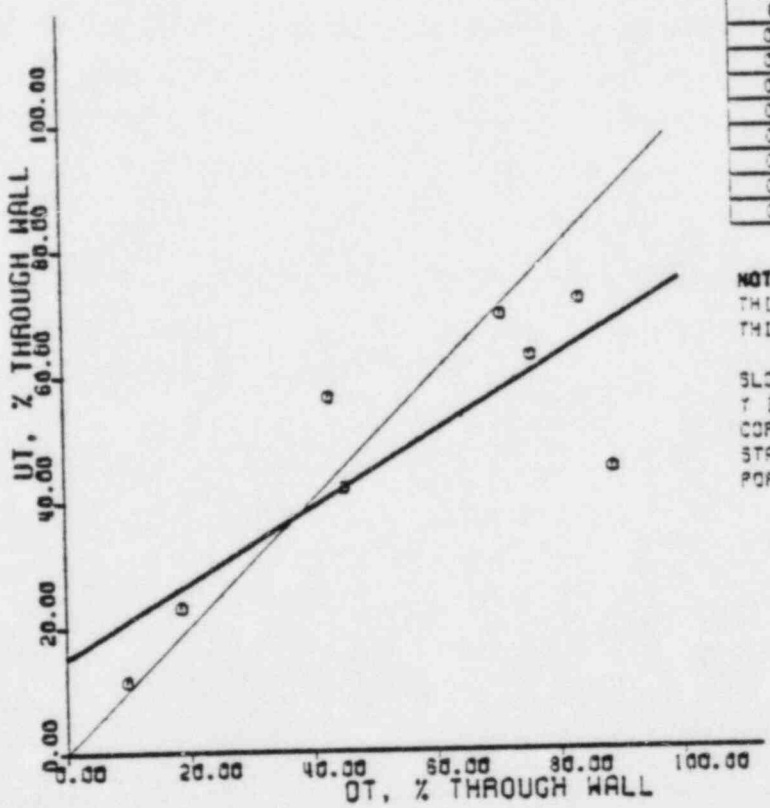

PIPE THK. (IN)	DEPTH (IN)	
	OT	UT
0.820	0.280	0.260
0.820	0.440	0.430
0.820	0.080	0.070
0.585	0.105	0.130
0.780	0.590	0.490
0.780	0.652	0.560
0.780	0.334	0.440
0.780	0.692	0.760

NOTES:
THIN LINE: IDEAL CASE
THICK LINE: LINEAR REGRESSION
Y = AX + B
SLOPE (A) = 0.80
Y INTERCEPT (B) = 15.1
CORRELATION COEFF. = 0.82
STANDARD DEVIATION = 21.8
POPULATION (N) = 8

FIGURE 6-2.

The second advanced approach used a special transducer called the Axicon (8 and 9). This transducer has a lens assembly that focuses the ultrasonic beam into a small diameter, well collimated beam several inches in length. It is analogous to an optical telephoto lens with the depth of field of a wide angle lens. One of the EPRI contractors (Amdata) was evaluating a transducer of this type for a different use. When this was discovered they were asked to size some IGSCC samples as a laboratory test. The results were so encouraging that the contractor was asked to examine as many of the round robin samples as possible in the 1½ days prior to their shipment for destructive evaluation. Five samples were evaluated with the transducer mounted on the AMAPS scanner. The data was generated by driving the scanner in the axial direction under manual control while noting the difference in the arrival time of the crack-corner reflection and the crack tip diffraction signals. This time difference was then used to calculate crack depth. Again the process was much more difficult than described because of the lack of experience with this type transducer on IGSCC. However, the results displayed in Figure 6-3 are very encouraging and strongly suggest greater consideration of this approach. The presentation format of Figure 6-3 is the same as for Figure 6-2.

In summary, the advanced methods performed very well producing very creditable results. Furthermore all of the major electronic and mechanical hardware is already developed as well as most of the software. Thus, field deployment can occur in the near term (months as opposed to years).

TEAM NO. 15
TRUE VS. MEASURED DEPTH

EPRI NDE CENTER

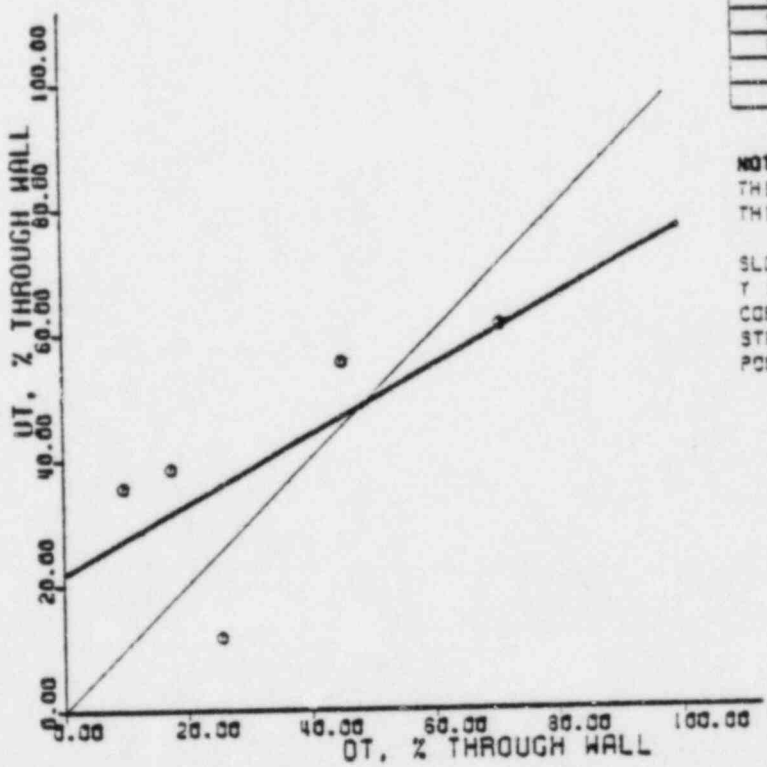

PIPE THK. (IN)	DEPTH (IN)	
	OT	UT
0.620	0.280	0.344
0.620	0.440	0.380
0.620	0.260	0.220
1.050	0.184	0.404
1.253	0.319	0.146

NOTES:
THIN LINE: IDEAL CASE
THICK LINE: LINEAR REGRESSION
Y = AX + B
SLOPE (A) = 0.55
Y INTERCEPT (B) = 21.9
CORRELATION COEFF = 0.70
STANDARD DEVIATION = 19.5
POPULATION (N) = 5

FIGURE 6-3.

VII. TRAINING PROGRAMS

It was necessary for the NDE Center to provide additional training to some inspection groups in order to meet the requirements of IE Bulletin 82-03 (3). This was accomplished on a short notice Ad Hoc basis. Later the NDE Center built on this experience to develop appropriate training courses. A course for UT operators in the detection and characterization of IGSCC has already been offered once and is scheduled on approximately an every other week basis for the next fourteen weeks. A course in sizing of IGSCC is being organized for the earliest possible availability with a target date of September 6, 1983.

With the advent of IE 82-03 and 83-02, the NDEC developed a 40-hour course to train and qualify UT operators in the detection and characterization of IGSCC in BWR's. The course content was established by an industry advisory group and members of the center staff and was subsequently authored by individuals with recognized skills in specific areas of IGSCC examination. This course is characterized by large amounts of hands-on work on realistic cracked samples plus a series of examinations containing a practical examination which utilizes Nine Mile Point samples. This examination is very similar to the IE 83-02 qualification test. A significant difference between the course practical examination and the IE 83-02 exercise is that the course requires an individual verification of skills rather than a group verification.

The first IGSCC course was conducted on June 27-July 1, 1983. It was attended by 19 individuals representing utilities, ISI vendors, and the NRC. Attendees gave the training program a very high rating and a later analysis of competency testing showed the results to correlate well with the guidelines in IE 83-02. In addition to the practical examination, each participant had to pass written General and Specific examination with a score of 80% or better. These assure that the stu-

dents have the required knowledge of the inspection method and the characteristics of the specific application. Additional detection and characterization courses now scheduled are shown below:

- o August 8-12
- o August 15-19
- o August 29-September 2
- o September 12-16
- o September 26-30
- o October 10-14
- o October 17-21

As the UT detection and characterization performance has been measured sequentially in IE 82-03, IE 83-02, and in the first NDE Center course, a steady improvement has been demonstrated. This is illustrated in Figure 7-1. The vertical axis of the figure is sensitivity, which refers to the percentage of 1 inch long cracked "cells" correctly identified as cracked by the participant. The horizontal axis of the figure is false alarm rate, which refers to the percentage of 1 inch long uncracked "cells" mistakenly called cracked by the participant. Perfect performance would be 100% sensitivity with a 0% false call rate. It is, of course, unrealistic to expect such a level of performance. The two curves represent averages of all the team performances during IE 82-03 and during IE 83-02 and the first NDE Center training course practical examination. Performance numbers have been essentially identical during these last two activities. Note the improvement with passing time and increased relevant experience.

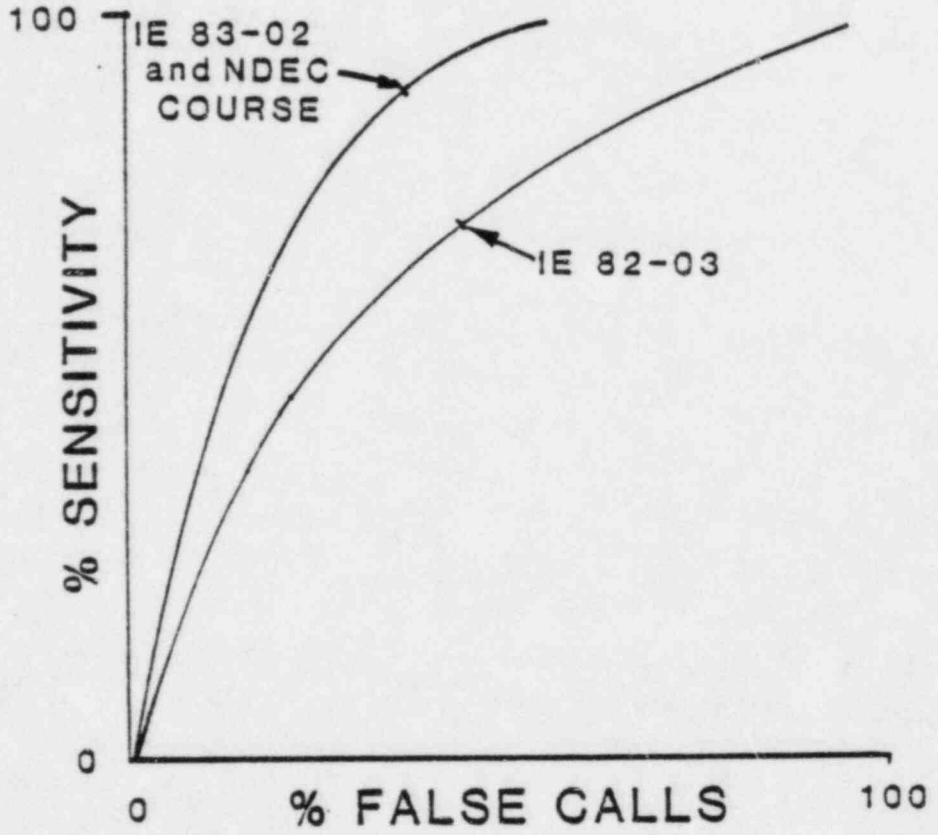

Figure 7-1. Progression Of Detection And Characterization Performance

The results of the IGSCC sizing round robin show that there is a need to offer additional training in specific sizing techniques. This course will be separate from the detection and characterization course and will be of 2-3 day duration. The format, however, will be similar to the 40 hour course. It is being generated through involvement of personnel who are skilled in the theoretical understanding of the physics of the sizing process as well as individuals who demonstrated practical capability to size defects with ultrasonic methods.

The target for the first offering is September with alternate week presentations thereafter. A class size of 12 to 16 participants is planned.

As a general approach to training, the NDE Center provides individual students with a transcript of test scores and training hours (CEU's) for all training that utilizes materials developed under the guidance of EPRI. For example, the Center has a complete Visual Examination (VE) Program to train Level I-III NDE personnel in accordance with ASME Section XI. The General, Specific and Practical examinations given by the Center at the conclusion of a VE training course are typically used by the utility to certify their NDE personnel. Of course, before the certification is issued, each utility would need to verify actual NDE experience and any other specific plant requirements. This same approach is possible with the specialized IGSCC courses.

VIII. QUALIFICATION PROGRAM FOR IGSCC SIZING

The previous section discussed the sequential improvement in detection performance which has occurred under IEB 82-03, IEB 83-02, and the recently completed IGSCC detection training course at the NDEC. It is expected that a similar improvement in ultrasonic sizing capability can be achieved with the development and implementation of the IGSCC sizing course discussed previously.

It would also be advisable to verify the level of performance of those performing IGSCC sizing. The significant results achieved under IEB 82-03 and IEB 83-02 and the practical examination portion of the IGSCC detection course provides a good model to follow for a qualification process.

It is recommended that a similar set of minimum performance standards be established for IGSCC depth sizing and a qualificaion program be established. It would be required that all people performing sizing operations on IGSCC satisfactorily complete the qualification procedure. It is planned that a practical final examination which will serve as the qualification procedure for the IGSCC sizing will constitute a part of the subject training course.

The following items will be considered during development of qualification criteria, accuracy of depth measurement, allowable precision bands, number of flaws, range of depths, type of reflector, i.e. IGSCC and EDM slots, time to make the measurements, etc.

The establishment of suitable samples must be given considerable attention as it is not possible to do a destructive evaluation for each qualification procedure. Rather, it will be necessary to establish flaw depths of IGSCC by nondestructive

means prior to the qualification. Perhaps this could be done by some of the newer approaches such as X-ray tomography, neutron radiography, high resolution ultrasonic methods (e.g. Axicon, imaging, etc.). In addition the data from the round robin for electro-discharge machined (EDM) slots strongly suggest that use of some of these reflectors properly placed in the heated affected zone can be useful for a sizing qualification effort. This is particularly attractive as depth measurement can be precise and the process is economical.

It is expected that the qualification program would be conducted in a manner analogous to IEB 83-02, i.e., the industry would provide the samples, facilities and necessary logistic support, while NRC representatives would proctor the qualification demonstration.

IX. MAN-REM CONSIDERATION

The available pool of skilled inspection personnel is relatively small. The heavy inspection schedule throughout 1983 means that many of these people are rapidly approaching their annual radiation exposure limits. In addition, other required inservice inspections on both PWR and BWR plants draw from this same body of people. As a consequence, the possibility of having several plants down and undergoing simultaneous inspections deserves careful review from the perspective of radiation exposure to skilled personnel.

One way of analyzing this is as follows. In recognition of the potential shortage of trained and qualified people, the EPRI NDE Center has increased the rate of offering its IGSCC detection course. It is now scheduled to be held seven times between August 8 and November 1, 1983. Each class contains 18 students, thus during this time 18 x 7 = 126 people will receive training. If a 70% passing rate is achieved, 90 people will be qualified in this period. Furthermore, assume each has a low enough accumulation to date to allow receiving an additional 1.5 REM by December 31, 1983 for a total of 135 MAN-REM available during this time. One BWR owner now undergoing the inspection and repair process has reported accumulation of 55 REM during the initial inspection process and estimates another 25 REM will be received before inspection of the repairs are completed. This is a total radiation dosage accumulation of 80 REM for inspection personnel only. Thus, the additional people from the training program can accommodate the equivalent of two plant inspection and repair processes in which dosages are this high.

Considering the radiation dosage for nine plants for which estimates have been obtained, a total dosage of approximately 400 MAN-REM have been accumulated during the inspection (before and after repair) of about 640 welds. Thus approximately 0.6 MAN-REM per weld are being accumulated on an average number of about 70 welds

examined per plant. Using these average numbers the additional people from the training programs could examine three plants with average radiation conditions.

X. POSSIBLE DEPLOYMENT OF ADVANCED HARDWARE

As discussed in the earlier section on the Round Robin process, the integrated EPRI-BWROG R&D effort has produced the necessary hardware and much of the software needed to automate the IGSCC inspection process. The system is now undergoing evaluation in the data acquisition mode to permit an appraisal of all the electronic and mechanical functions of the system independent of the automatic decision software, which is in the final development stage. The current status of the system is that it successfully completed one field test in a nuclear power plant in early June 1983 and was subsequently used to record magnetic tape records of UT signal and position information for all samples used in the Round Robin. All this operation was in the data acquisition mode. This latter exercise provided over 200 hours of successful operating experience with the system. The ability to record this data on magnetic tape cassettes and transfer these records to computers remote from the site has been demonstrated. Furthermore, an evaluation of the ability to use this permanently recorded, very detailed data for independent or third party computer analysis to determine flaw size is underway. The data presented as Team 17 was in fact generated in this manner. In addition, three other contractors are using the same data to analyze different computer evaluation processes. One effort is pursuing refinement of the technique used by Team 17 while the other two are exploring different analysis methods.

The above discussion illustrated the use of the data acquisition system for recording data for off-line analysis to produce sizing information. The same system can also be used to acquire data from the plant for off-line analysis for detection and discrimination as well.

All elements of the above system for acquiring field data and performing off-line analysis are available. A schematic representation of how this operation could be

conducted is shown in Figure 10-1. The overall system has not yet been exercised to the extent needed to establish overall system performance, reliability, and an optimized mode of operation. However, results to date are very encouraging, encouraging to the point that plans are being developed to provide the EPRI owned equipment to those utilities willing to use it. These arrangements will be implemented by the J.A. Jones Applied Research Company on a cost recovery basis.

At the present time, it is believed that the previously fielded system can be refitted and be ready for deployment between August 15 and September 1. An identical system will be configured as soon as possible after September 1.

In addition, two other systems are being acquired for integration at the NDEC to perform automated detection, discrimination and recording of results as a function of position. These systems would provide immediate results at the inspection site. Components of the system included the AMAPS scanner with ALN 4033 controller, Mark III transducer, and the ALN 4060 flaw discriminator. All of these components are commercially available today and their performance evaluated in different ways. The next step is integration of the components into a complete system, evaluate its performance and then put it through a qualification exercise. This will be done as rapidly as resources permit.

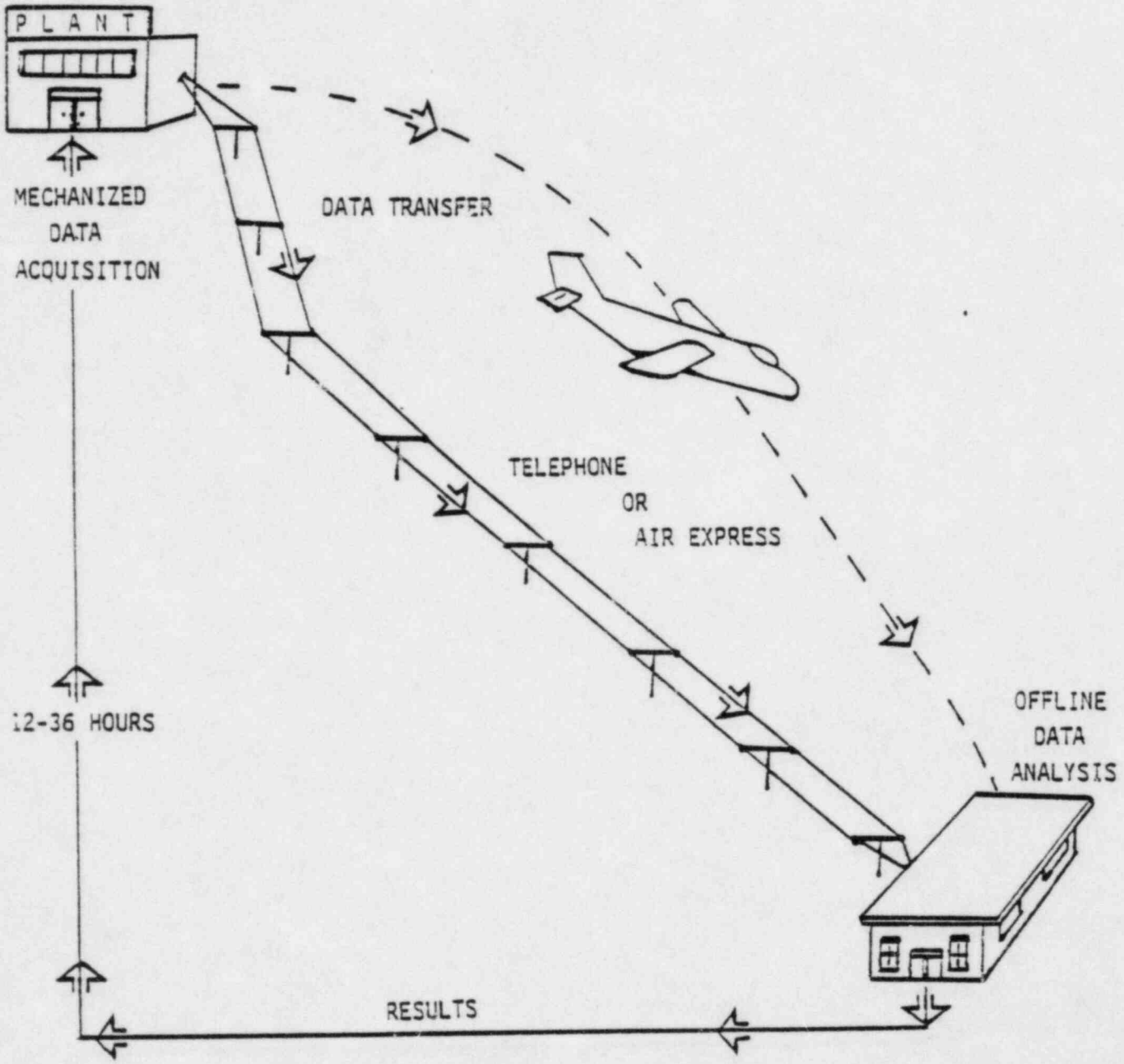

Figure 10-1. Possible Mode Of Field Deployment
Of Automated Hardware.

XI. REFERENCES

1. G.J. Dau "Codes and Standards for Inservice Inspection of Nuclear Power Plants" pp. 38-52 of NONDESTRUCTIVE TESTING STANDARDS - A REVIEW edited by Harold Berger, ASTM Special Technical Publication 624, American Society for Testing and Materials, Philadelphia, PA 19103

2. C.Y. Cheng, et. al. "Technical Report on Material Selection and Processing Guidelines for BWR Coolant Pressure Boundary Piping," NUREG-0313, Rev. 1. US Nuclear Regulatory Commission, Washington, DC. July 1980.

3. IE Bulletin No. 82-03, "Stress Corrosion Cracking in Thick-Wall, Large-Diameter, Stainless Steel, Recirculation System Piping at BWR Plants," US Nuclear Regulatory Commission, Office of Inspection and Enforcement, Washington, DC. October 14, 1982.

4. IE Bulletin No. 83-02, "Stress Corrosion Cracking in Large-Diameter Stainless Steel Recirculation System Piping at BWR Plants", US Nuclear Regulatory Commission, Office of Inspection and Enforcement, Washington, DC. March 4, 1983.

5. G.J. Dau, et. al. "Nondestructive Evaluation Program: Progress in 1982," EPRI NP-2728-SR, Electric Power Research Institute, Palo Alto, CA. February 1983.

6. G.J. Dau, et. al. "Nondestructive Evaluation Program: Progress in 1981," EPRI NP-2088-SR, Electric Power Research Institute, Palo Alto, CA. January 1982.

7. A.N. Mucciardi, et. al. "Signal Processing for ISI," EPRI NP1421, Electric Power Research Institute, Palo Alto, CA. May 1980.

8. R.V. Murphy "Toroidial, Conical, Spherical Lenses In Ultrasonic Inspection," Vol. 39, No. 4, pp. 391-395, Materials Evaluation, March 1981.

9. S. Nagai and K. Iizuka "A Practical Ultrasound Axicon For Nondestructive Testing," pp. 265-270, Ultrasonics, November 1982.

APPENDIX A

UT DATA FOR FLAWS

Appendix A

ULTRASONICS SIZING DATA

All manual teams participating in the round robin were requested to use their own equipment and procedures and report their results on the forms that were provided (see Figure A-1). In particular all teams were requested to use more than one set of equipment/procedure on each flaw to provide themselves the opportunity to check the applicability and accuracy of their different techniques on a given flaw once the destructive results became available. Where multiple depth estimates were made on a particular crack, the team was requested to select and identify their best estimate for reporting. Team 3 produced multiple results on a number of flaws without selecting their best estimates and indicated that when forced to make a choice they would take the conservative approach and report the deepest estimate. Team 14 produced multiple estimates on majority of the flaws and elected not to make any choices.

The following pages are tabulations of teams data for each flaw. Where a particular team does not show an estimate for a given flaw, it indicates that the team did not examine that particular flaw. Where no details of UT sizing beyond the depth estimate are given, it indicates that either the technique was among the advanced techniques or the team used a combination of frequencies, angles, etc. to arrive at their final estimates. Each of the manual teams have copies of their original raw data in the same format as they submitted to the NDE Center at the conclusion of their participation in the round robin.

ROUND ROBIN ON UT SIZING OF IGSCC
EPRI NDE Center
Charlotte, NC

Crack No. _____

Inspector/Level _____
ISI Company _____
Utility _____

Date _____

UT Instrument, Make & Model _____

Transducer: Single ( ) Dual ( )

Make & Model _____
Size _____
Frequency _____
Band width, if known _____
Angle _____°
Mode: shear ( ), longitudinal ( )

Method of Sizing:

( ) Amplitude drop, at _____% of Peak ( ), DAC ( )
( ) Crack tip diffraction
( ) Others, describe briefly
_____
_____

Measurements from: Near Side ( ), Far Side ( )
Sound Path: 1/2V ( ), 3/2V ( ), other _____
Beam Spread: Accounted for ( ), Not accounted for ( )

Measured crack depth: _____ inch

FIGURE A-1. EXAMPLE OF DATA FORM USED IN ROUND ROBIN

Wall thickness at C. Bore 0.785"

FLAW	PROBE SIDE	FLAW SIDE	FLAW SIDE	PROBE SIDE
1	X	X	☐	☐

No.

19%

FLAW DEPTH 0.147 inch

TEAM	UT DEPTH INCH	SIZING METHOD: AMPLITUDE TIP	AMPLITUDE % PEAK	AMPLITUDE % DAC	OTHER	TRANSDUCER: θ°	f, MHz	MODE S	MODE L	TYPE S	TYPE D	SIZE	MAKE	SOUND PATH ½V	SOUND PATH ¾V	OTHER	BEAM SPREAD ACCOUNTED? YES	BEAM SPREAD ACCOUNTED? NO	UT INSTRUMENT
1	0.160		10			43	2¼	✓		✓		¼"	AERO	✓			✓		USL 38
2	0.055		10			56	4	✓		✓		9x10mm	KRAUT	✓			✓		USL 38
3	0.203	✓				56	2¼	✓		✓		0.5	AERO	✓			✓		NORTEC
4	0.30		20			60	1.5	✓		✓		0.5	AERO	✓				✓	USL 38
5	0.43	✓				60	1.5	✓		✓		0.5	AERO	✓				✓	USL 38
6	0.150		50			43	1.5	✓			✓	¾x¾	AERO	✓			✓		USL 38
7	0.160		50			45 60	2¼	✓	✓	✓		0.5	AERO	✓				✓	NORTEC
8	0.370		10		✓	60	1.5	✓		✓		0.5	AERO	✓				✓	USL 38
9	0.45	✓				52	3.3	✓		✓		¾	NOT CI NOVA	✓				✓	USIP 11
10	0.32		50			45	2¼	✓		✓		0.5	AERO	✓					USK 6
11	0.263		50			60	2¼	✓		✓		¼	AERO	✓			✓		USL 38
13	0.04																		
14	0.158 0.356 0.553		50			45 60 70	1.5 2¼	✓		✓		¾x¾ 0.5	AERO	✓				✓	USL 38
16	0.270		5			45	2¼	✓		✓		0.5	AERO					✓	USL 38

· Wall thickness at C. Bore 0.812"

11%

FLAW NO.	PROBE SIDE	FLAW SIDE		FLAW SIDE	PROBE SIDE
2	X	X			

FLAW DEPTH 0.094 inch

TEAM	UT DEPTH INCH	SIZING METHOD: AMPLITUDE TIP	AMPLITUDE % PEAK	AMPLITUDE % DAC	OTHER	TRANSDUCER: θ°	f. MHz	MODE S	MODE L	TYPE S	TYPE D	SIZE	MAKE	SOUND PATH ½V	SOUND PATH ¾V	SOUND PATH OTHER	BEAM SPREAD ACCOUNTED? YES	BEAM SPREAD ACCOUNTED? NO	UT INSTRUMENT
1	.060		10			43	2¼	✓		✓		¼"	AERO	✓			✓		USL 38
2	0.025				✓	45	4	✓		✓		9X10 mm	KRAUT		✓		✓		USL 38
3	0.234	✓				56	2¼	✓		✓		0.5	AERO	✓			✓		NORTEC
4	0.25		20			60	1.5	✓		✓		0.5	AERO	✓				✓	USL 38
5	0.16	✓				60	1.5	✓		✓		0.5	AERO	✓				✓	USL 38
6	0.150		50			43	1.5	✓			✓	¾x¾	AERO	✓			✓		USL 38
7	0.150		50			45 60	2¼	✓	✓	✓		0.5	AERO	✓				✓	NORTEC
8	0.330		10		✓	60	1.5	✓		✓		0.5	AERO	✓			✓		USL 38
9	0.24	✓				52	3.5	✓		✓		⅜	NDTCI NOVA	✓				✓	USIP 11
10	0.22		50			45	2¼	✓		✓		0.5	AERO	✓					USK 6
11	0.282		50			60	2¼	✓		✓		¼	AERO	✓			✓		USL 38
13	0.08																		
14	0.250 0.5 0.284		50			45 60 70	1.5 2¼	✓		✓		¾x¾ 0.5	AERO	✓				✓	USL 38
16	0.287		5			45	2¼	✓		✓		0.5	AERO	✓				✓	USL 38

Wall thickness at C-Bore 0.620"

45%

FLAW NO.	PROBE SIDE	FLAW SIDE	FLAW SIDE	PROBE SIDE
3	X	X		

FLAW DEPTH 0-28 inch

ITEM	UT DEPTH IN.	SIZING METHOD: AMPLITUDE TIP	AMPLITUDE % PEAK	AMPLITUDE % DAC	OTHER	TRANSDUCER: ∠, MM's	MODE S	MODE L	TYPE S	TYPE D	SIZE	MAKE	SOUND PATH ½ V	SOUND PATH ¾ V	SOUND PATH OTHER	BEAM SPREAD ACCOUNTED FOR: YES	BEAM SPREAD ACCOUNTED FOR: NO	UT INSTRUMENT
1	0-120		10			43 2¼	✓		✓		¼"	AERO	✓			✓		USL 38
2	0-130		10			45 4	✓		✓		9x10 mi	KRAUT	✓	✓		✓		USL 38
3	0-298		25			56 2¼	✓				0.5	AERO	✓			✓		NORTEC
4	0-30		20			60 1-5	✓		✓		0.5	AERO	✓				✓	USL 38
5	0-18	✓				60 1-5	✓		✓		0.5	AERO	✓				✓	USL 38
6	0-115		50			43 1-5	✓			✓	⅔x¾	AERO	✓			✓		USL 38
7	0-150		50			45 60 2¼	✓	✓	✓		0.5	AERO	✓				✓	NORTEC
8	0-345		10		✓	60 1-5	✓		✓		0.5	AERO	✓			✓		USL 38
9	0-26	✓				52 3-3	✓		✓		⅔	NOT CI NOVA	✓				✓	USIP 11
10	0-25		50			45 2¼	✓		✓		0.5	AERO	✓					USK 6
11	0-292			25		45 2¼	✓			✓	.5x.5	H'SONIC		✓		✓		USL 38
13	0-44																	
14	0-115 0-338 0-440		50			45 60 70 1-5 2-25	✓		✓	✓	¾x¾ 0.5	AERO	✓				✓	USL 38
15	0-344																	
16	0-298		5			45 2¼	✓		✓		0.5	AERO	✓				✓	USL 38
17	0-26																	

Wall thickness at C. Bore 0.620"

FLAW NO.	PROBE SIDE	FLAW SIDE	FLAW SIDE	PROBE SIDE
4	X	X		

71%

FLAW DEPTH 0.44 inch

ITEM	UT DEPTH INCH	SIZING METHOD: CRACK TIP	AMPLITUDE: % PEAK	AMPLITUDE: % DAC	SIZING METHOD: OTHER	TRANSDUCER: θ°	f, MHz	MODE: S	MODE: L	TYPE: S	TYPE: D	SIZE	MAKE	SOUND PATH: ½V	SOUND PATH: ¾V	SOUND PATH: OTHER	BEAM SPREAD ACCOUNTED ?: YES	BEAM SPREAD ACCOUNTED ?: NO	UT INSTRUMENT
1	0.025		10			43	2¼	✓		✓		¼"	AERO	✓			✓		USL 38
2	0.050		10			45	4	✓		✓									
3	0.296	✓				52	2¼	✓		✓		0.5	AERO	✓			✓		NORTEC
4	0.40		20			60	1.5	✓		✓		0.5	AERO	✓			✓		USL 38
5	0.26	✓				60	1.5	✓		✓		0.5	AERO	✓				✓	USL 38
6	0.095		50			43	1.5	✓			✓	⅜ x ¾	AERO	✓			✓		USL 38
7	0.150		50			45 60	2¼	✓	✓	✓		0.5	AERO	✓				✓	NORTEC
8	0.319		10		✓	60	1.5	✓		✓		0.5	AERO	✓			✓		USL 38
9	0.40	✓				52	3.8	✓		✓		⅜	NOT CI NOVA	✓				✓	USIP 11
10	0.35		50			45	2¼	✓		✓		0.5	AERO	✓					USK 6
11	0.278			25		45	2¼	✓			✓	.5 x .5	H'SONIC		✓		✓		USL 38
13	0.55																		
14	0.121 0.303 0.639		50			45 60 70	1.5 2¼	✓		✓	✓	½ x ½ 0.5	AERO	✓				✓	USL 38
	0.330																		
16	0.315		5			45	2¼	✓		✓		0.5	AERO	✓				✓	USL 38
17	0.43"																		

Wall thickness at C. Bore 0.620"

FLAW	PROBE SIDE	FLAW SIDE	FLAW SIDE	PROBE SIDE
5	X	X		
No				

10%

FLAW DEPTH 0.06 inch

TEAM	UT DEPTH INCH	SIZING METHOD: CODE	AMPLITUDE: AMP	% PEAK	% DAC	OTHER	TRANSDUCER: θ°	f. MHz	MODE: S	L	TYPE: S	D	SIZE	MAKE	SOUND PATH: ½V	¾V	OTHER	BEAM SPREAD ACCOUNTED ?: YES	NO	UT INSTRUMENT
1	0.04			10			43	2¼	✓		✓		¼"	AERO	✓			✓		USL 38
2	0.060			10			60	4			✓		4x4 m	KRAUT	✓	✓		✓		USL 38
3	0.183			25			56	2¼	✓		✓		0.5	AERO	✓			✓		NORTEC
4	0.25			20			60	1.5	✓		✓		0.5	AERO	✓				✓	USL 38
5	0.18	✓					60	1.5	✓		✓		0.5	AERO	✓				✓	USL 38
6	0.115			50			43	1.5	✓			✓	⅞ x 1½	AERO	✓			✓		USL 38
7	0.200			50			45/60	2¼	✓	✓	✓		0.5	AERO	✓				✓	NORTEC
8	0.250			10		✓	60	1.5	✓		✓		0.5	AERO	✓			✓		USL 38
9	0.33	✓					52	3.3	✓		✓		¾	NDT CI NOVA	✓				✓	USIP 11
10	0.30			50			45	2¼	✓		✓		0.5	AERO	✓					USK 6
11	0.135				25		60	2¼	✓		✓		¼	AERO	✓			✓		USL 38
13	0.08																			
14	0.122 0.223 0.439			50			45 60 70	1.5 2¼	✓		✓	✓	¾x¾ 0.5	AERO	✓				✓	USL 38
15	0.22																			
16	0.315			50			45	2¼	✓		✓		0.5	AERO	✓				✓	USL 38
17	0.07																			

Wall thickness at C. Bore 0.565"

FLAW	PROBE SIDE	FLAW SIDE	FLAW SIDE	PROBE SIDE
6	X	X		
No.				

19%

FLAW DEPTH 0.105 inch

ITEM	UT DEPTH, INCH	SIZING METHOD: CRACK TIP	AMPLITUDE: % FSH PEAK	AMPLITUDE: % DAC	AMPLITUDE: OTHER	TRANSDUCER: θ°	f, MHz	MODE: S	MODE: L	TYPE: S	TYPE: D	SIZE	MAKE	SOUND PATH: ½V	SOUND PATH: ¾V	SOUND PATH: OTHER	BEAM SPREAD ACCOUNTED FOR: YES	BEAM SPREAD ACCOUNTED FOR: NO	UT INSTRUMENT
1	0.08		10			43	2¼	✓		✓		¼"	AERO	✓			✓		USL 38
2	0.075		10			60	4			✓		4X10 m	KRAUT	✓	✓		✓		USL 38
3	0.171	✓				56	2¼	✓		✓		0.5	AERO	✓			✓		NORTEC
4	0.15		20			60	1.5	✓		✓		0.5	AERO	✓				✓	USL 38
5	0.14	✓				60	1.5	✓		✓		0.5	AERO	✓				✓	USL 38
6	0.105		50			43	1.5	✓			✓	3mmX3½	AERO	✓			✓		USL 38
7	0.100		50			45 60	2¼	✓	✓	✓		0.5	AERO	✓				✓	NORTEC
8	0.250		10		✓	60	1.5	✓		✓		0.5	AERO	✓			✓		USL 38
9	0.41	✓				52	3.3	✓		✓		⅜	NDT CI NOVA	✓				✓	USIP 11
10	0.30		50			45	2¼	✓		✓		0.5	AERO	✓					USK 6
11	0.166			25		60	2¼	✓		✓		¼	AERO	✓			✓		USL 38
12	0.073	✓				45	1.5	✓		✓		⅜	AERO	✓				✓	USL 38
13	0.12																		
14	0.045 0.174 0.364		50			45 60 70	1.5 2¼	✓		✓	✓	¾X¾ 0.5	AERO	✓				✓	USL 38
16	0.225		5			45	2¼	✓		✓		2¼	AERO	✓				✓	USL 38
17	0.13																		

Wall thickness at C. Bore 1.050"

FLAW NO.	PROBE SIDE	FLAW SIDE	FLAW SIDE	PROBE SIDE
7	X	X		

18%

FLAW DEPTH 0.184 inch

ITEM	UT DEPTH, INCH	SIZING METHOD: CIRCUS	AMPLITUDE: TIP	AMPLITUDE: % PEAK	AMPLITUDE: % DAC	AMPLITUDE: OTHER	TRANSDUCER: θ°	f, MHz	MODE: S	MODE: L	TYPE: S	TYPE: D	SIZE	MAKE	SOUND PATH: ½V	SOUND PATH: ¾V	SOUND PATH: OTHER	BEAM SPREAD ACCOUNTED?: YES	BEAM SPREAD ACCOUNTED?: NO	UT INSTRUMENT
1	0.140			10			43	2¼	✓		✓		¼"	AERO	✓			✓		USL 38
2	0.100			10			60	4	✓		✓		9X10 m/m	KRAUT	✓			✓		USL 38
3	0.125	✓					56	2¼	✓		✓		0.5	AERO	✓			✓		NORTEC
4	0.30			20			60	1.5	✓		✓		0.5	AERO	✓				✓	USL 38
5	0.25	✓					60	1.5	✓		✓		0.5	AERO	✓				✓	USL38
6	0.150			50			43	1.5	✓			✓	⅜x⅜	AERO	✓			✓		USL 38
7	0.150			50			60	2¼	✓	✓	✓		0.5	AERO	✓				✓	NORTEC
8	0.330			10		✓	60	1.5	✓		✓		0.5	AERO	✓			✓		USL 38
9	0.60	✓					53	3.8	✓		✓		½	NOT CI NOVA	✓				✓	USIP 11
10	0.15			50			45	2¼	✓		✓		0.5	AERO	✓					USK 6
11	0.282				25		60	2¼	✓		✓		¼	AERO	✓			✓		USL38
13	0.12																			
14	0.052			50			45	1.5	✓			✓	⅞x¾	AERO	✓				✓	USL 38
15	0.404																			
16	0.250			5			45	2¼	✓		✓		0.5	AERO	✓				✓	USL 38

Wall thickness at C. Bore 1.253"

FLAW NO.	PROBE SIDE	FLAW SIDE	FLAW SIDE	PROBE SIDE
8	X	X		

25%

FLAW DEPTH 0.318 inch

ITEM	UT DEPTH INCH	SIZING METHOD: CRACK TIP	AMPLITUDE: % FSH PEAK	AMPLITUDE: % DAC	OTHER	TRANSDUCER: θ	F. MHz	MODE: S	MODE: L	TYPE: S	TYPE: D	SIZE	MAKE	SOUND PATH: ½V	SOUND PATH: ¾V	SOUND PATH: OTHER	BEAM SPREAD ACCOUNTED?: YES	BEAM SPREAD ACCOUNTED?: NO	UT INSTRUMENT
1	0.050		10			43	2¼	✓		✓		¼"	AERO	✓			✓		USL 38
2	0.060				✓	60	4	✓		✓		4x10 mm	KRAUT	✓	✓		✓		USL 38
3	0.046	✓				56	2¼	✓		✓		0.5	AERO	✓			✓		NORTEC
4	0.25		20			60	1.5	✓		✓		0.5	AERO	✓				✓	USL 38
5	0.30	✓				60	1.5	✓		✓		0.5	AERO	✓				✓	USL 38
6	0.115		50			43	1.5	✓			✓	⅜x¾	AERO	✓			✓		USL 38
7	0.150		50			45 60	2¼	✓	✓	✓		0.5	AERO	✓				✓	NORTEC
8	0.200		10		✓	60	1.5	✓		✓		0.5	AERO	✓			✓		USL 38
9	0.82	✓				45	3.3	✓		✓		⅜	NOT CI NOVA	✓				✓	USIP11
10	0.24		50			45	2¼	✓		✓		0.5	AERO	✓					USK 6
11	0.274			25		60	2¼	✓		✓		¼	AERO	✓			✓		USL 38
13	0.08																		
14	0.129 0.9 1.157		50			45 60 70	1.5 2¼	✓		✓	✓	⅜x¼ 0.5	AERO	✓				✓	USL38
15	.146																		
16	0.270		5			45	2¼	✓		✓		0.5	AERO	✓				✓	USL 38

Wall thickness at C-Bore 0.780"

FLAW NO.	PROBE SIDE	FLAW SIDE	FLAW SIDE	PROBE SIDE
9	X	X	☐	☐

76%

FLAW DEPTH 0.590 inch

ITEM	UT DEPTH INCH	SIZING METHOD: CRACK TIP	AMPLITUDE: % PEAK	AMPLITUDE: % DAC	OTHER	TRANSDUCER: θ°	f, MHz	MODE: S	MODE: L	TYPE: S	TYPE: D	SIZE	MAKE	SOUND PATH: ½V	SOUND PATH: ¾V	SOUND PATH: OTHER	BEAM SPREAD ACCOUNTED FOR: YES	BEAM SPREAD ACCOUNTED FOR: NO	UT INSTRUMENT
1	0.08		50			45	2¼	✓		✓		¼"	AERO			✓	✓		USL 32
2	0.250		10			60	4	✓		✓		AXIOM	KRAUT	✓	✓		✓		USL 38
3	0.137		50			45	1.5	✓		✓		⅜	H'SONIC	✓				✓	NORTEC
5	0.39	✓				60	1.5	✓		✓		0.5	AERO	✓				✓	USL 38
6	0.140		50			45	1.5	✓			✓	¾x¾	AERO	✓			✓		MGFX ATTN
7	0.275		50			45	2¼	✓	✓	✓		0.5	H'SONIC	✓				✓	NORTEC
8	0.30		10		✓	60	1.5	✓		✓		0.5	AERO	✓	✓		✓		USL 38
9	0.22	✓				45 52 60	4	✓		✓		⅜	NOT CI NOVA	✓				✓	USIP 11
11	0.193			25		60	2¼	✓		✓		¼	AERO	✓			✓		USL 38
12	0.104	✓				45	1.5	✓		✓		⅜	AERO	✓				✓	USL 38
13	0.2																		
14	0.035 0.336 0.5[illegible]		50			45 60 70	1.5 2¼	✓		✓		✓ ⅜x¼ 0.5	AERO	✓				✓	USL 38
16	0.300		5			45	2¼	✓		✓		0.5	AERO	✓				✓	USL 38
17	0.49																		

Wall thickness at C. Bore 0.730"

FLAW NO.	PROBE SIDE	FLAW SIDE	FLAW SIDE	PROBE SIDE
9	☐	☐	X	X

84%

FLAW DEPTH 0.653 inch

TEAM	UT DEPTH, INCH	SIZING METHOD: CRACK TIP	AMPLITUDE: % PEAK	AMPLITUDE: % DAC	SIZING METHOD: OTHER	TRANSDUCER: θ°	TRANSDUCER: f, MHz	MODE: S	MODE: L	TYPE: S	TYPE: D	TRANSDUCER: SIZE	TRANSDUCER: MAKE	SOUND PATH: ½V	SOUND PATH: ¾V	SOUND PATH: OTHER	BEAM SPREAD ACC COUNTED ?: YES	BEAM SPREAD ACC COUNTED ?: NO	UT INSTRUMENT
1	0.05		50			45	2¼	✓		✓		¼"	AERO			✓	✓		USL 32
3	0.182		50			45	1.5	✓		✓		⅜	H'SONIC	✓				✓	NORTEC
6	0.140		50			45	1.5	✓			✓	⅜ x ¾	AERO	✓			✓		AGFX 710
12	0.139	✓				45	1.5	✓		✓		⅜	AERO	✓				✓	USL 38
13	0.6																		
14	0.109 0.543 0.652		50			60 70	1.5 2¼	✓		✓	✓	½ x ¼ 0.5	AERO	✓				✓	USL 38
16	0.260		5			45	2¼	✓		✓		0.5	AERO	✓				✓	USL 38
17	0.56																		

Wall thickness at C. Bore 0.780"

FLAW NO.	PROBE SIDE	FLAW SIDE	FLAW SIDE	PROBE SIDE
10	X	X		

43%

FLAW DEPTH 0.334 inch

TEAM	UT DEPTH INCH	SIZING METHOD: AMPLITUDE TIP	AMPLITUDE % PEAK	AMPLITUDE % DAC	OTHER	TRANSDUCER: θ°	f, MHz	MODE S	MODE L	TYPE S	TYPE D	SIZE	MAKE	SOUND PATH ½V	SOUND PATH ¾V	SOUND PATH OTHER	BEAM SPREAD ACCOUNTED? YES	BEAM SPREAD ACCOUNTED? NO	UT INSTRUMENT
1	0.08		50			45	2¼	✓		✓		¼	AERO			✓	✓		USL 32
2	0.750		10		1	60	4	✓		✓		9X10 mi	KRAUT	✓	✓		✓		USL 38
3	0.106		50			45	1·5	✓		✓		⅜	H'SONIC	✓				✓	NORTEC
5	0.22	✓				60	1·5	✓		✓		0.5	AERO	✓				✓	USL 38
6	0.105		50			45	1·5	✓			✓	⅜ x ¾	AERO	✓			✓		MG-FX 710
7	0.325		50			45	2¼	✓	✓	✓		0.5	H'SONIC	✓				✓	NORTEC
8	0.76		10		1	60	1·5	✓		✓		0.5	AERO	✓	✓		✓		USL 38
9	0.15	✓				45 5=60	4	✓		✓		⅜	NDT CI NOVA	✓				✓	USIP 11
12	0.150					45	1·5	✓		✓		⅜	AERO	✓				✓	USL 38
13	0.08																		
14	0.093 0.233		50			45 70	1·5 2¼	✓		✓	✓	⅜ x 2¼ 0.5	AERO	✓				✓	USL 38
16	0.220		5			45	2¼	✓		✓		0.5	AERO	✓				✓	USL 38
17	0.44																		

Wall thickness at C. Bore 0.780"

89%

FLAW NO.	PROBE SIDE	FLAW SIDE	FLAW SIDE	PROBE SIDE
10	☐	☐	X	X

FLAW DEPTH 0.692 inch

ITEM	UT DEPTH INCH	SIZING METHOD: CREEP TIP	AMPLITUDE: % PEAK	AMPLITUDE: % DAC	SIZING METHOD: OTHER	TRANSDUCER: θ°	f. MHz	MODE: S	MODE: L	TYPE: S	TYPE: D	TRANSDUCER: SIZE	TRANSDUCER: MAKE	SOUND PATH: ½ V	SOUND PATH: 3/2 V	SOUND PATH: OTHER	BEAM SPREAD ACCOUNTED FOR: YES	BEAM SPREAD ACCOUNTED FOR: NO	UT INSTRUMENT
1	0.04		50			45	2.25	✓		✓		1/4"	AERO			✓	✓		USL 32
3	0.661		50			45	1.5	✓		✓		3/8	H'SONIC	✓				✓	NORTEC
6	0.140		50			45	1.5	✓			✓	3/4 x 3/4	AERO	✓			✓		M&F 710
11	0.531			25		60	2¼	✓		✓		¼	AERO	✓			1		USL 38
12	0.589					45	1.5	✓		✓		3/3	AERO	✓				✓	USL 38
13	0.67																		
14	0.507 0.741 0.614		50			45 70	1.5 2¼	✓		✓	✓	3/4 x 1/4 9.5	AERO	✓		✓		✓	USL 38
16	0.360		5			45	2¼	✓		✓		0.5	AERO	✓				✓	USL 38
17	0.35																		

Wall thickness at C. Bore 1.1"

15%

FLAW NO.	PROBE SIDE	FLAW SIDE	FLAW SIDE	PROBE SIDE
11	X	X		

NS

FLAW DEPTH 0.160 inch

ITEM	UT DEPTH INCH	SIZING METHOD: CRACK TIP	AMPLITUDE: % PEAK	AMPLITUDE: % DAC	OTHER	TRANSDUCER: θ°	f, MHz	MODE: S	MODE: L	TYPE: S	TYPE: D	SIZE	MAKE	SOUND PATH: ½V	SOUND PATH: ¾V	SOUND PATH: OTHER	BEAM SPREAD ACCOUNTED FOR?: YES	BEAM SPREAD ACCOUNTED FOR?: NO	UT INSTRUMENT
1	0.07		50			45	2¼	✓		✓		¼"	AERO			✓	✓		USL 32
2	0.210		10		✓	60	4	✓		✓		9x10mm	KRAUT	✓			✓		USL 38
3	0.158		50			45	1.5	✓		✓		⅜	H'SONIC	✓				✓	NORTEC
5	0.21	✓				60	1.5	✓		✓		0.5	AERO	✓				✓	USL 38
6	0.190		50			45	1.5	✓			✓	⅜x¾	AERO	✓			✓		KBGFX 710
7	0.250		50			45	2¼	✓	✓	✓		0.5	AERO	✓				✓	NORTEC
8	0.400		10		✓	60	1.5	✓		✓		0.5	AERO	✓			✓		USL 38
9	0.33	✓				45 52 60	4	✓		✓		⅜	NOT CI NOVA	✓				✓	USIP 11
11	0.113		50			45	2¼	✓		✓		¼	AERO	✓			✓		USL 38

Wall thickness at C'bore 1.1"

15%

FLAW No.	PROBE SIDE	FLAW SIDE	FLAW SIDE	PROBE SIDE
11	☐	☐	X	X

FLAW DEPTH 0.170 inch

ITEM	UT DEPTH INCH	SIZING METHOD: CURVE	AMPLITUDE: TIP	AMPLITUDE: % PEAK	AMPLITUDE: % DAC	OTHER	TRANSDUCER: θ°	f, MHz	MODE: S	MODE: L	TYPE: S	TYPE: D	SIZE	MAKE	SOUND PATH: ½V	SOUND PATH: ¾V	SOUND PATH: OTHER	BEAM SPREAD ACCOUNTED ?: YES	BEAM SPREAD ACCOUNTED ?: NO	UT INSTRUMENT
1	0.16			50			45	2¼	✓		✓		½"	AERO			✓	✓		USL 32
2	0.210			10			60	4	✓		✓		4x10 mm	KRAUT	✓			✓		USL 38
3	0.134			50			45	1.5	✓		✓		⅜	H'SONIC	✓				✓	NORTEC
5	0.17	✓					60	1.5	✓		✓		0.5	AERO	✓				✓	USL 38
6	0.220			50			45	1.5	✓			✓	⅜x¾	AERO	✓			✓		MGFX 7/C
7	0.200			50			45/60	2¼	✓	✓	✓		0.5	H'SONIC AERO	✓				✓	NORTEC
8	0.300			10		✓	60	1.5	✓		✓		0.5	AERO	✓			✓		USL 38
9	0.34	✓					45/52/60	4	✓		✓		⅜	NOT CII NOVA	✓				✓	USIP 11
11	0.155			50			45	2¼	✓		✓		¼	AERO	✓			✓		USL 38

Wall thickness at C. Bore 1.1"

17%

FLAW	PROBE SIDE	FLAW SIDE	FLAW SIDE	PROBE SIDE
12	X	X	☐	☐

NO

N3

FLAW DEPTH 0.185 inch

TEAM	UT DEPTH INCH	SIZING METHOD: CRACK TIP	AMPLITUDE: ½ PEAK	AMPLITUDE: ½ DAC	GRAY	TRANSDUCER: θ°	f MHz	MODE: S	MODE: L	TYPE: S	TYPE: D	SIZE	MAKE	SOUND PATH: ¼ V	SOUND PATH: ½ V	SOUND PATH: OTHER	BEAM SPREAD ACCOUNTED ?: YES	BEAM SPREAD ACCOUNTED ?: NO	UT INSTRUMENT
1	0.05		50			45	2¼	✓		✓		½"	AERO			✓	✓		USL 32
2	0.180		10			60	4	✓		✓		9x10mm	KRAUT	✓					USL 38
3	0.195		50			45	1.5	✓		✓		¾	H'SONIC	✓				✓	NORTEC
5	0.28	✓				60	1.5	✓		✓		0.5	AERO	✓				✓	USL 38
6	0.190		50			45	1.5	✓			✓	¾x¾	AERO	✓			✓		AGFK 710
7	0.275		50			45 60	2¼	✓	✓	✓		0.5	H'SONIC AERO	✓				✓	NORTEC
8	0.200		10		✓	60	1.5	✓		✓		0.5	AERO	✓			✓		USL 38
9	0.43	✓				45 52 70	4	✓		✓		¾	NDT OI NOVA	✓				✓	USIP 11
11	0.157		50			60	2¼	✓		✓		¼	AERO	✓			✓		USL 38
17	?																		

Wall thickness at C-Bore 1.1"

17%

FLAW	PROBE SIDE	FLAW SIDE	FLAW SIDE	PROBE SIDE
12	☐	☐	X	X

NO

N2

FLAW DEPTH 0.185 inch

ITEM	UT DEPTH INCH	SIZING METHOD: CRACK TIP	AMPLITUDE: % PEAK	AMPLITUDE: % DAC	OTHER	TRANSDUCER: ANGLE	FREQ MHz	MODE: S	MODE: L	TYPE: S	TYPE: D	SIZE	MAKE	SOUND PATH: ½V	SOUND PATH: ¾V	SOUND PATH: OTHER	BEAM SPREAD ACCOUNTED FOR?: YES	BEAM SPREAD ACCOUNTED FOR?: NO	UT INSTRUMENT
1	0.11		50			45	2½	✓		✓		¼"	AERO			✓	✓		USL 32
2	0.150		10			60	4	✓		✓		9x10 m	KRAUT	✓					USL 38
3	0.158		50			45	1.5	✓		✓		⅜	H'SONIC	✓				✓	NORTEC
5	0.19	✓				60	1.5	✓		✓		0.5"	AERO	✓				✓	USL 38
6	0.190		50			45	1.5	✓			✓	9x10 3/4	AERO	✓			✓		MGFx 710
7	0.180		50			45 60	2¼	✓	✓	✓		0.5"	H'SONIC AERO	✓				✓	NORTEC
8	0.450		10		✓	60	1.5	✓		✓		0.5"	AERO	✓			✓		USL 38
9	0.39	✓				45 60	4	✓		✓		⅜	NOT CI NOVA	✓				✓	USIP 11
11	0.184		50			60	2½	✓		✓		¼	AERO	✓			✓		USL 38
1																			
17	0.12																		

FLAW NO.	PROBE SIDE	FLAW SIDE	FLAW SIDE	PROBE SIDE
13	X	X		

FLAW DEPTH _____ inch

ITEM	UT DEPTH INCH	SIZING METHOD: CRACK TIP	AMPLITUDE: % PEAK MAX	AMPLITUDE: % DAC	OTHER	TRANSDUCER: θ°	f, MHz	MODE: S	MODE: L	TYPE: S	TYPE: D	SIZE	MAKE	SOUND PATH: ½V	SOUND PATH: ¾V	SOUND PATH: OTHER	BEAM SPREAD ACCOUNTED FOR?: YES	BEAM SPREAD ACCOUNTED FOR?: NO	UT INSTRUMENT
1	0.16		50			45	2¼	✓		✓		¼"	AERO			✓	✓		USL 32
2	0.150				✓	60	4	✓		✓		9X10M	KRAUT	✓					USL 33
3	0.151		50			55	2¼	✓		✓		⅜	H'SONIC	✓				✓	NORTEC
5	0.15	✓				60	1.5	✓		✓		0.5"	AERO	✓				✓	USL 38
6	0.125		50			45	1.5	✓			✓	⅜x¾	AERO	✓			✓		MGFX 710
7	0.350		50			45 60	2¼	✓	✓	✓		0.5	H'SONIC AERO	✓				✓	NORTEC
8	0.250		10		✓	60	1.5	✓		✓		0.5	AERO	✓			✓		USL 33
9	0.19	✓				45 52 60	4	✓		✓		⅜	NDT CI NOVA	✓				✓	USIP 11
11	0.120		50			60	2¼	✓		✓		¼	AERO	✓			✓		USL 33

FLAW NO.	PROBE SIDE	FLAW SIDE	FLAW SIDE	PROBE SIDE
13	☐	☐	X	X

FLAW DEPTH _____ inch

ITEM	UT DEPTH INCH	SIZING METHOD: CURVE	AMPLITUDE: TIP	AMPLITUDE: % PEAK	AMPLITUDE: % DAC	AMPLITUDE: OTHER	TRANSDUCER: ∠°	TRANSDUCER: f, MHz	MODE: S	MODE: L	TYPE: S	TYPE: D	TRANSDUCER: SIZE	TRANSDUCER: MAKE	SOUND PATH: ½ V	SOUND PATH: ¾ V	SOUND PATH: OTHER	BEAM SPREAD ACCOUNTED FOR: YES	BEAM SPREAD ACCOUNTED FOR: NO	UT INSTRUMENT
1	0.06			50			45	2¼	✓		✓		¼"	AERO			✓	✓		USL 32
2	0.150					✓	60	4	✓		✓		Axiom	KRAUT	✓					USL 33
3	0.140			50			55	2¼	✓		✓		⅜	H'SONIC	✓				✓	NORTEC
5	0.20	✓					60	1.5	✓		✓		0.5	AERO	✓				✓	USL 33
6	0.160			50			45	1.5	✓			✓	¾ x ¾	AERO	✓			✓		DGFx 710
7	0.300			50			+5 60	2¼	✓	✓	✓		0.5	H'SONIC AERO	✓				✓	NORTEC
8	0.240			10		✓	60	1.5	✓		✓		0.5	AERO	✓			✓		USL 33
9	0.11	✓					+5 -5 60	4	✓		✓		⅜	NOT CI	✓				✓	USIP 11
11	0.262			50			60	2¼	✓		✓		¼	AERO	✓			✓		USL 33

FLAW NO.	PROBE SIDE	FLAW SIDE	FLAW SIDE	PROBE SIDE
14	X	X		

FLAW DEPTH _____ inch

ITEM	UT DEPTH INCH	SIZING METHOD: AMPLITUDE TMP	AMPLITUDE % PEAK	AMPLITUDE % DAC	OTHER	TRANSDUCER: θ°	F. MHz	MODE S	MODE L	TYPE S	TYPE D	SIZE	MAKE	SOUND PATH ½V	SOUND PATH ¾V	SOUND PATH OTHER	BEAM SPREAD ACCOUNTED? YES	BEAM SPREAD ACCOUNTED? NO	UT INSTRUMENT
1	0.10		50			45	2¼	✓		✓		¼"	AERO			✓	✓		USL 32
2	0.210				✓	60	4	✓		✓		9x10mm	KRAUT	✓					USL 38
3	0.090		50			55	2¼	✓		✓		⅜	H'SONIC	✓				✓	NORTEC
5	0.16	✓				60	1.5	✓		✓		0.5	AERO	✓				✓	USL 38
6	0.110		50			45	1.5	✓			✓	⅜x¾		✓			✓		MGFX 710
7	0.300		50			45 60	2¼	✓	✓	✓		0.5	H'SONIC AERO	✓				✓	NORTEC
8	0.420		10		✓	60	1.5	✓		✓		0.5	AERO	✓			✓		USL 38
9	0.25	✓				45 52 60	4	✓		✓		⅜	NUT CI	✓				✓	USIP 11
11	0.176					60	2¼	✓		✓		½	AERO	✓			✓		USL 38

FLAW NO.	PROBE SIDE	FLAW SIDE	FLAW SIDE	PROBE SIDE
14	☐	☐	X	X

FLAW DEPTH _____ inch

TEAM	UT DEPTH INCH	SIZING METHOD: AMPLITUDE TIP	AMPLITUDE % PEAK	AMPLITUDE % DAC	SIZING METHOD: OTHER	TRANSDUCER: θ°	f, MHz	MODE S	MODE L	TYPE S	TYPE D	SIZE	MAKE	SOUND PATH ½V	SOUND PATH ¾V	SOUND PATH OTHER	DEPTH SPREAD ACCOUNTED FOR: YES	DEPTH SPREAD ACCOUNTED FOR: NO	UT INSTRUMENT
1	0.07		50			45	2¼	✓		✓		¼"	AERO			✓	✓		USL 32
2	0.210				✓	60	4	✓		✓		AXIOM	KRAUT	✓					USL 38
3	0.440		50			55	2¼	✓		✓		¾	H'SONIC	✓				✓	NORTEC
5	0.23	✓				60	1·5	✓		✓		0·5	AERO	✓				✓	USL 38
6	0.190		50			45	1·5	✓			✓	¾ x ¾	AERO	✓			✓		MGFX 710
7	0.280		50			45 60	2¼	✓	✓	✓		0·5	H'SONIC AERO	✓				✓	NORTEC
8	1·1		10		✓	60	1·5	✓		✓		0·5	AERO	✓	✓		✓		USL 38
9	0.82	✓				45 52½ 60	4	✓		✓		¾	NOT CI	✓				✓	USIP 11

FLAW NO.	PROBE SIDE	FLAW SIDE	FLAW SIDE	PROBE SIDE
15	X	X		

FLAW DEPTH _____ inch

ITEM	UT DEPTH INCH	SIZING METHOD: AMPLITUDE TIP	AMPLITUDE % PEAK	AMPLITUDE % DAC	SIZING METHOD: OTHER	TRANSDUCER: θ°	f, MHz	MODE S	MODE L	TYPE S	TYPE D	SIZE	MAKE	SOUND PATH ½V	SOUND PATH ¾V	SOUND PATH OTHER	BEAM SPREAD ACCOUNTED FOR? YES	BEAM SPREAD ACCOUNTED FOR? NO	UT INSTRUMENT
1	0.04		50			45	2¼	✓		✓		½"	AERO			✓	✓		USL32
2	0.210				✓	60	4	✓		✓		9x10 mm	KRAUT	✓					USL38
3	0.205		50			55	2¼	✓		✓		⅜	H'SONIC	✓				✓	NORTEC
5	0.08	✓				60	1-5	✓		✓		0.5	AERO	✓				✓	USL38
6	0.095		50			45	1-5	✓			✓	⅜x¾	AERO	✓			✓		~~KB~~ 710
7	0.100		50			45 60	2¼	✓	✓	✓		0.5	H'SONIC AERO	✓				✓	NORTEC
8	0.300		10		✓	60	1-5	✓		✓		0.5	AERO	✓			✓		USL38
9	0.33	✓				45 52 60	4	✓		✓		⅜	NOTCH	✓				✓	USIP 11
11	0.196		50			60	2¼	✓		✓		¼	AERO	✓			✓		USL30

FLAW NO.	PROBE SIDE	FLAW SIDE	FLAW SIDE	PROBE SIDE
15	☐	☐	X	X

FLAW DEPTH _____ inch

ITEM	UT DEPTH INCH	SIZING METHOD: AMPLITUDE TIP	AMPLITUDE % PEAK	AMPLITUDE % DAC	OTHER	TRANSDUCER: θ°	f, MHz	MODE S	MODE L	TYPE S	TYPE D	SIZE	MAKE	SOUND PATH ½V	SOUND PATH ¾V	SOUND PATH OTHER	BEAM SPREAD ACCOUNTED? YES	BEAM SPREAD ACCOUNTED? NO	UT INSTRUMENT
1	0.06		50			45	2¼	✓		✓		¼"	AERO			✓	✓		USL 32
2	0.210				✓	60	4	✓		✓		9x10 mm	KRAUT	✓					USL 38
3	0.216		50			55	2¼	✓		✓		⅜	H'SONIC	✓					NORTEC
5	0.07	✓				60	1.5	✓		✓		0.5	AERO	✓				✓	USL 38
6	0.250		50			45	1.5	✓			✓	⅜x¾	AERO	✓			✓		ATEX 7/8
7	0.175		50			45 60	2¼	✓	✓	✓		0.5	H'SONIC AERO	✓				✓	NORTEC
8	0.250		10		✓	60	1.5	✓		✓		0.5	AERO	✓			✓		USL 38
9	0.22	✓				45 52 60	4	✓		✓		⅜	NOT CI	✓				✓	USIP 11
11	0.222		50			60	2¼	✓		✓		¼	AERO	✓			✓		USL 38

FLAW NO.	PROBE SIDE	FLAW SIDE	FLAW SIDE	PROBE SIDE
16	X	X	☐	☐

FLAW DEPTH _____ inch

TERM	UT DEPTH INCH	SIZING METHOD: CROSS TIP	AMPLITUDE: % PEAK	AMPLITUDE: % DAC	AMPLITUDE: OTHER	TRANSDUCER: θ°	f, MHz	MODE: S	MODE: L	TYPE: S	TYPE: D	SIZE	MAKE	SOUND PATH: ½V	SOUND PATH: ¾V	SOUND PATH: OTHER	BEAM SPREAD ACCOUNTED ?: YES	BEAM SPREAD ACCOUNTED ?: NO	UT INSTRUMENT
1	0.18		50			45	2¼	✓		✓		¼"	AERO			✓	✓		USL 32
2	0.20				✓	60	4	✓		✓		9X10 M	KRAUT	✓					USL 38
3	0.26		50			55	2¼	✓		✓		⅜	H'SONIC	✓				✓	NORTEC
5	0.28	✓				60	1.5	✓		✓		0.5	AERO	✓				✓	USL 38
6	0.160		50			45	1.5	✓			✓	¾x¾	AERO	✓			✓		MGFX 710
7	0.250		50			45 60	2¼	✓	✓	✓		0.5	H'SONIC AERO	✓				✓	NORTEC
8	0.420		10		✓	60	1.5	✓		✓		0.5	AERO	✓			✓		USL 38
9	0.20	✓				45 52 60	4	✓		✓		⅜	NDT CI	✓				✓	USIP 11
11	0.035		50			45	2¼	✓		✓		¼	AERO	✓			✓		USL 38

FLAW NO.	PROBE SIDE	FLAW SIDE	FLAW SIDE	PROBE SIDE
16	☐	☐	☒	☒

FLAW DEPTH _____ inch

ITEM	UT DEPTH INCH	SIZING METHOD: CURVE	AMPLITUDE: TIP	AMPLITUDE: % PEAK	AMPLITUDE: % DAC	AMPLITUDE: OTHER	TRANSDUCER: θ°	F. MHz	MODE: S	MODE: L	TYPE: S	TYPE: D	SIZE	MAKE	SOUND PATH: ½V	SOUND PATH: ¾V	SOUND PATH: OTHER	BEAM SPREAD ACCOUNTED ?: YES	BEAM SPREAD ACCOUNTED ?: NO	UT INSTRUMENT
1	0.06			50			45	2¼	✓		✓		¼"	AERO			✓	✓		USL 32
2	0.20					✓	60	4	✓		✓		9X10m	KRAUT	✓					USL 32
3	0.134			50			45	1.5	✓		✓		⅜	H'SONIC	✓				✓	NORTEC
5	0.33	✓					60	1.5	✓		✓		0.5	AERO	✓				✓	USL 38
6	0.125			50			45	1.5	✓			✓	⅜ x ¾	AERO	✓			✓		MGFX 710
7	0.250			50			45 60	2¼	✓	✓	✓		0.5	H SONIC AERO	✓				✓	NORTEC
8	0.300			10		✓	60	1.5	✓		✓		0.5	AERO	✓					USL 38
9	0.17	✓					45 52 60	4	✓		✓		⅜	NOT CI	✓				✓	USIP 11
11	0.127			50			60	2¼	✓		✓		¼	AERO	✓			✓		USL 38

APPENDIX B

DETAILS OF DESTRUCTIVE EXAMINATION

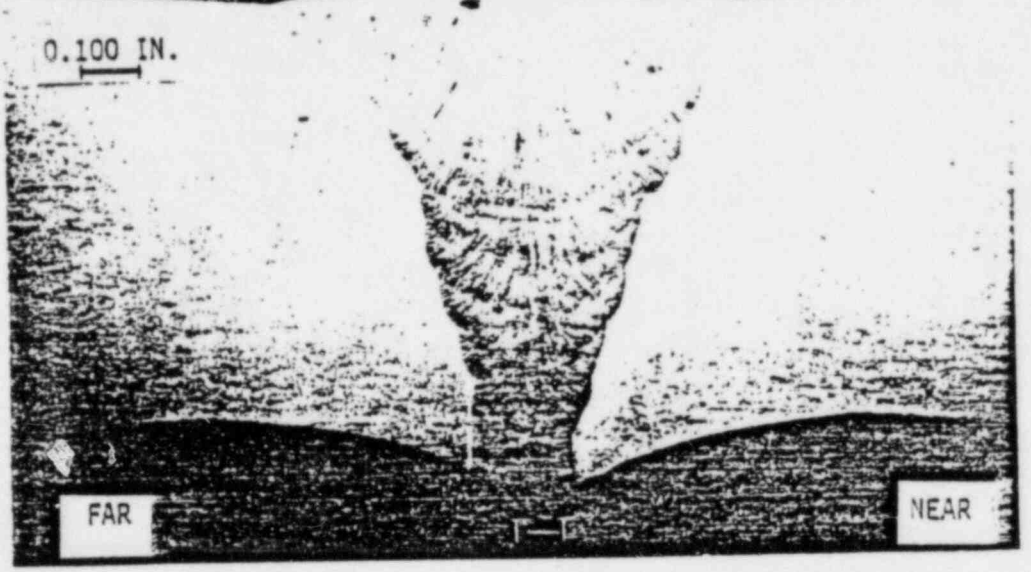

SAMPLE 1-1

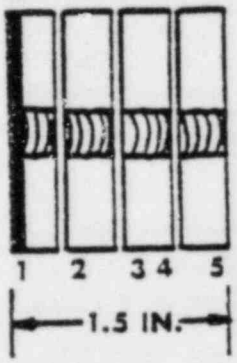

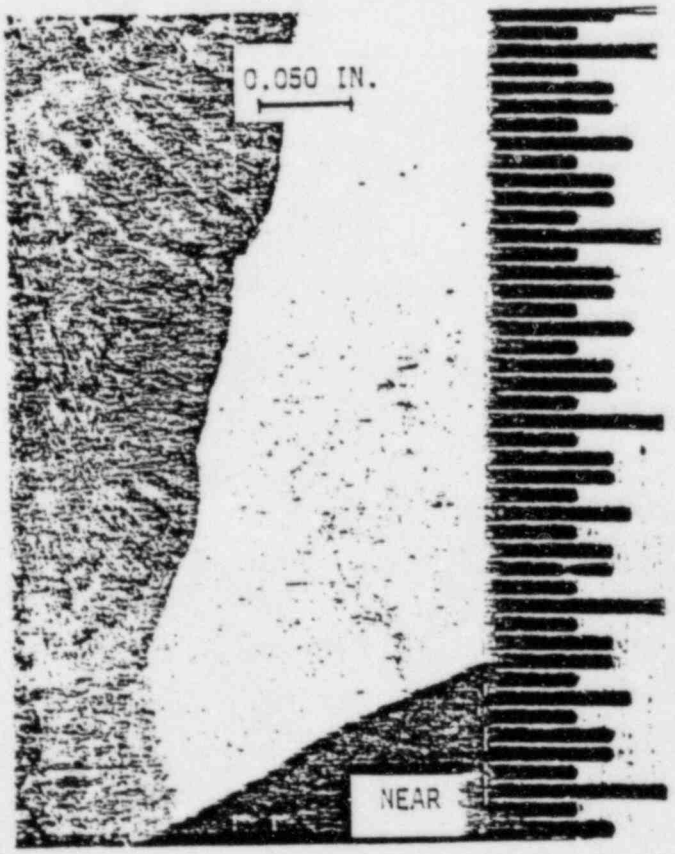

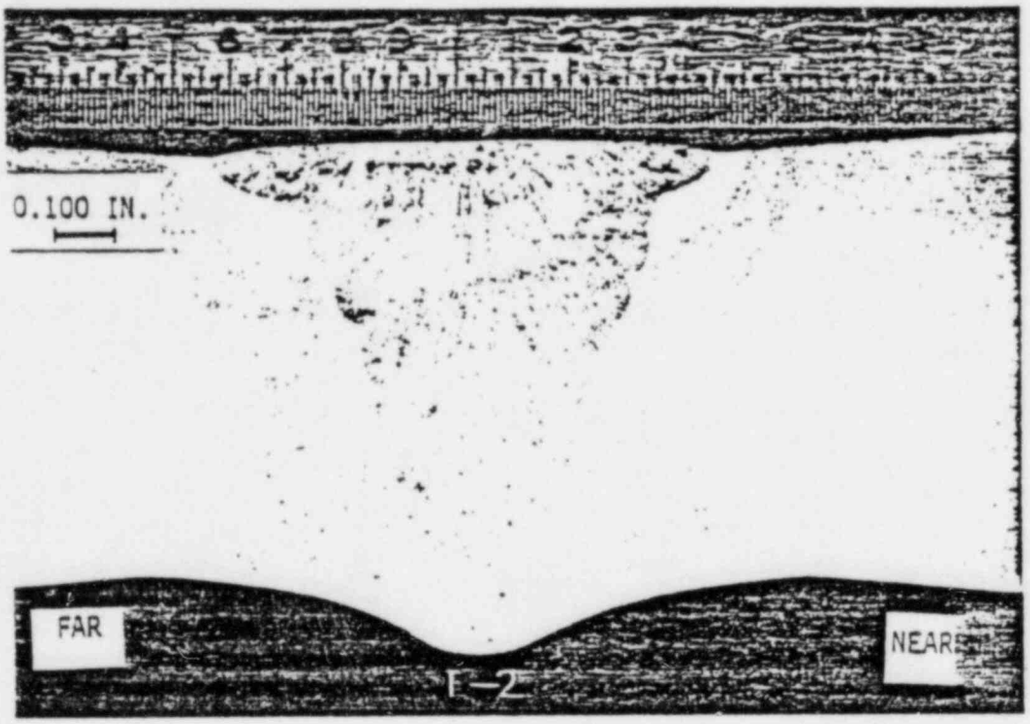

SAMPLE 1-2

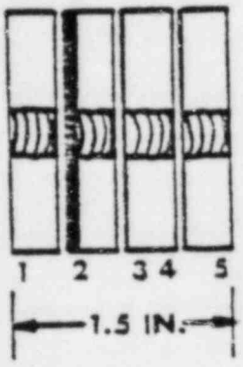

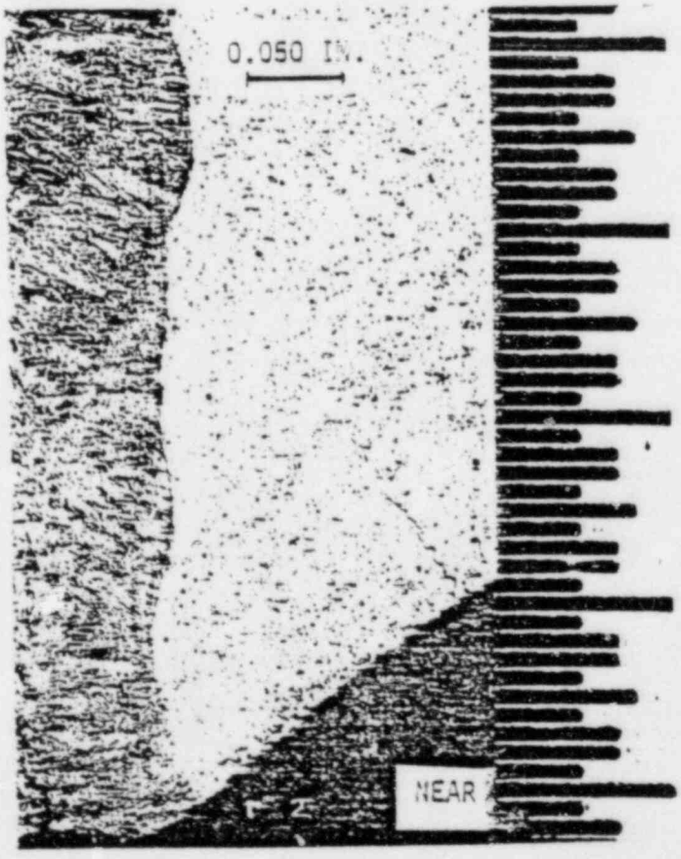

SAMPLE 1-3

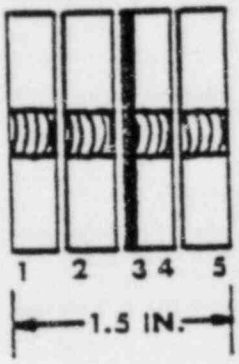

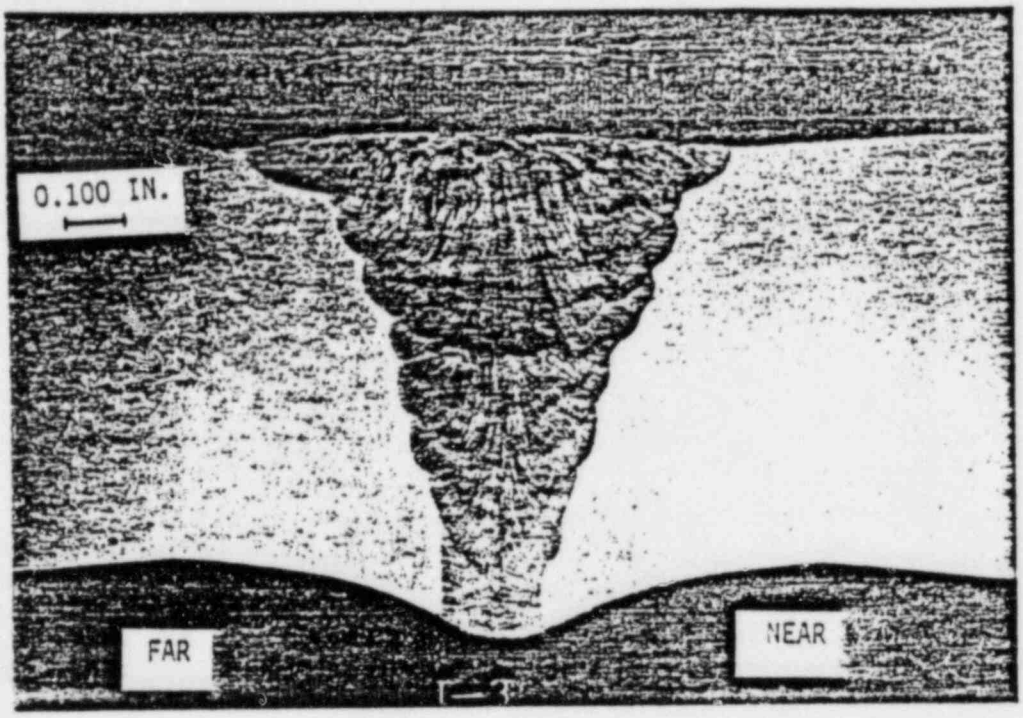

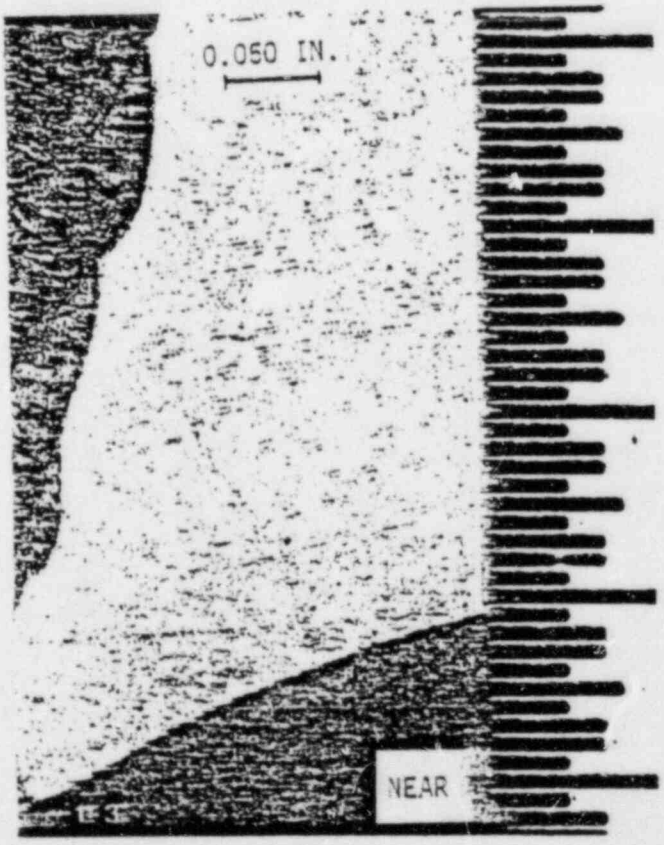

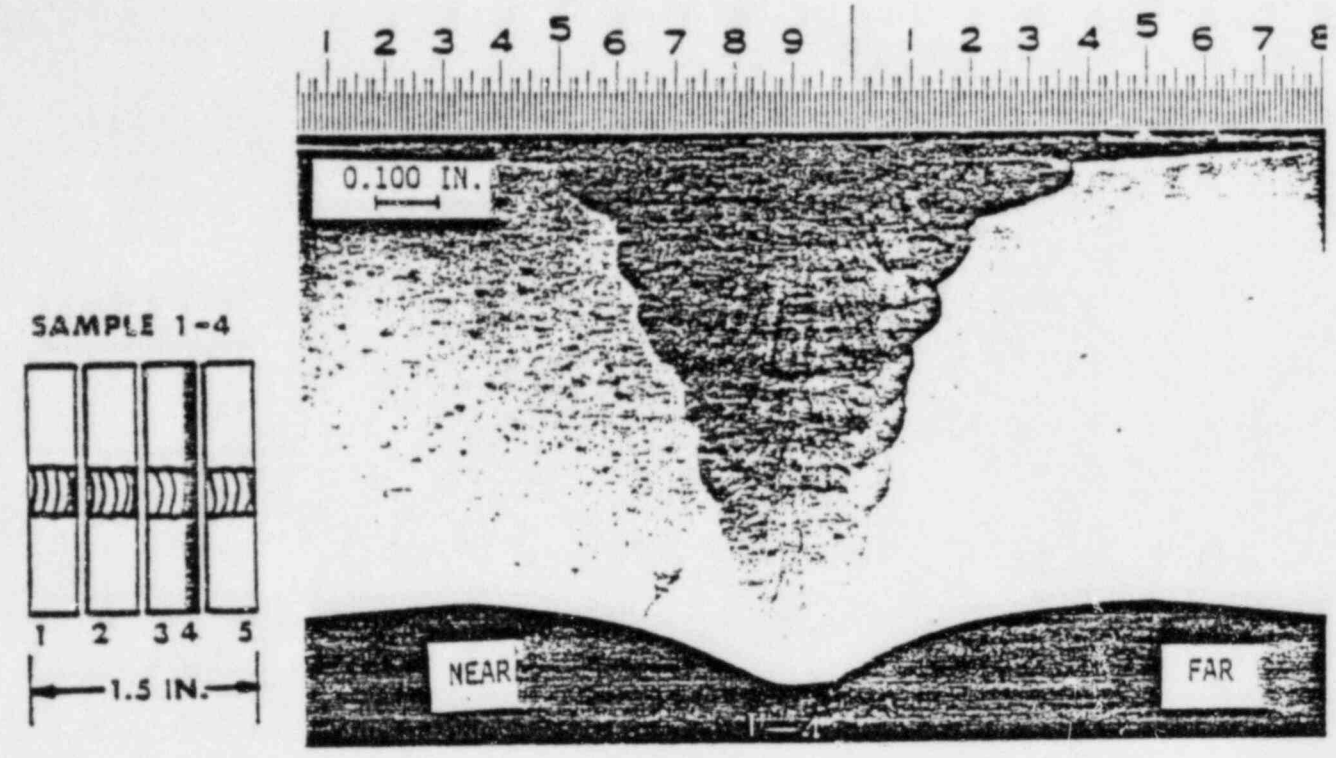
1 2 3 4 5 6 7 8 9 1 2 3 4 5 6 7 8
0.100 IN.
SAMPLE 1-4
1 2 3 4 5
1.5 IN.
NEAR
FAR

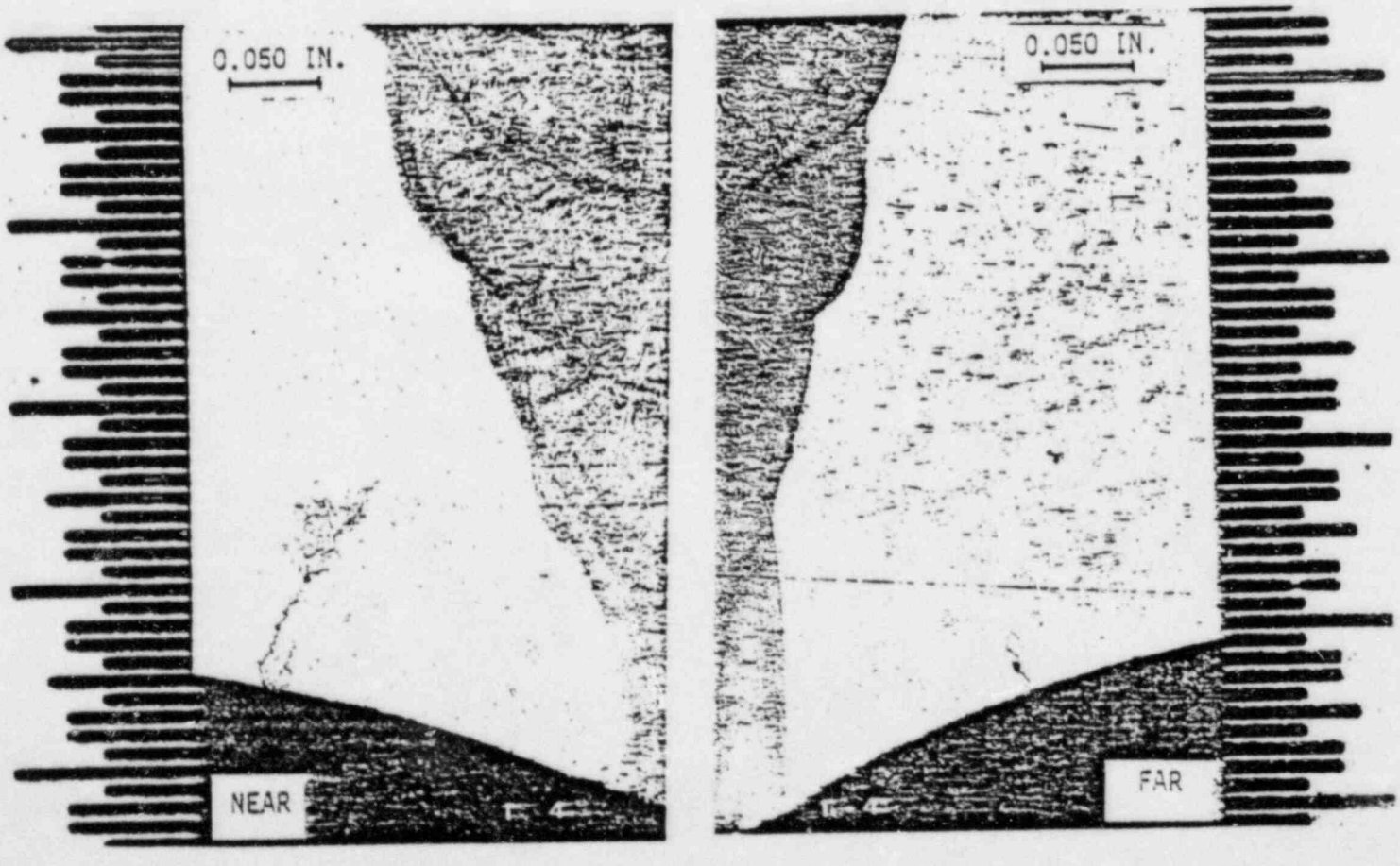
0.050 IN.
NEAR
0.050 IN.
FAR

SAMPLE 1-5

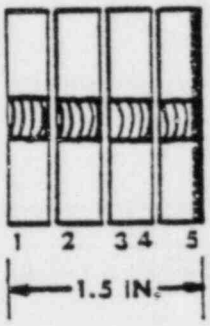

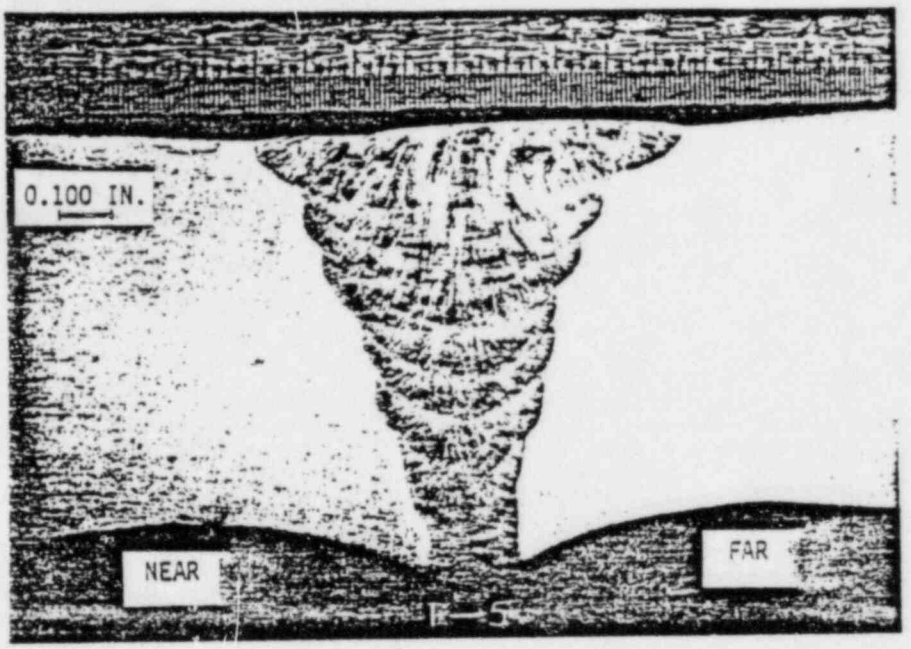

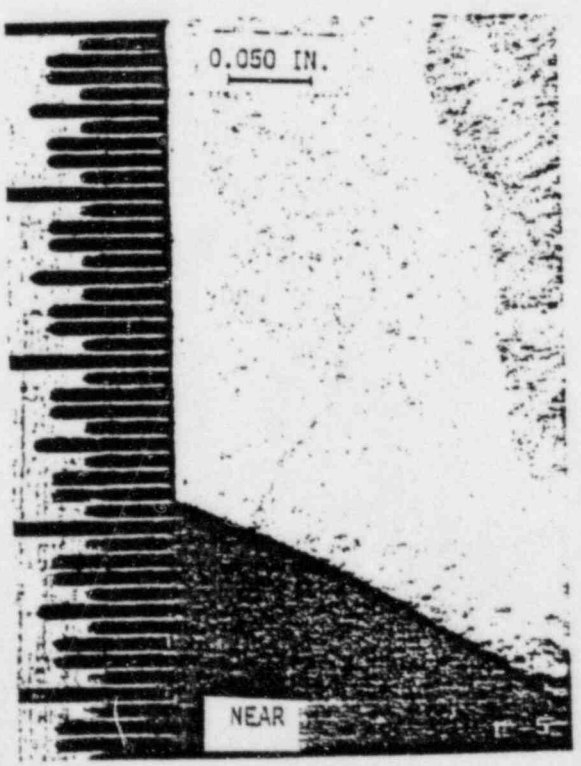

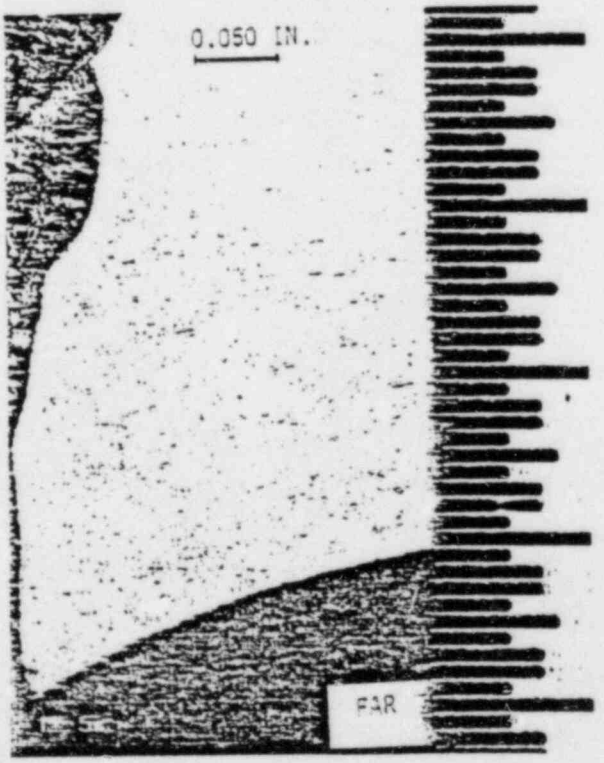

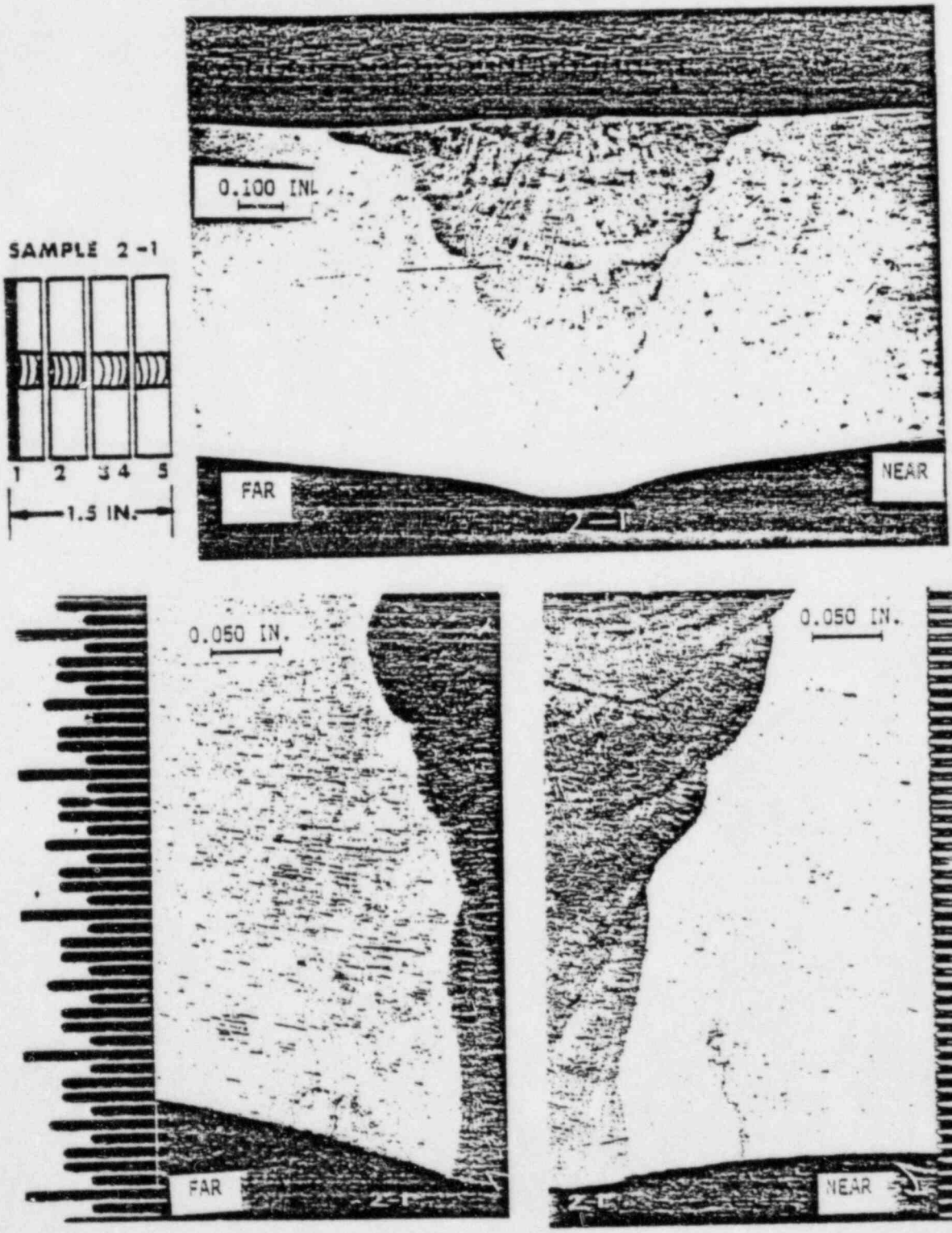
SAMPLE 2-1
1 2 3 4 5
1.5 IN.
0.100 IN.
FAR
NEAR
0.050 IN.
FAR
0.050 IN.
NEAR

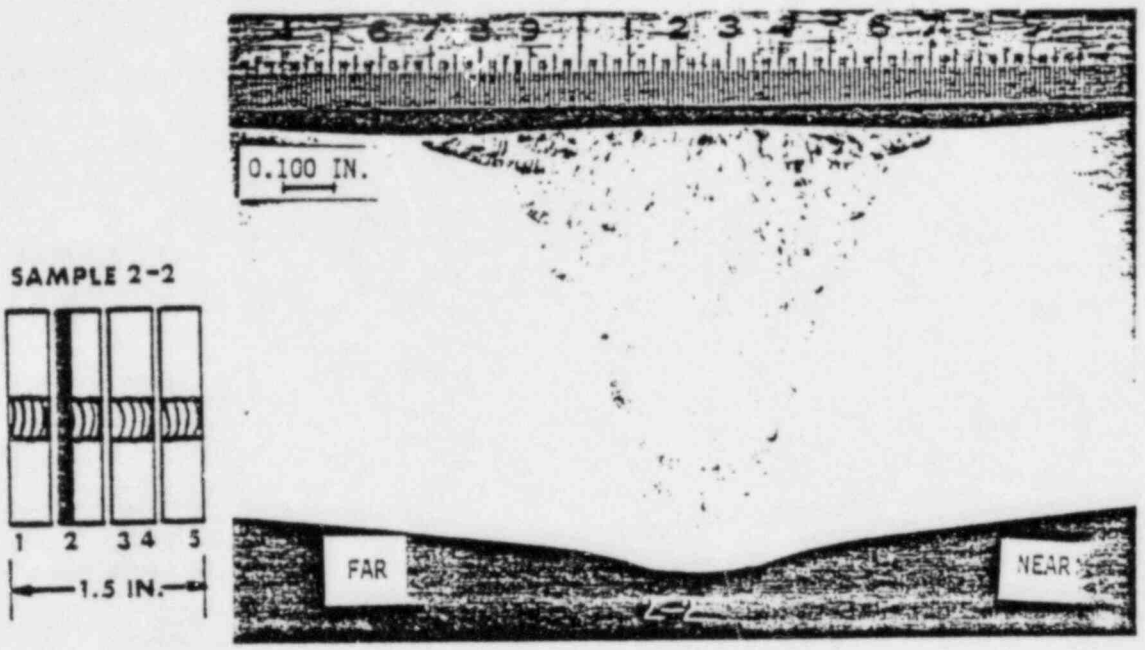
0.100 IN.
SAMPLE 2-2
1 2 3 4 5
1.5 IN.
FAR
NEAR

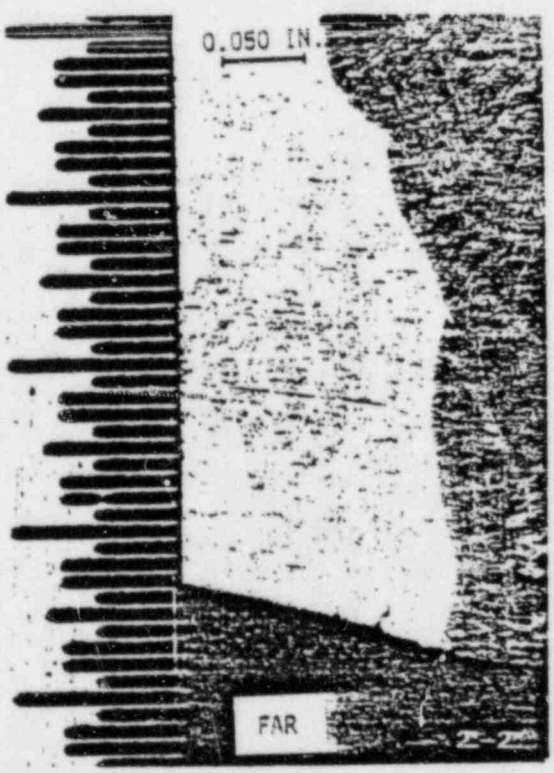
0.050 IN.
FAR
2-2

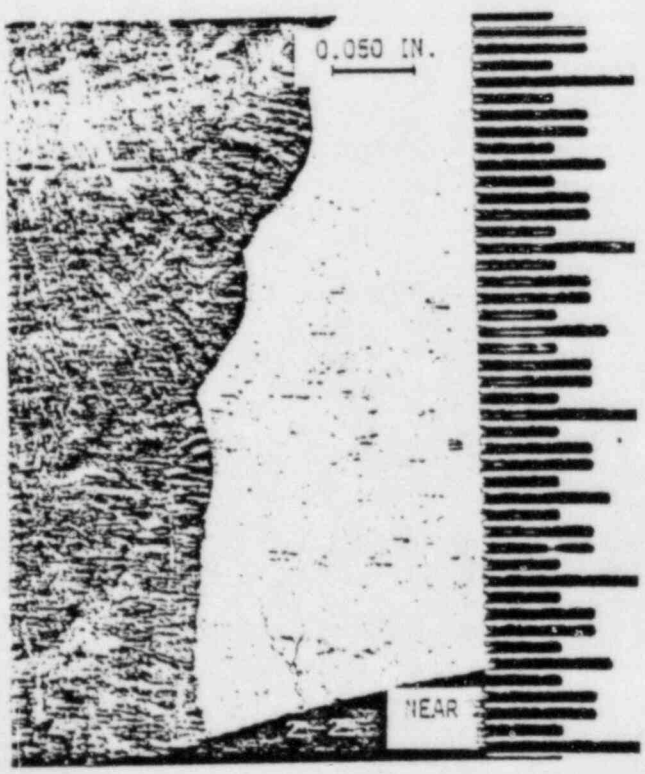
0.050 IN.
NEAR
2-2

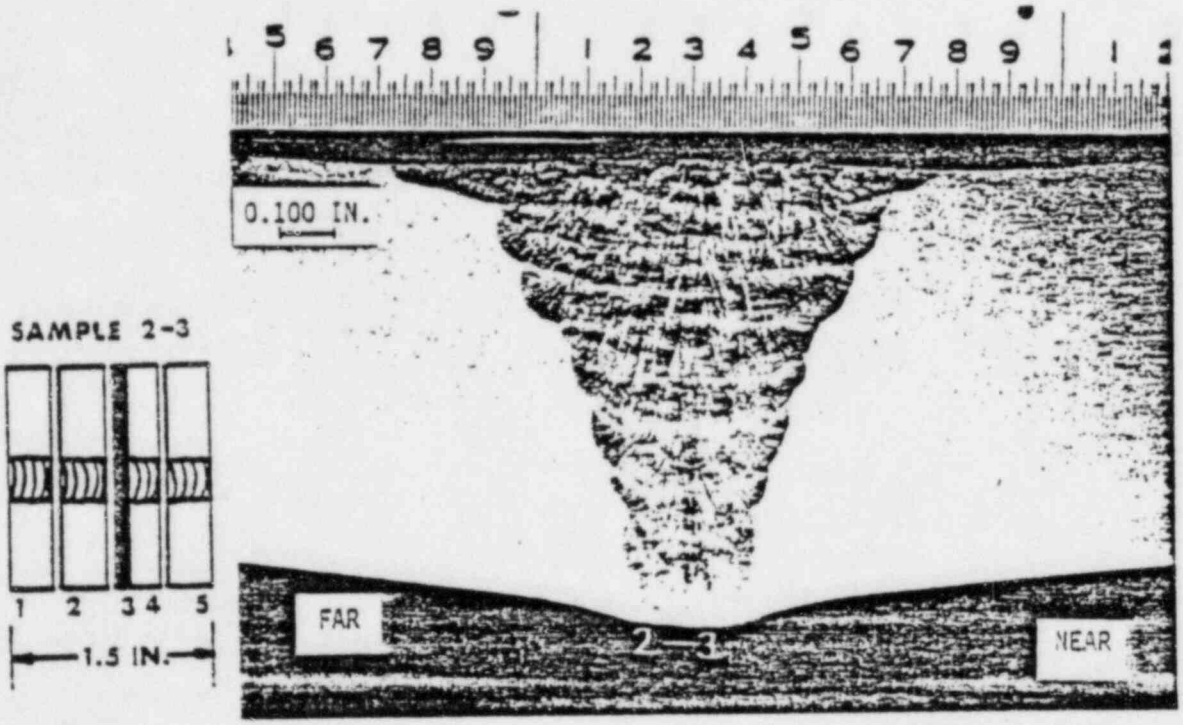
0.100 IN.
SAMPLE 2-3
1 2 3 4 5
1.5 IN.
FAR
NEAR

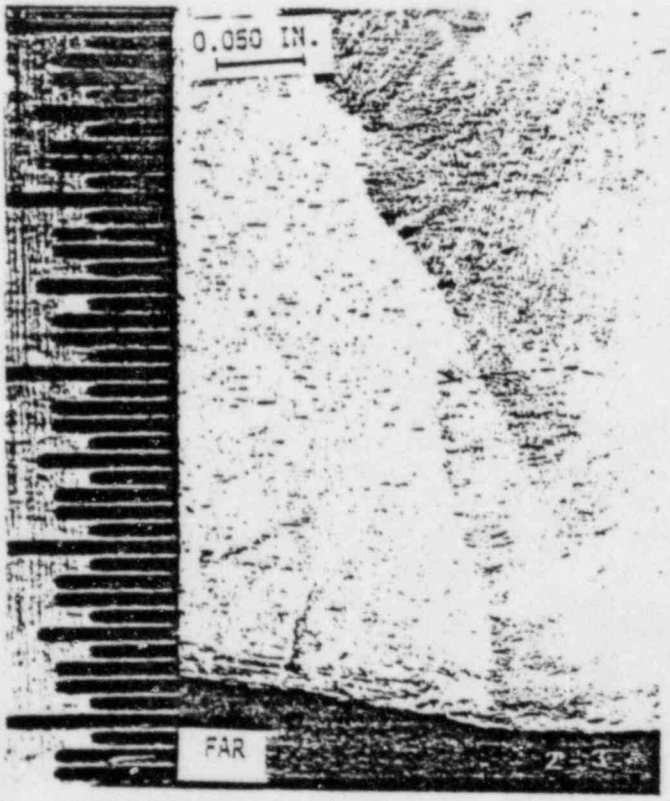
0.050 IN.
FAR

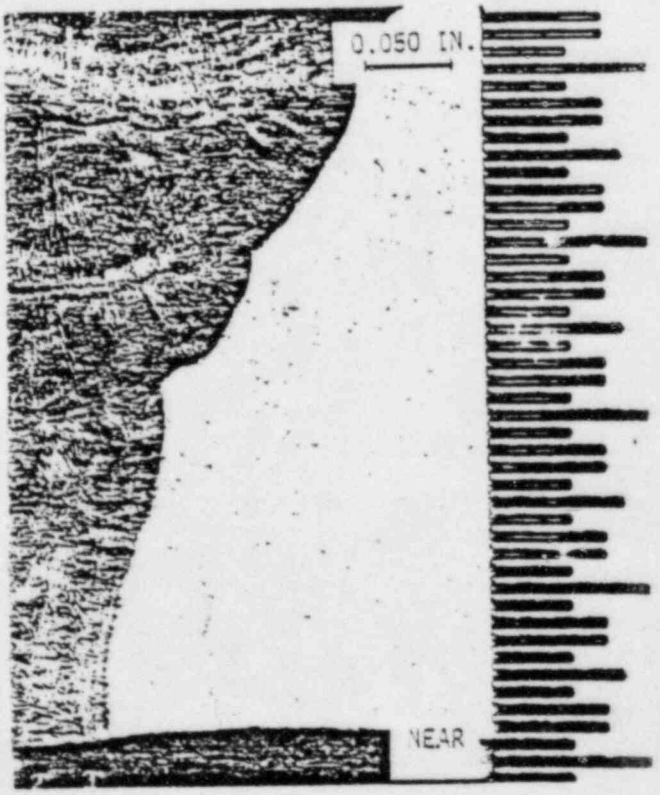
0.050 IN.
NEAR

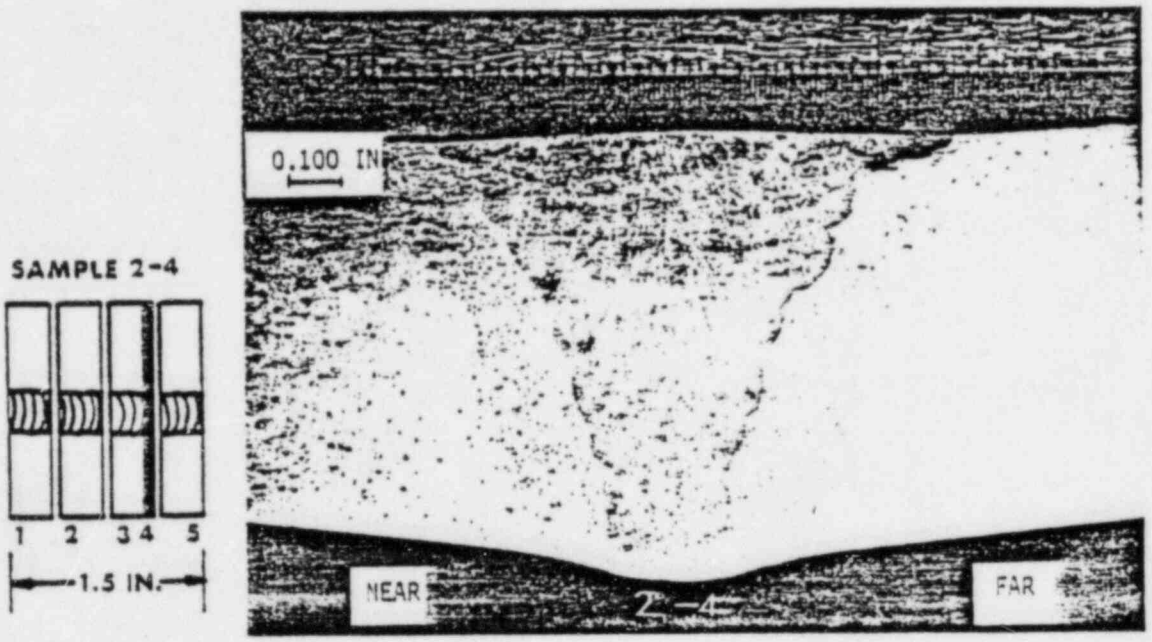
SAMPLE 2-4
1 2 3 4 5
1.5 IN.
0.100 IN.
NEAR
FAR
2-4

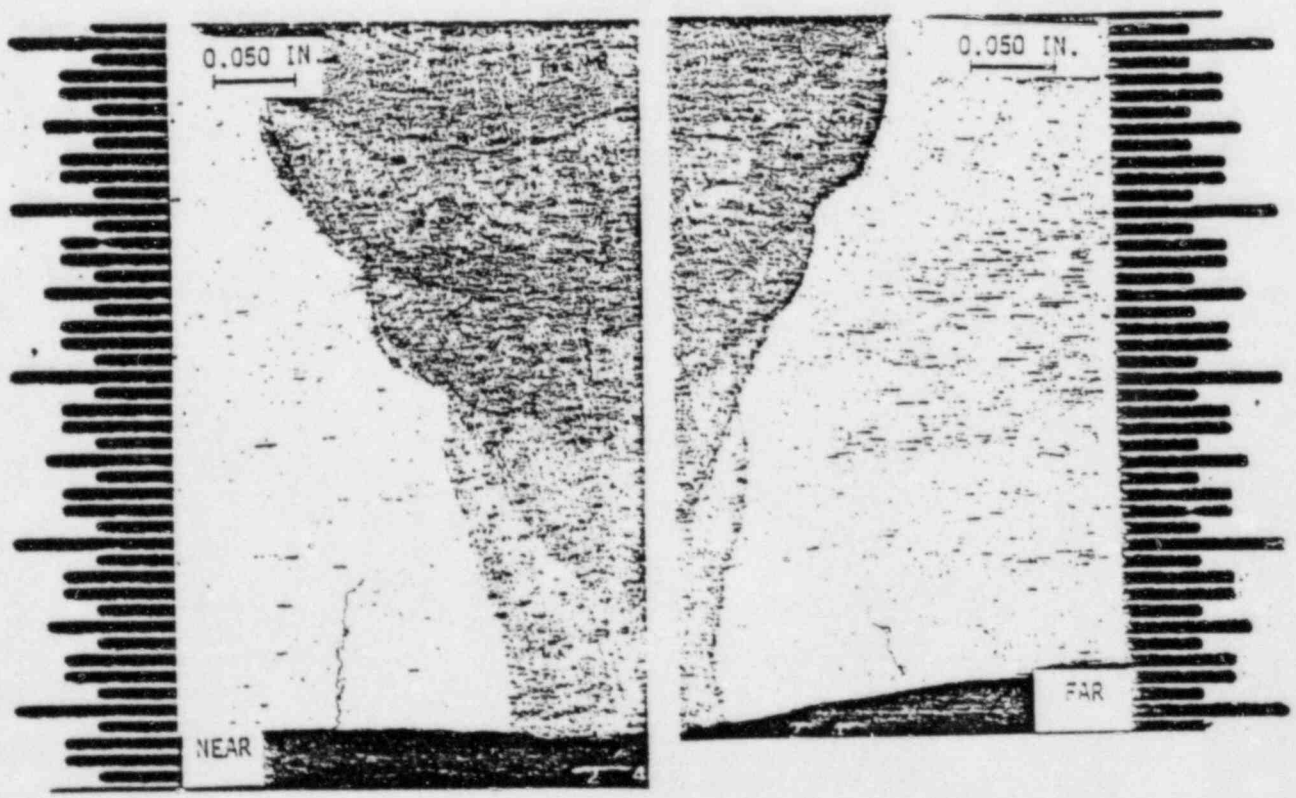
0.050 IN.
NEAR
2-4
0.050 IN.
FAR

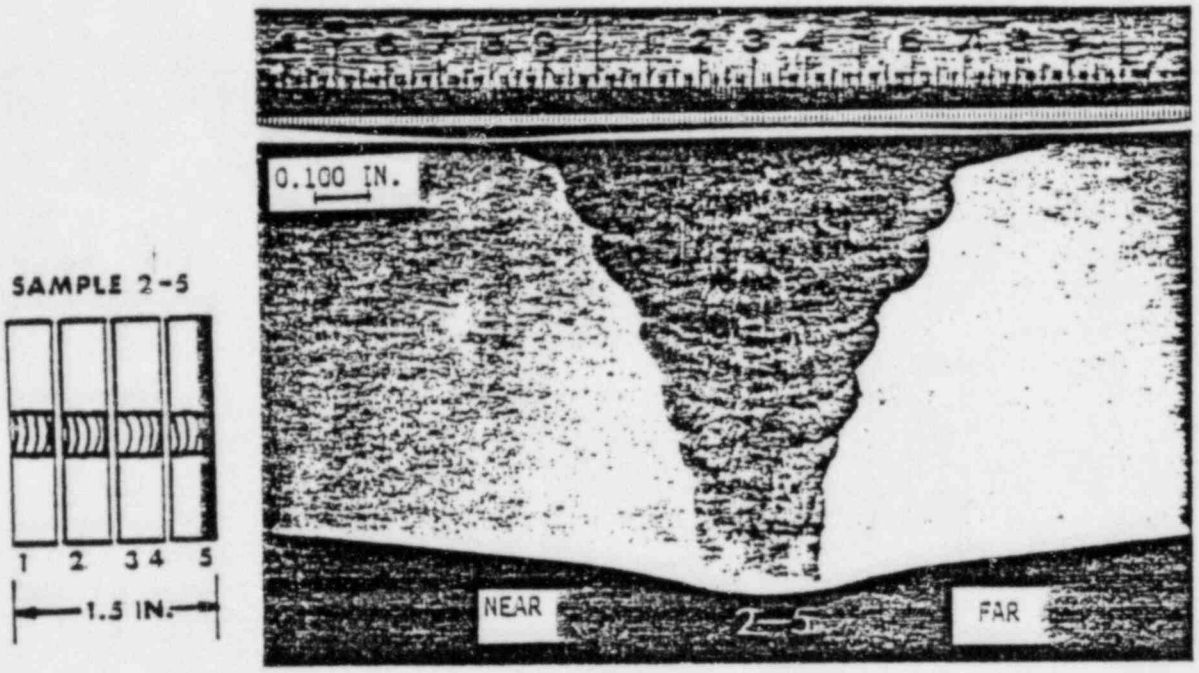
SAMPLE 2-5
1 2 3 4 5
1.5 IN.
0.100 IN.
NEAR
2-5
FAR

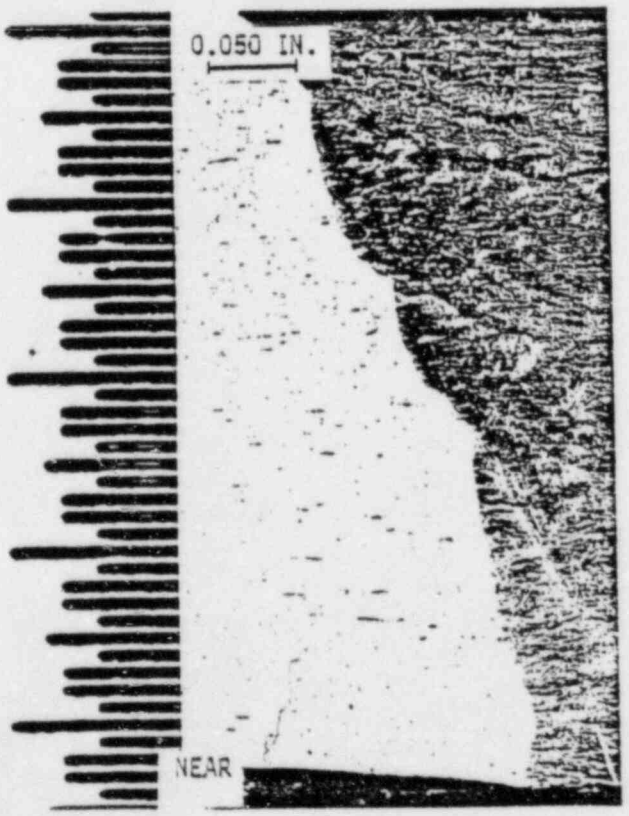
0.050 IN.
NEAR

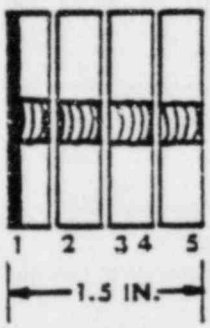
SAMPLE 6-1
1 2 3 4 5
1.5 IN.

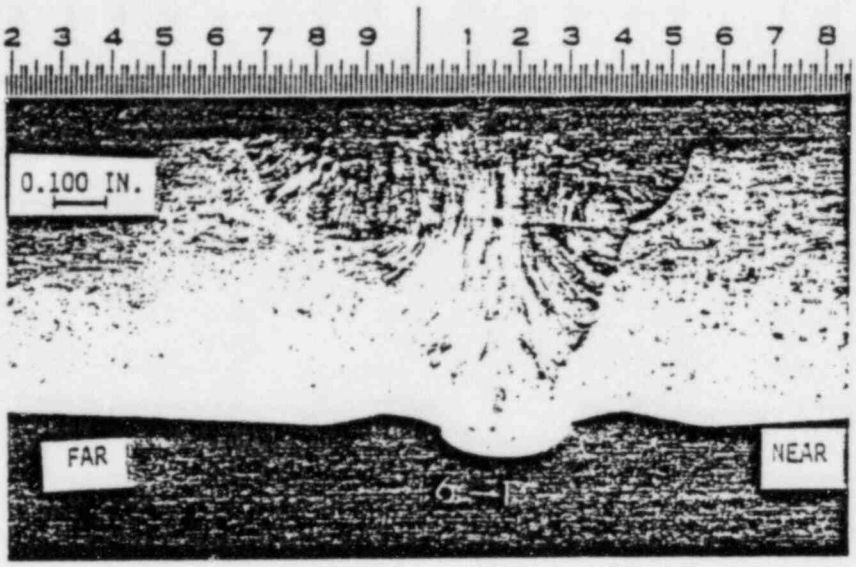
2 3 4 5 6 7 8 9 1 2 3 4 5 6 7 8
0.100 IN.
FAR
NEAR

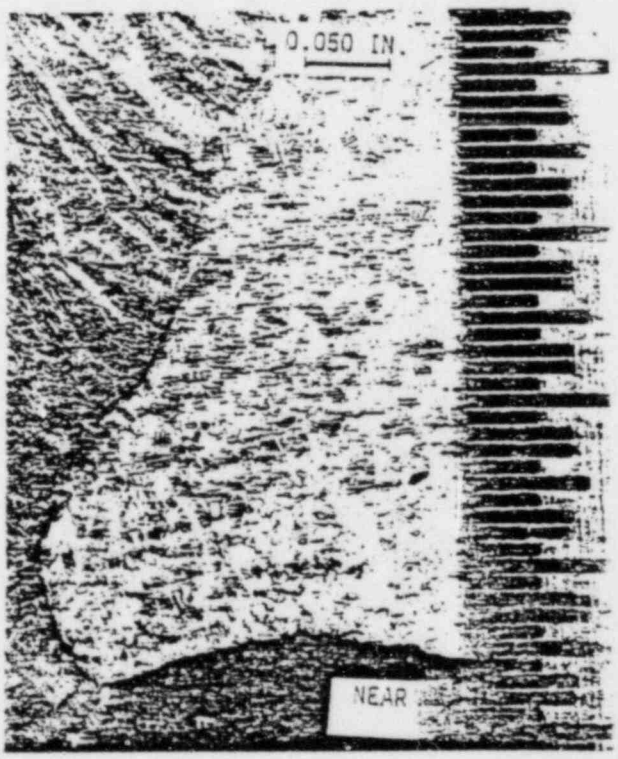
0.050 IN.
NEAR

SAMPLE 6-2

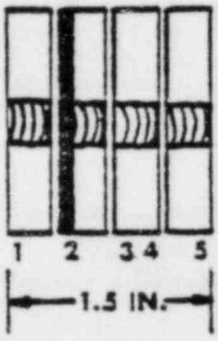

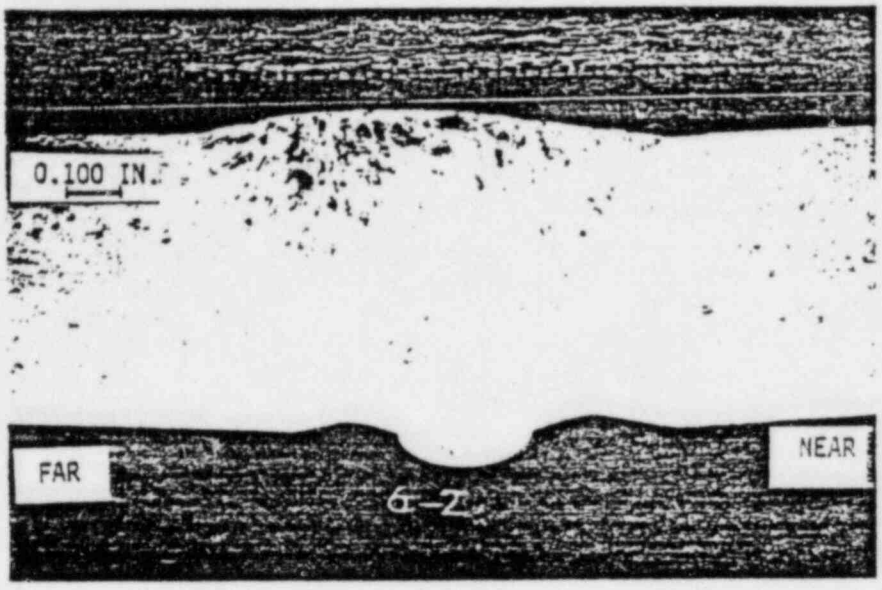

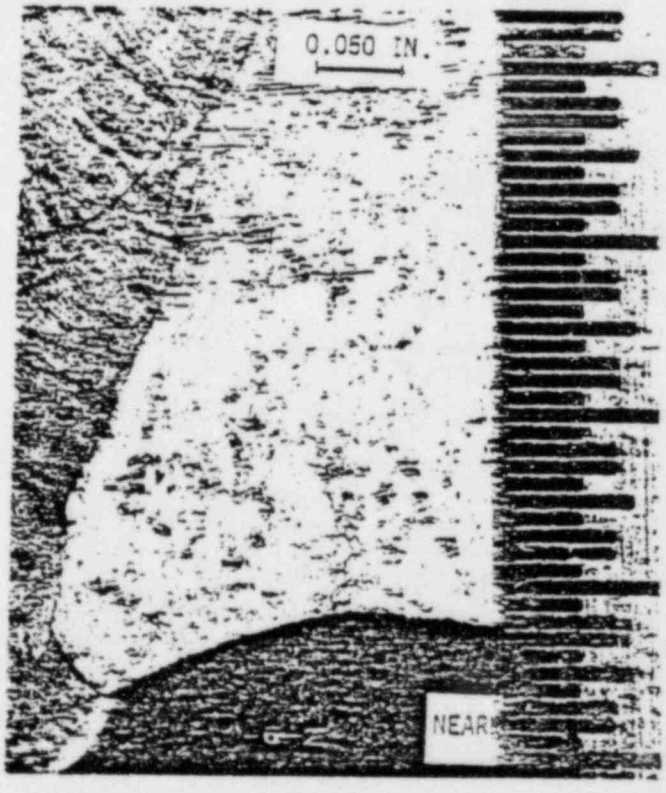

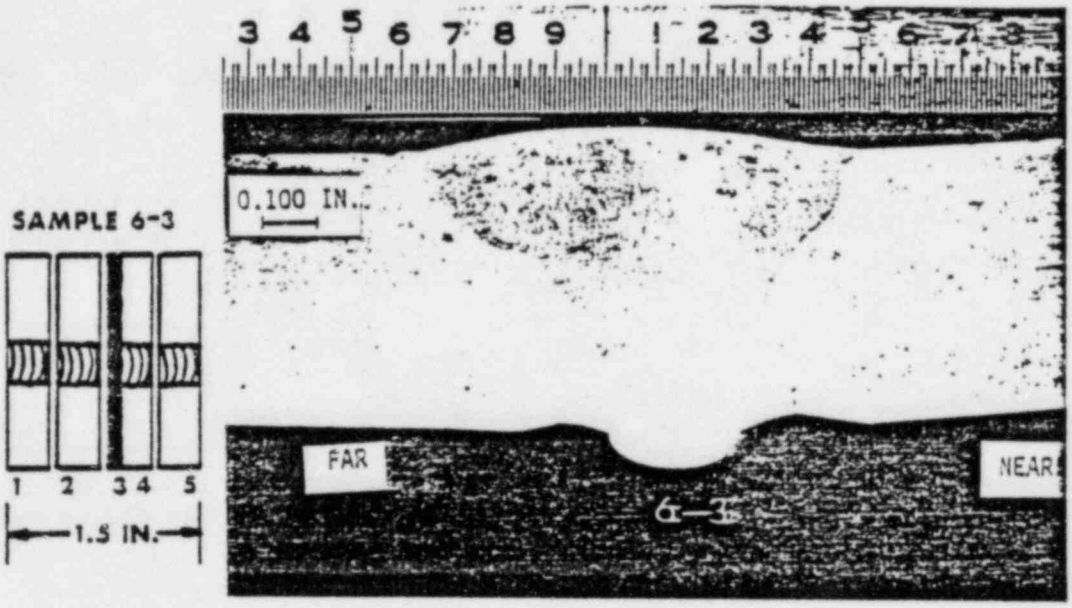
SAMPLE 6-3
1 2 3 4 5
1.5 IN.
0.100 IN.
FAR
NEAR
6-3

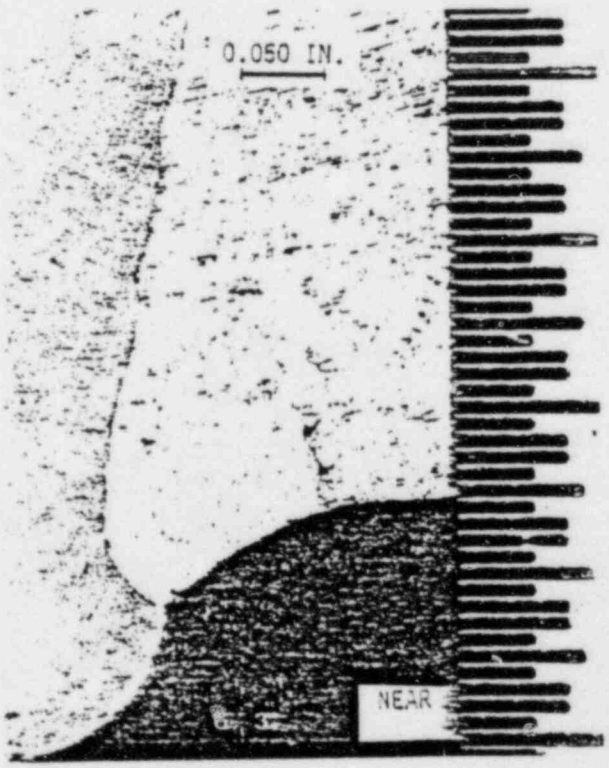
0.050 IN.
NEAR

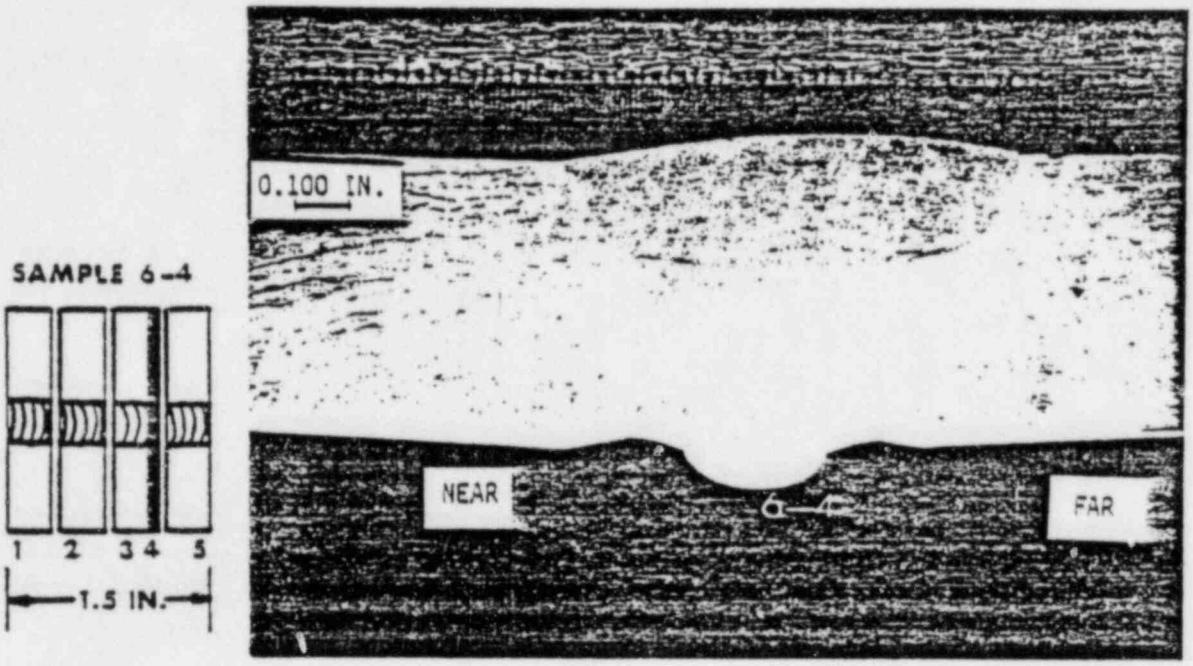
SAMPLE 6-4
1 2 3 4 5
1.5 IN.
0.100 IN.
NEAR
FAR

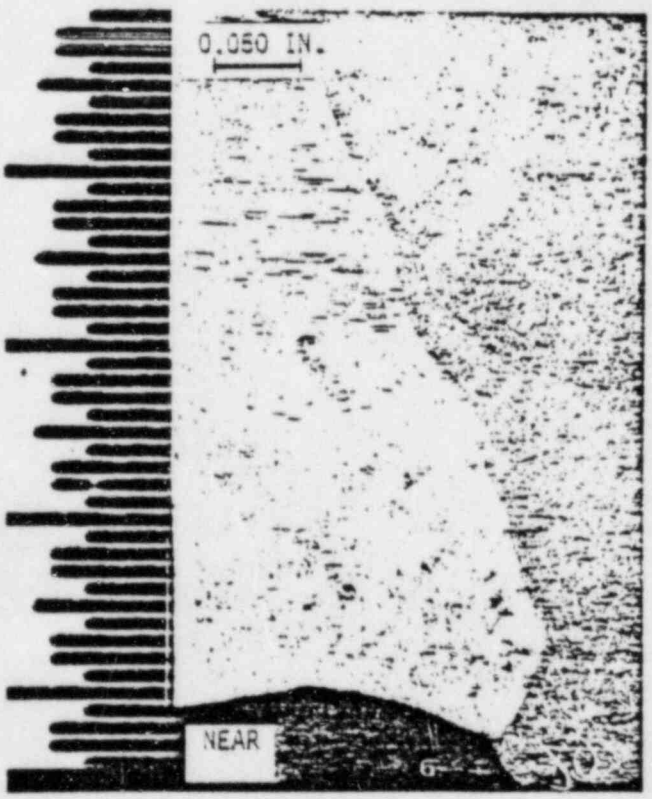
0.050 IN.
NEAR

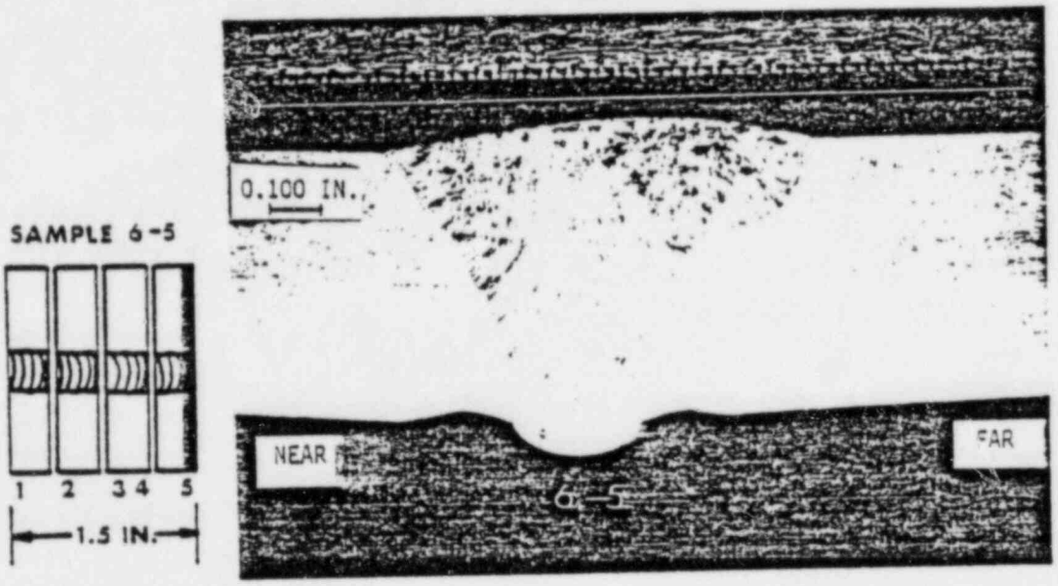
SAMPLE 6-5
1 2 3 4 5
1.5 IN.
0.100 IN.
NEAR
FAR
6-5

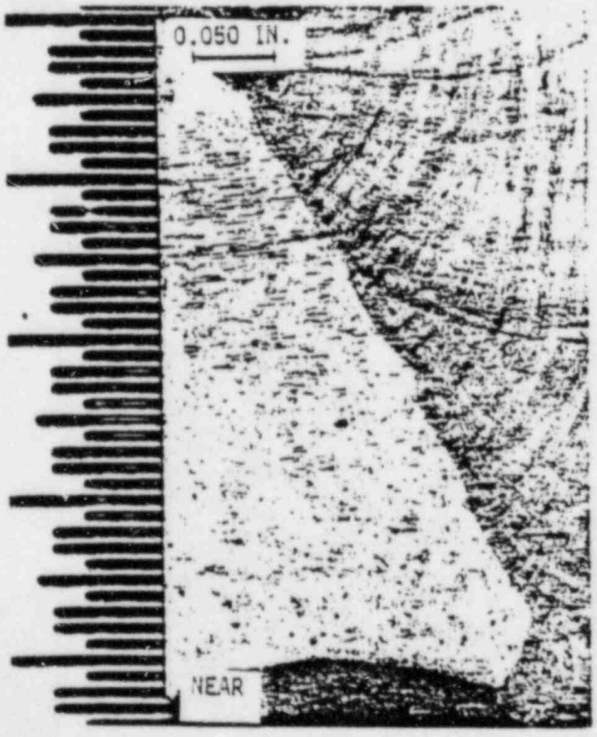
0.050 IN.
NEAR

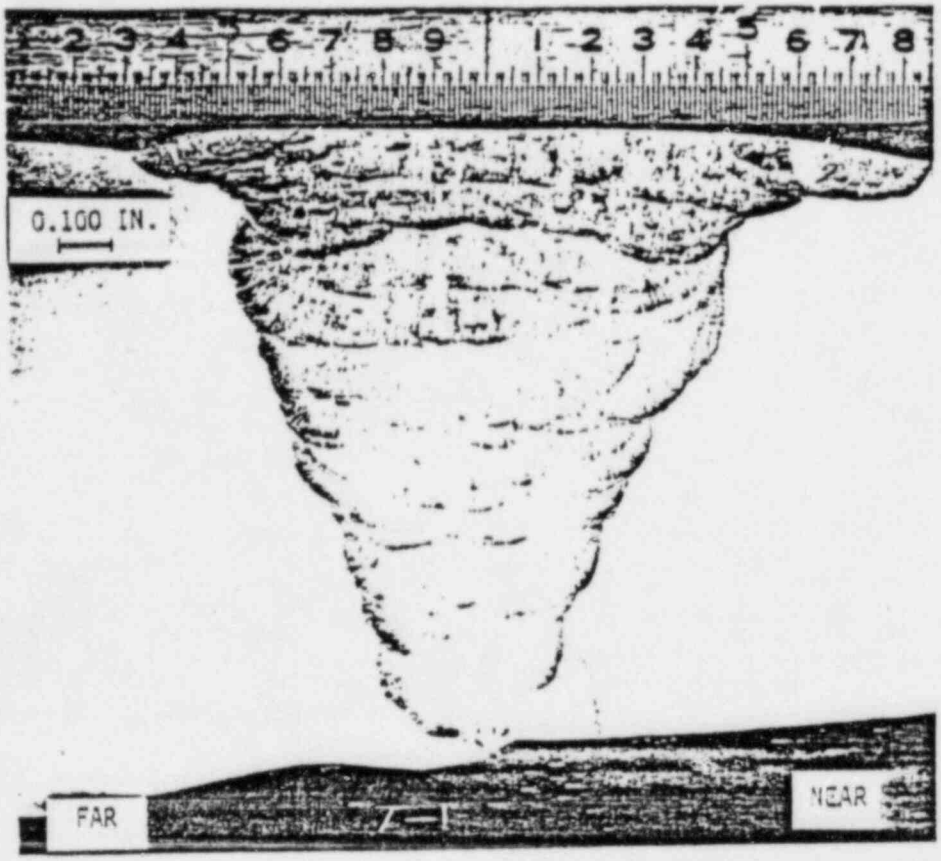

SAMPLE 7-1

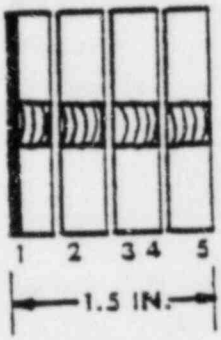

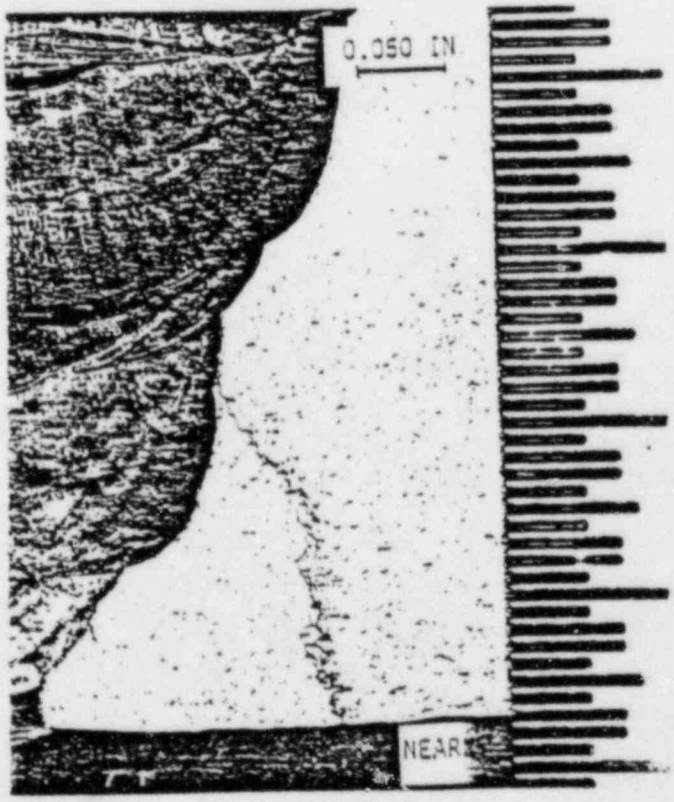

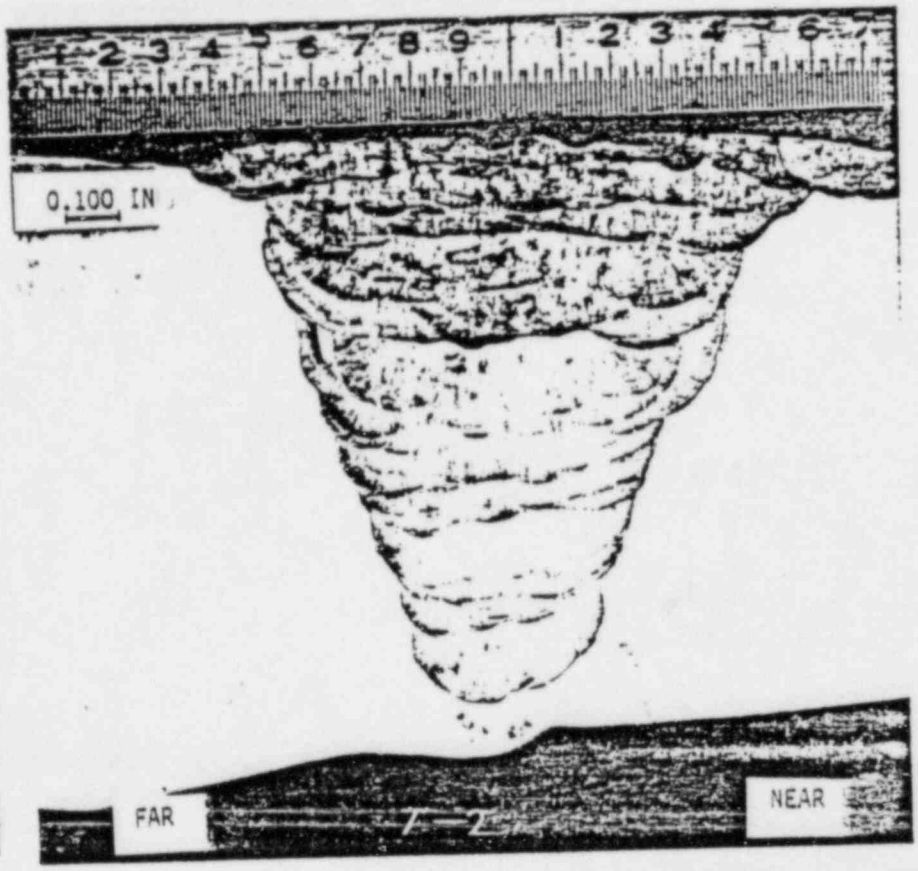

SAMPLE 7-2

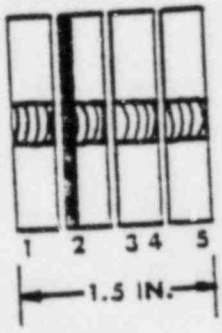

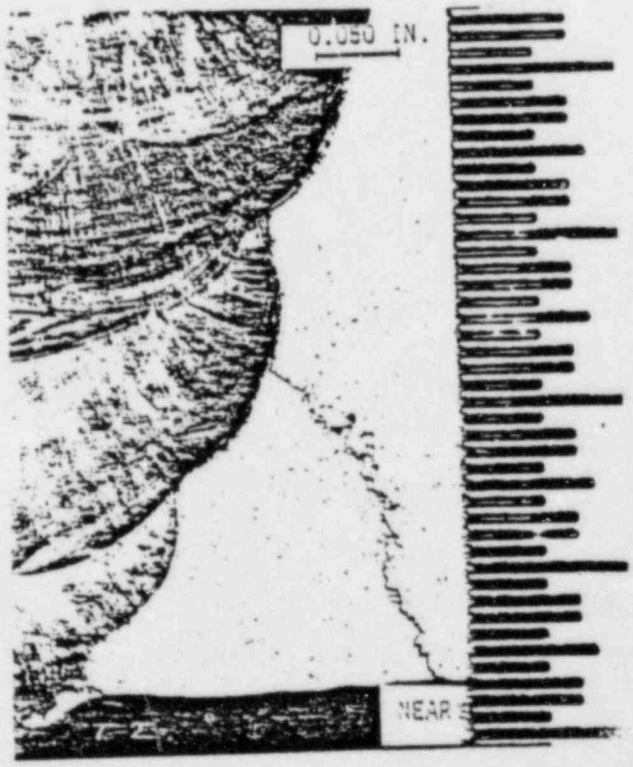

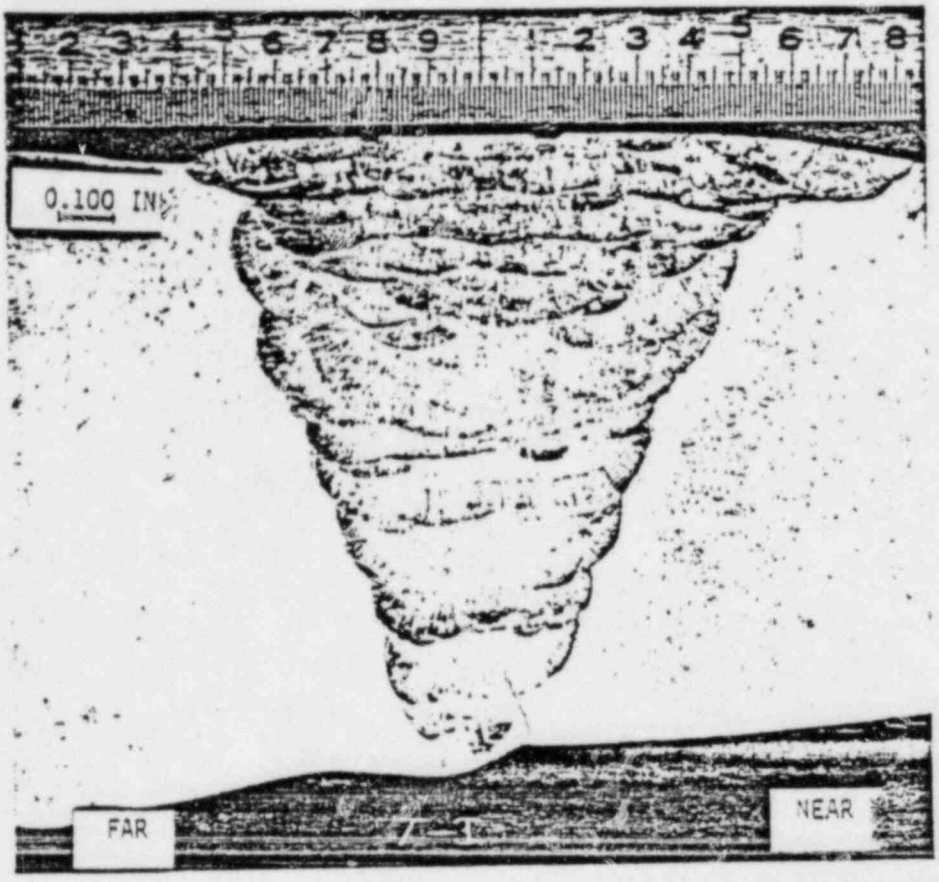

SAMPLE 7-3

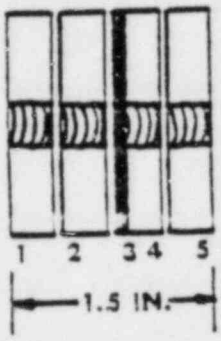

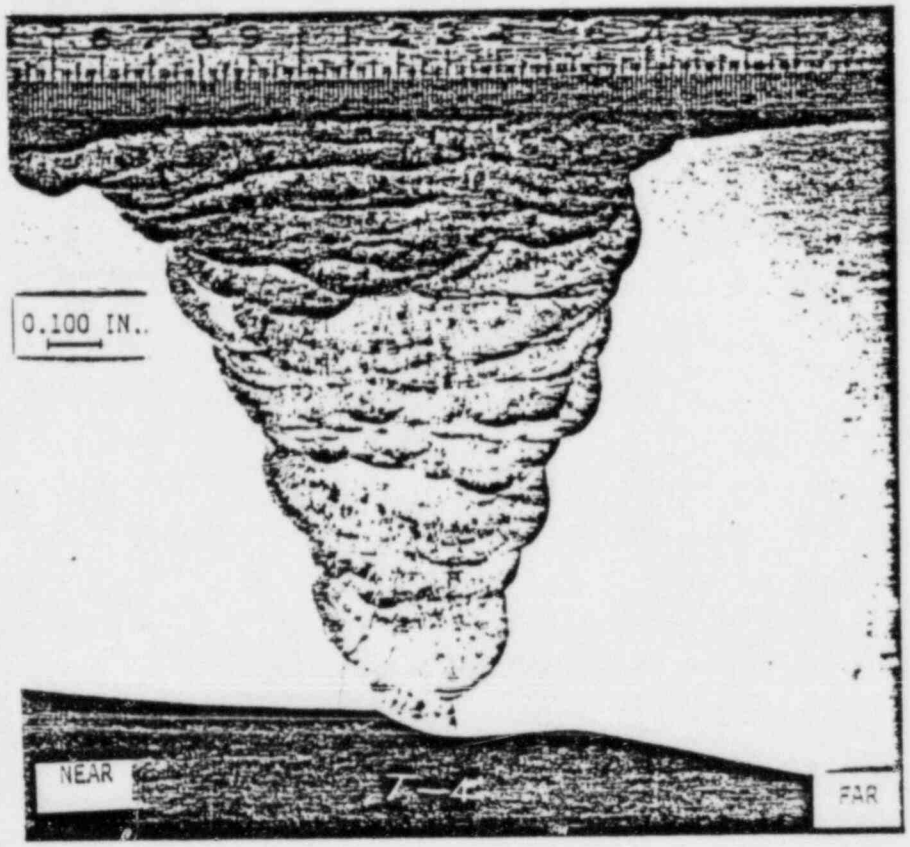

SAMPLE 7-4

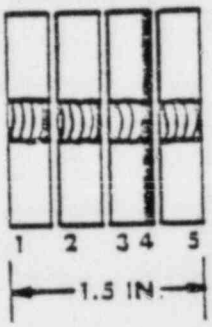

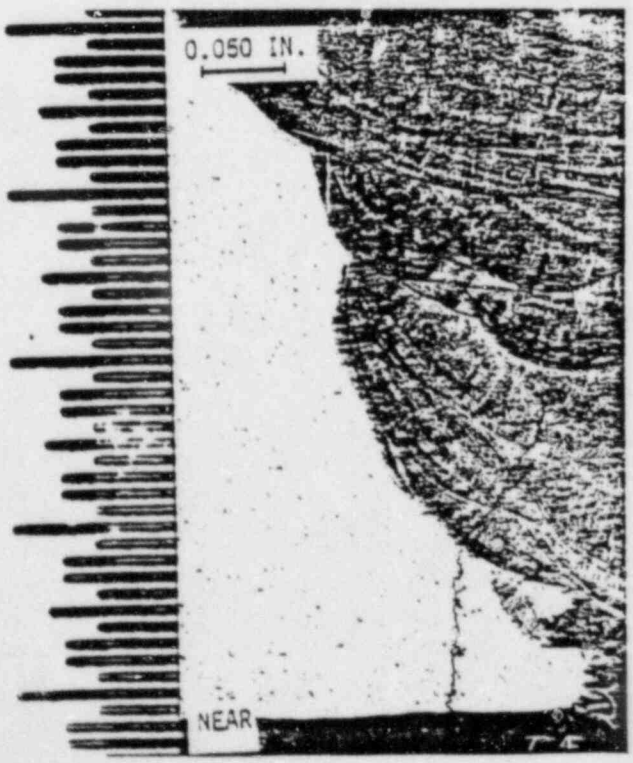

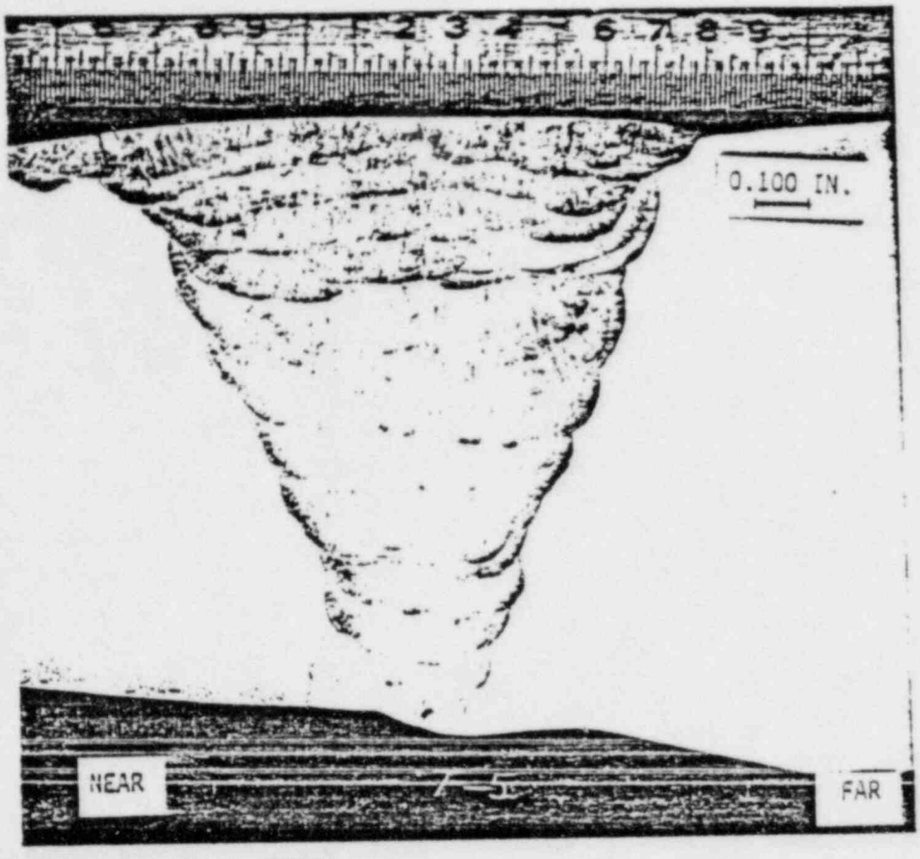

SAMPLE 7-5

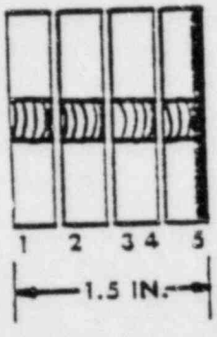

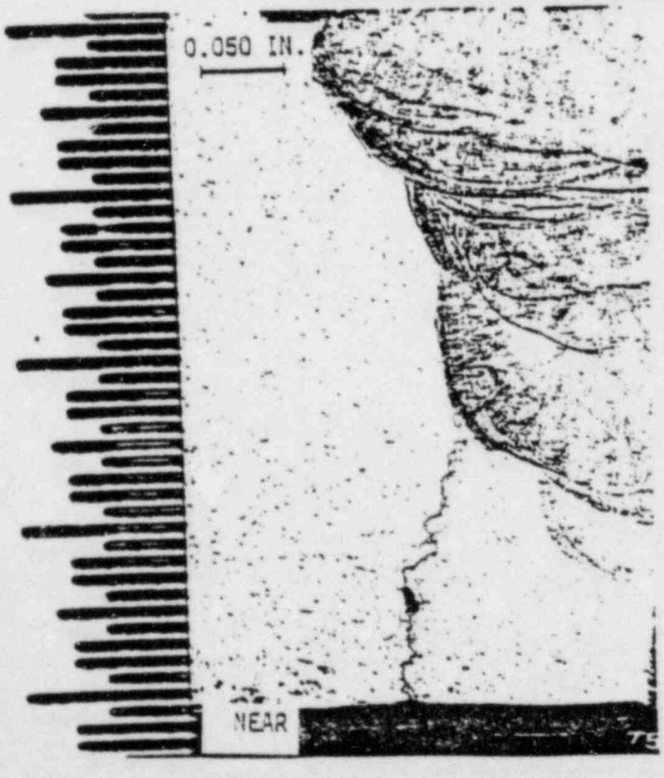

EPRI/NDE CENTER ROUND ROBIN ON ULTRASONIC SIZING OF IGSCC , JULY 1983

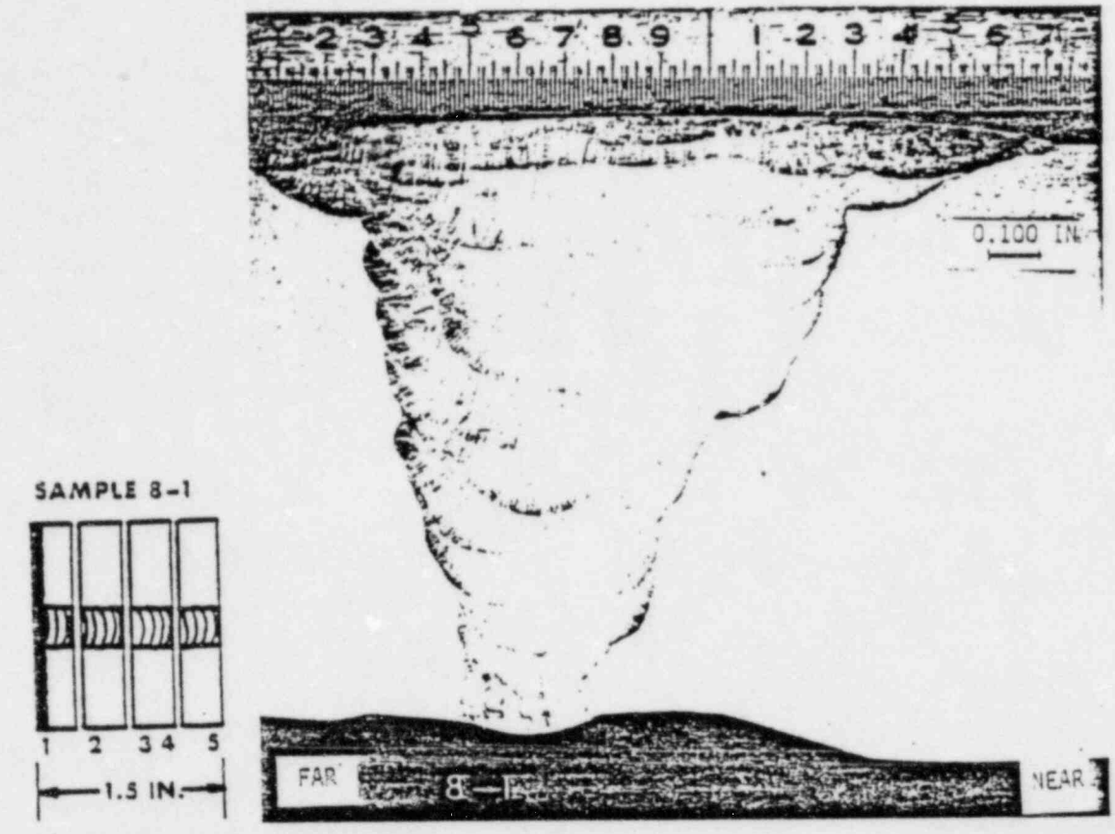

SAMPLE 8-1

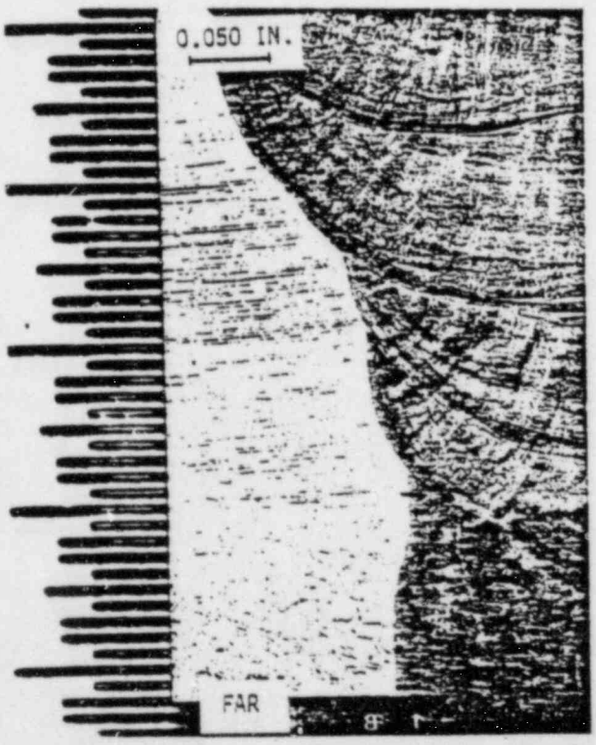

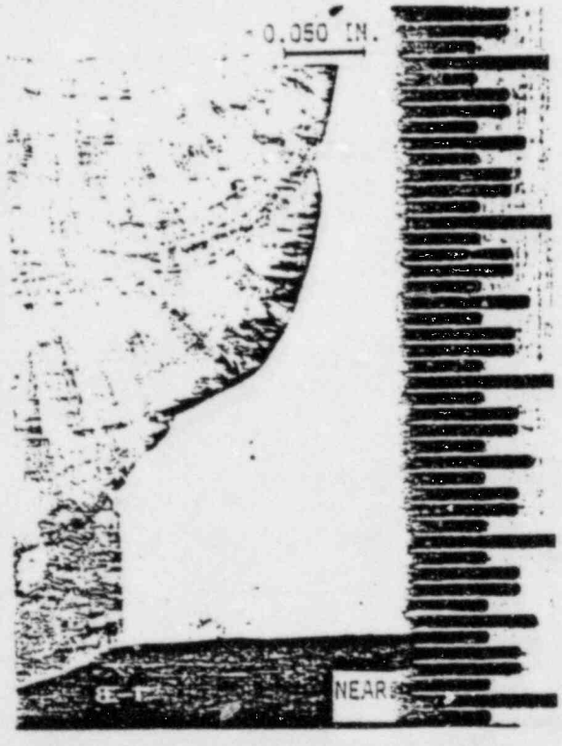

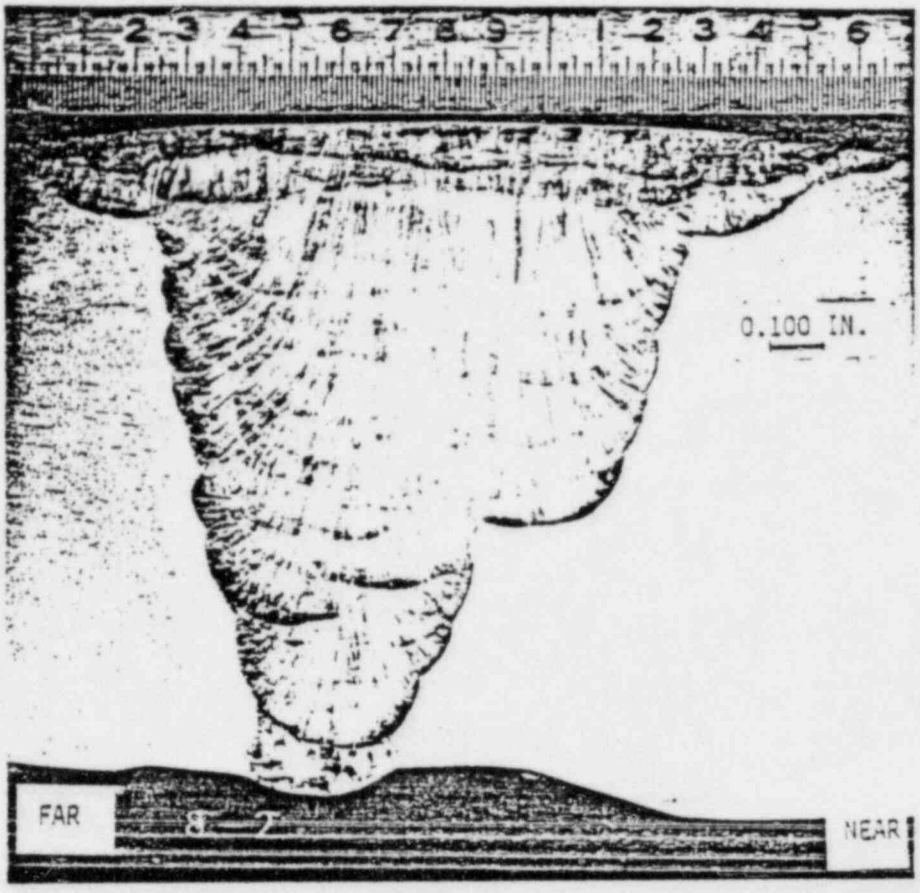

SAMPLE B-2

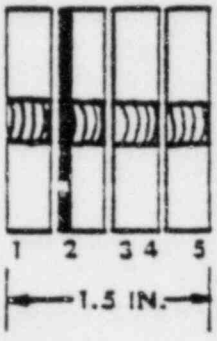

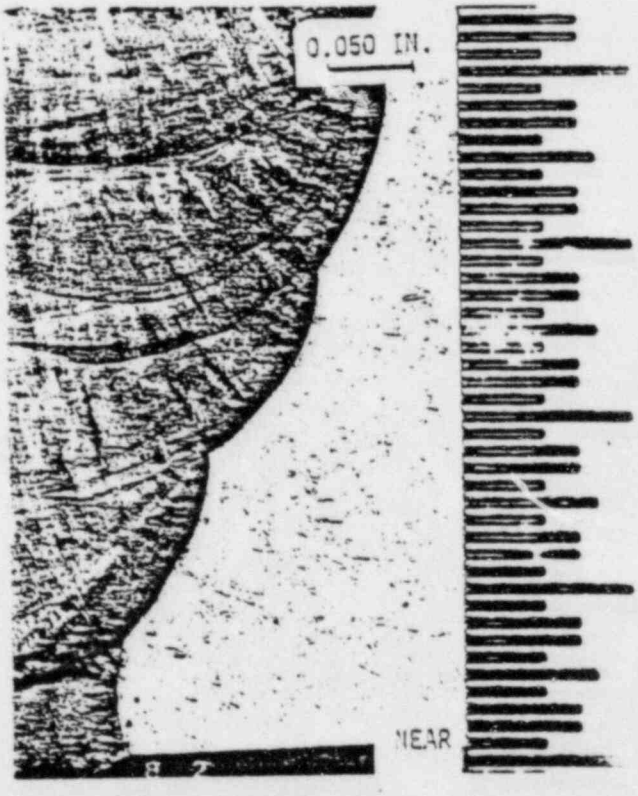

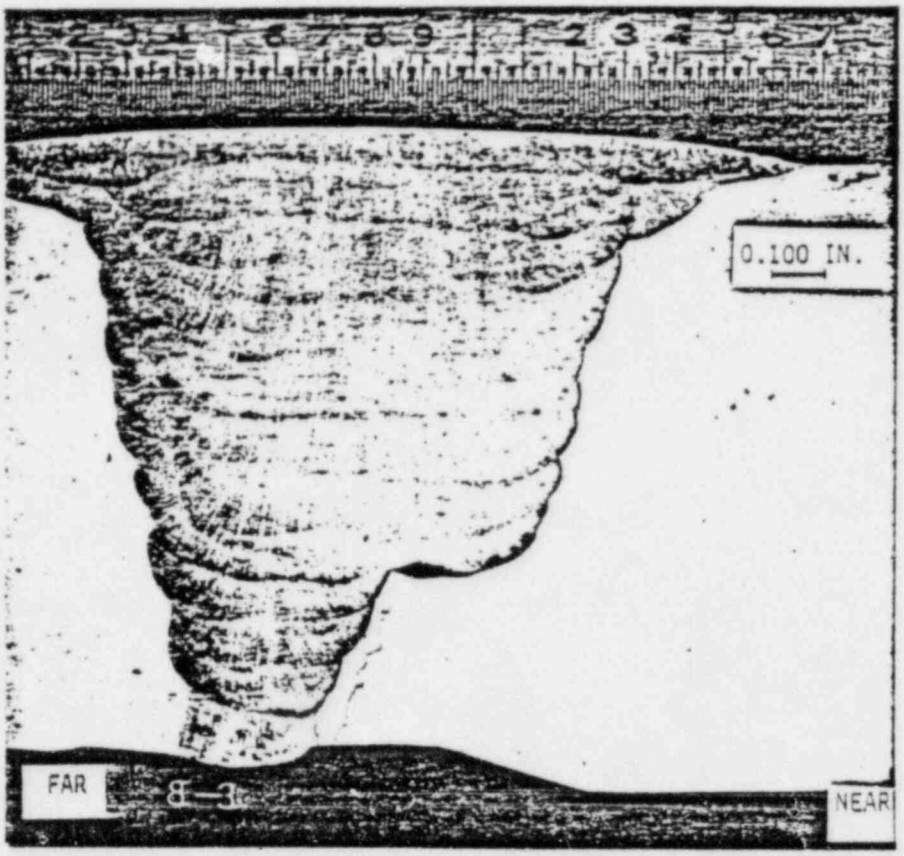

SAMPLE 8-3

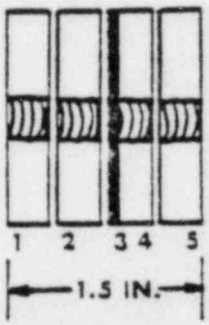

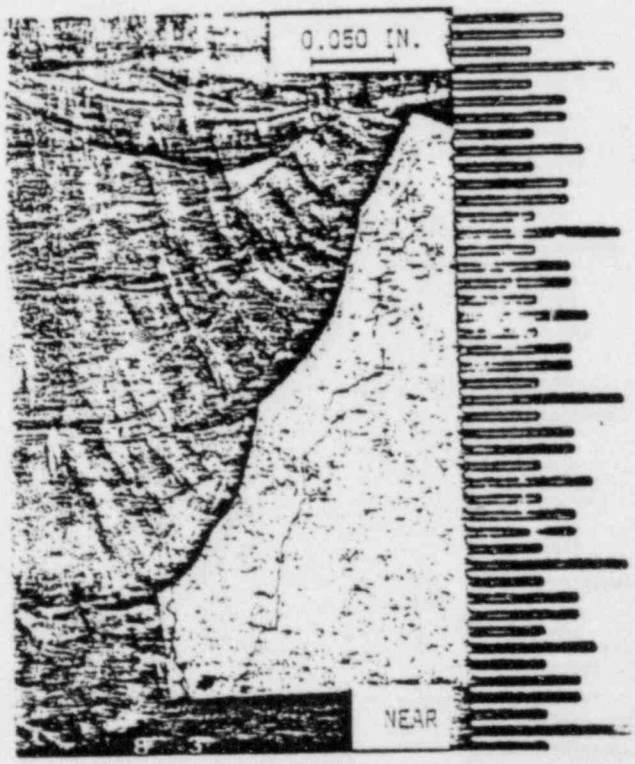

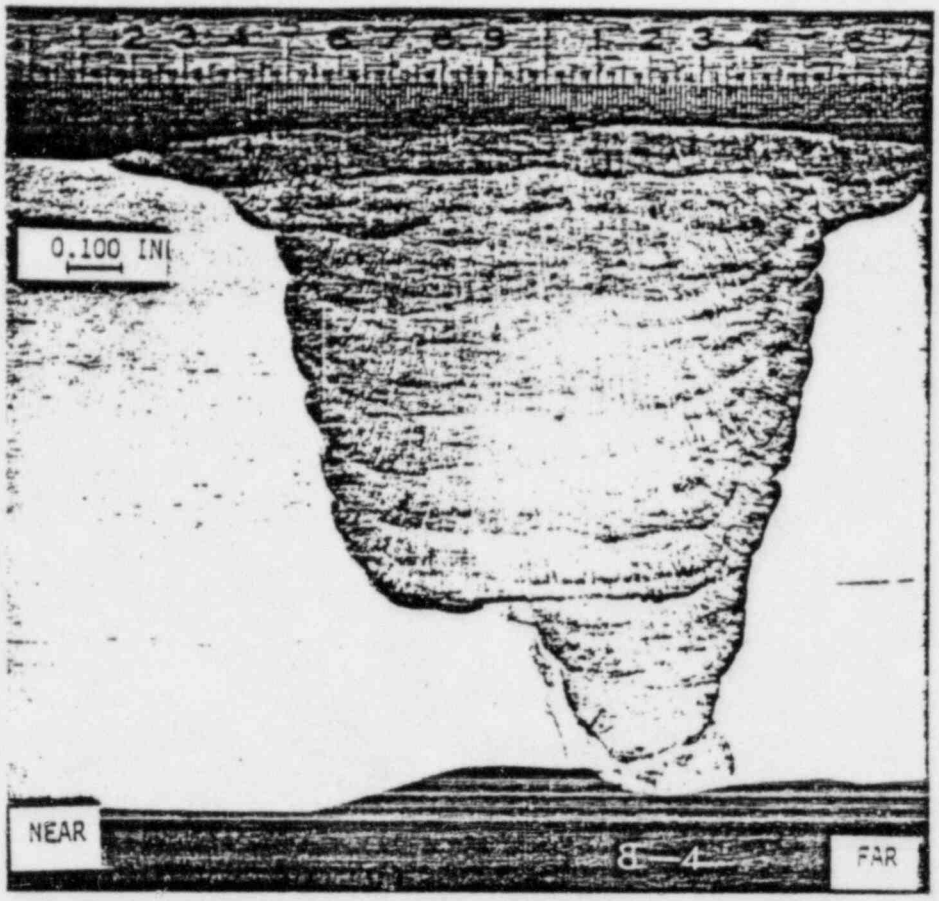

SAMPLE 8-4

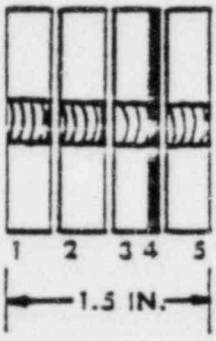

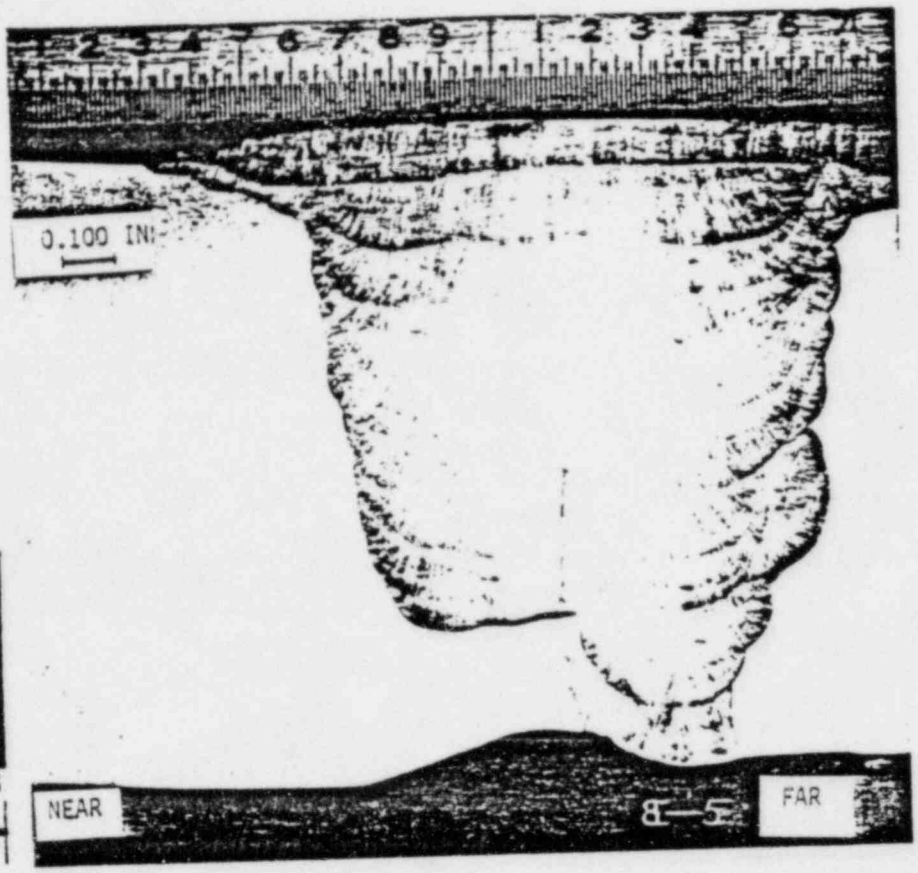

SAMPLE B-5

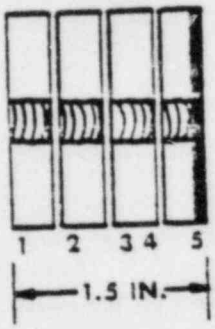

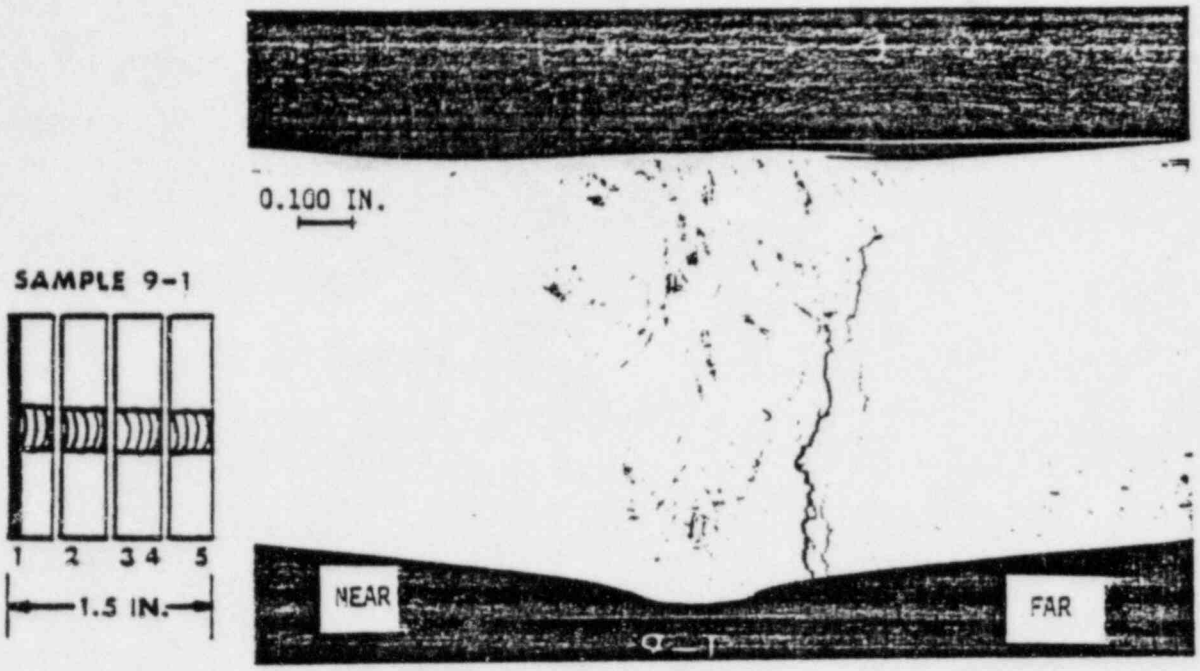
0.100 IN.
SAMPLE 9-1
1 2 3 4 5
1.5 IN.
NEAR
FAR

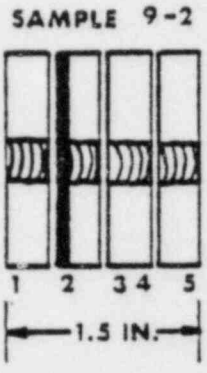
SAMPLE 9-2
1 2 3 4 5
1.5 IN.

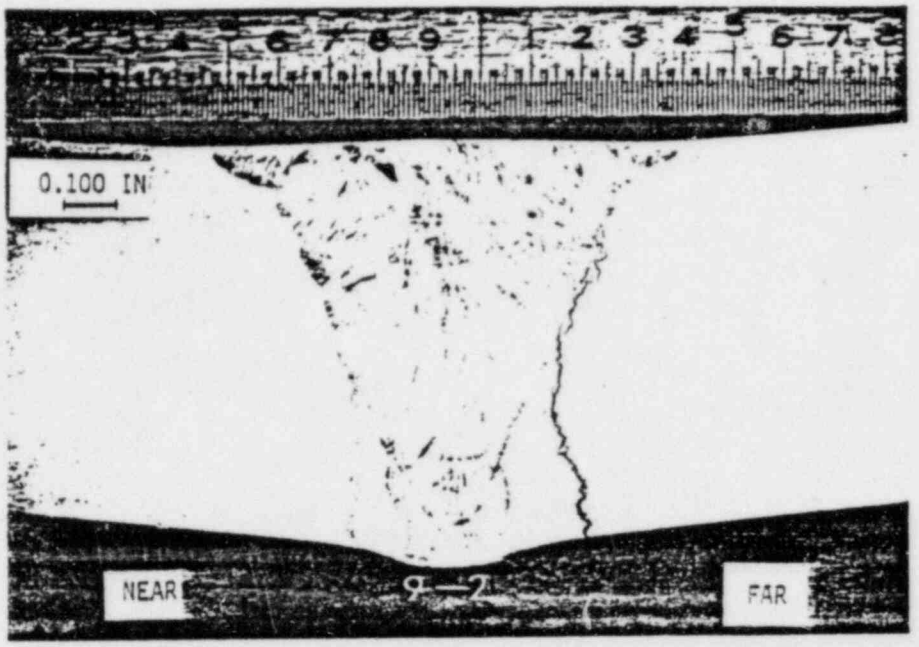
0.100 IN
NEAR
9-2
FAR

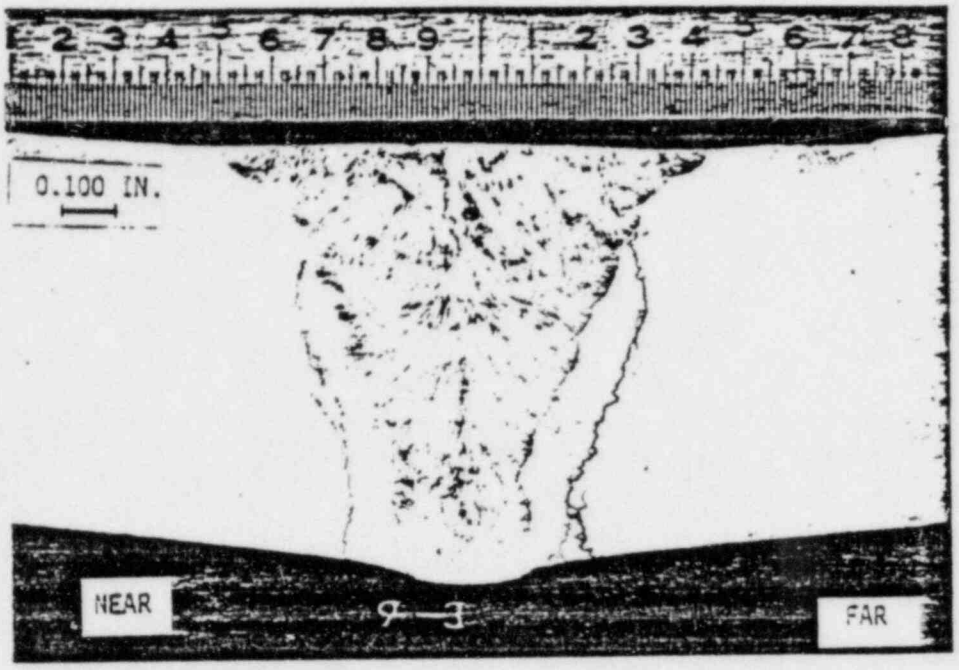

SAMPLE 9-3

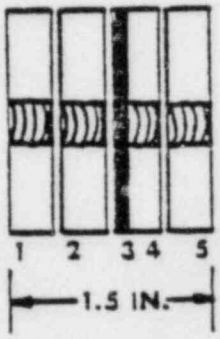

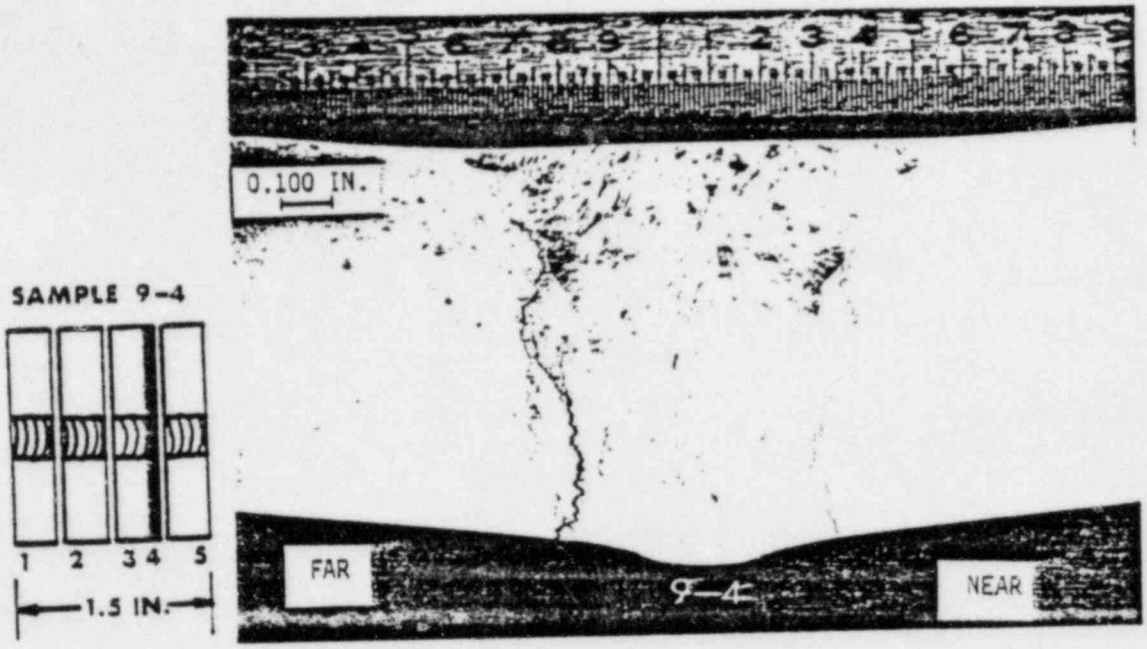
SAMPLE 9-4
1 2 3 4 5
1.5 IN.
0.100 IN.
FAR
9-4
NEAR

SAMPLE 9-5

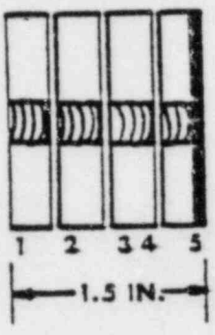

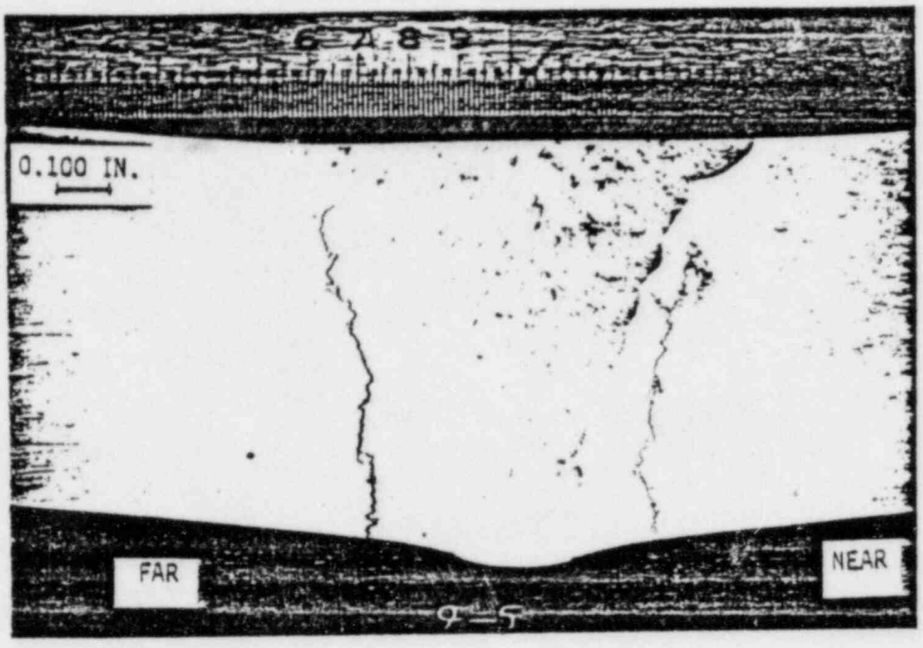

SAMPLE 10-1

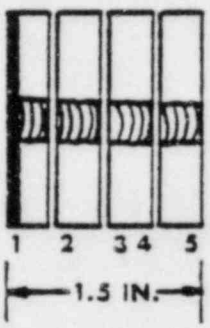

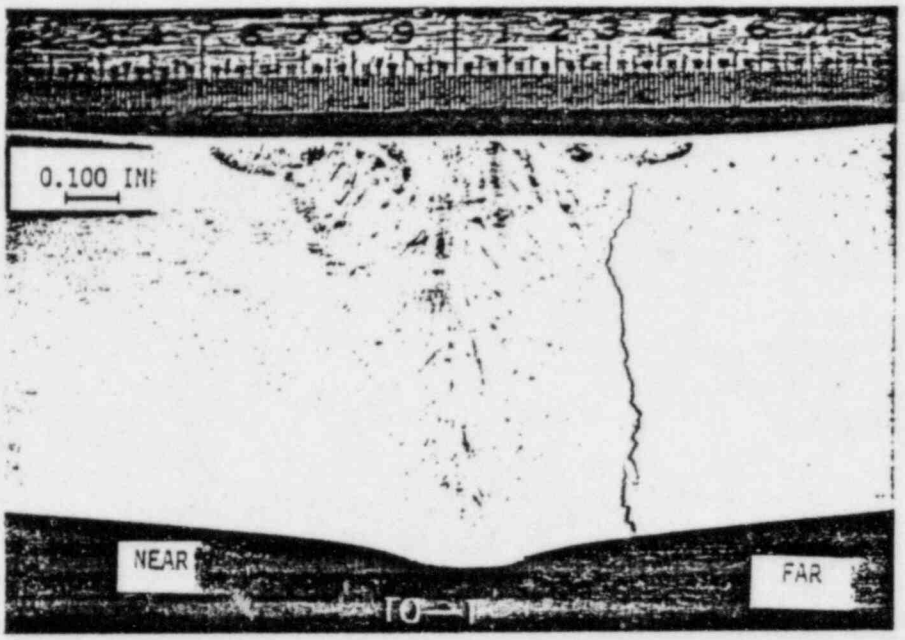

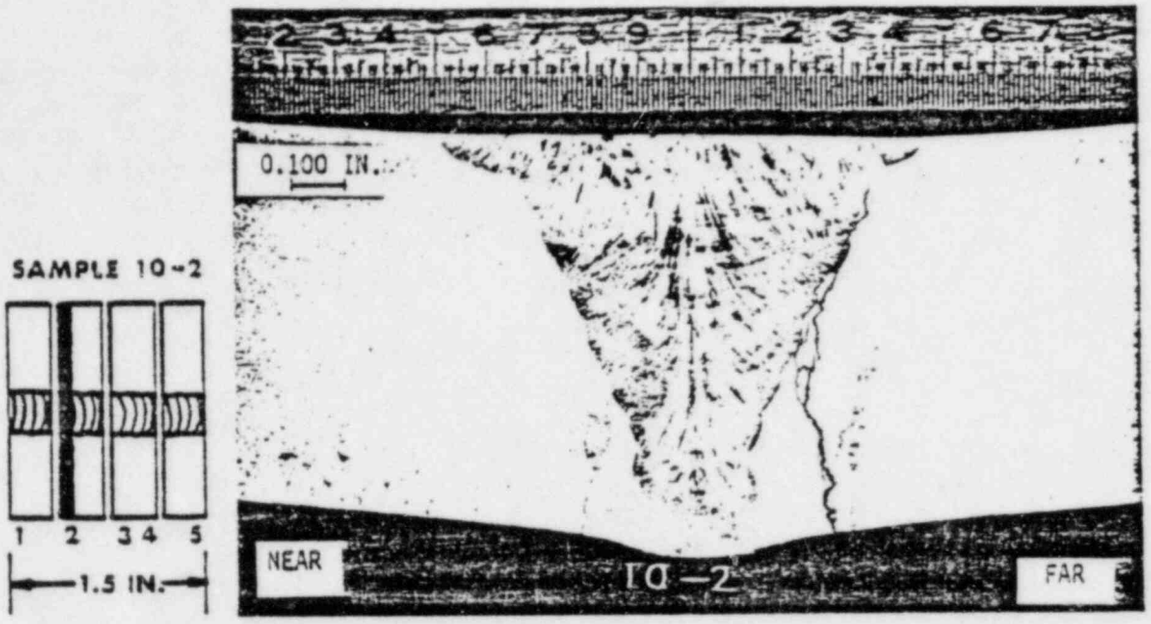
SAMPLE 10-2
1 2 3 4 5
1.5 IN.
0.100 IN.
NEAR
10-2
FAR

SAMPLE 10-3

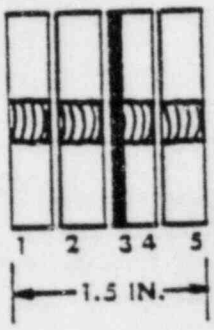

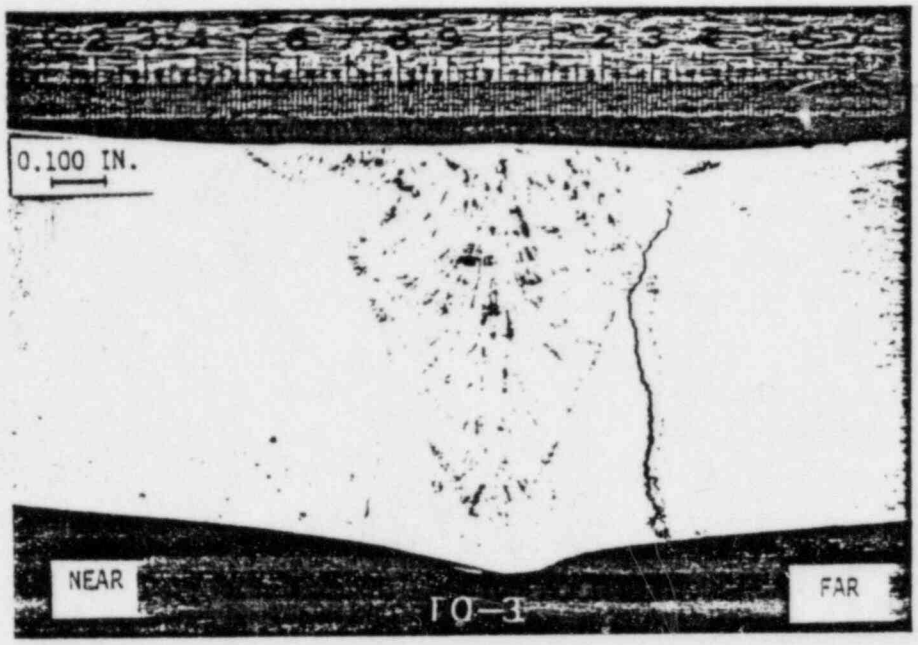

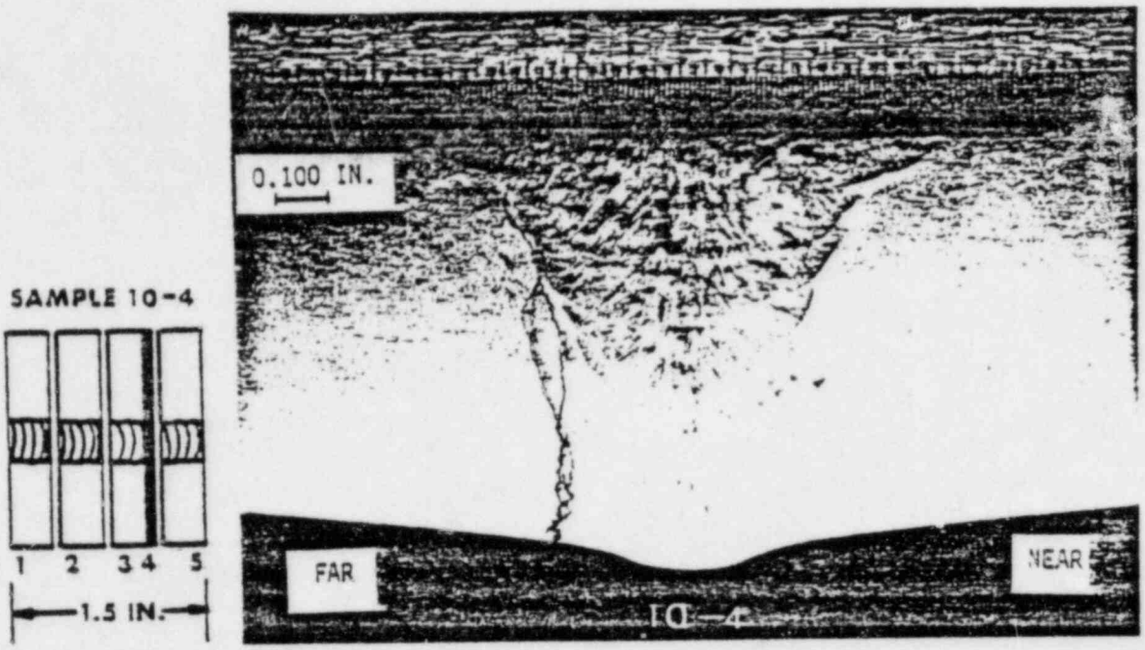
SAMPLE 10-4
1 2 3 4 5
1.5 IN.
0.100 IN.
FAR
NEAR
10-4

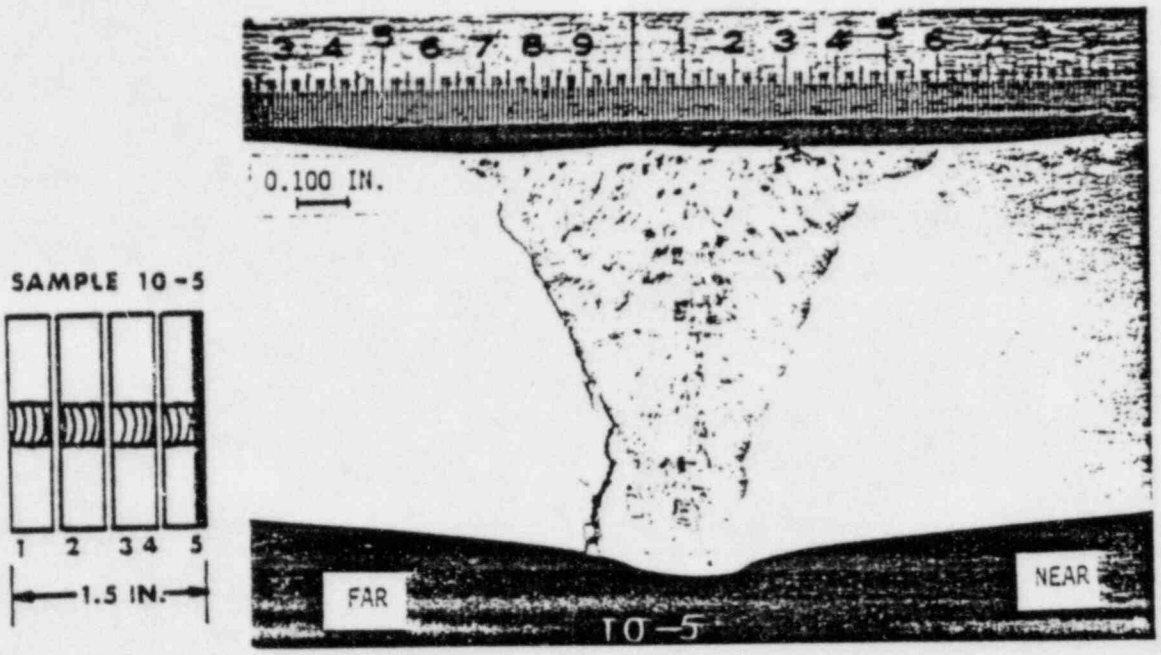
SAMPLE 10-5
1 2 3 4 5
1.5 IN.
0.100 IN.
FAR
NEAR
10-5

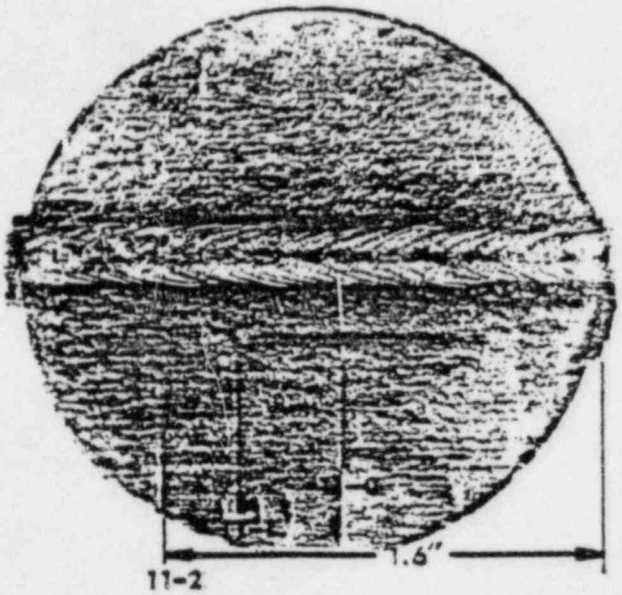

11-2

NEAR 11-0 FAR

NEAR 11-1 FAR

NEAR 11-2 FAR

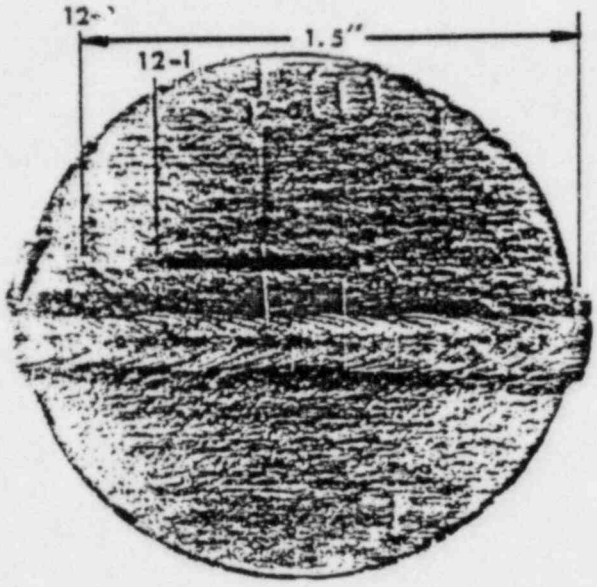

NEAR 12-0 FAR

NEAR 12-1 FAR

NEAR 12-2 FAR

APPENDIX C

FLAW EVALUATION APPROACH

Provided By Dave Norris During 7/22/83 Meeting

DRAFT NO. 10

EVALUATION PROCEDURE AND ACCEPTANCE CRITERIA FOR FLAWS IN AUSTENITIC STEEL PIPING

by S. Ranganath* and D. M. Norris*

CONTENTS

*S. Ranganath is with the General Electric Company, Nuclear Energy Engineering Division, San Jose, California. D. M. Norris is with the Electric Power Research Institute, Palo Alto, California.

Publication of this report was sponsored by the Subcommittee on Piping, Pumps, and Valves of the Pressure Vessel Research Committee of the Welding Research Council.

ABSTRACT

This Bulletin provides the technical basis for determining the acceptability for continued service of austenitic piping components containing axial and circumferential flaws that exceed the allowable flaw standards of IWB-3514.3. The methodology is based on a limit load evaluation of the net pipe section reduced by the flaw area and is appropriate for normal and faulted conditions in nuclear power plants of light-water reactor design. The allowable flaw size is determined by applying a safety factor on the net-section collapse loads. Flaws are evaluated by comparing the maximum flaw dimensions determined by flaw growth analysis at the end of a selected period of evaluation with the allowable flaw dimensions. Guidance is given on determination of critical flaw size, environmental flaw growth, flaw growth instability and leak-before-break, and leak rates and detection. The methodology can be used to determine the acceptability of the flawed piping component for continued service to the next inspection (or until the end of service lifetime) or to determine the inspection interval required.

1.0 INTRODUCTION

Section XI [1] of the ASME Code recognizes the possibility of flaws in structures and presents criteria for inspection and determination of the significance of these flaws. Acceptance standards are provided for vessels, nozzles, flanges, piping and bolts. If the defects discovered during inspection are smaller than the acceptance standards it can be assumed without flaw growth evaluation that the original design safety margins are not compromised. The acceptance standards for austenitic piping is given in IWB-3514.3; the maximum allowable flaw depth is 12.5% of the wall thickness.

If the flaw indication exceeds the standards continued operation can be

justified if it is shown that the inherent Code margin of safety is preserved even with the flaw. For heavy-walled ferritic vessels, an evaluation procedure based is presented in Nonmandatory Appendix A to Section XI. The background of this evaluation procedure with example calculations is discussed in [2,3]. However, an analogous evaluation procedure is not available for piping. Consequently, if an indication in a pipe exceeds the standard (~12% of the pipe wall), the flaw is unacceptable and must be repaired before the unit can be operated.

The basis for IWB-3514.3 limits is given by Maccary [3]. Maccary points out that "although the permissible flaw sizes...provide a conservative estimate of allowable indications in strain hardening materials, the acceptance standards were intentionally lowered for added conservatism to a level corresponding to flaw detectability limits attainable by ultrasonic examination techniques."

Substantial data are now available to more precisely define the margins of safety for flawed austenitic piping and, with new analysis techniques, make possible evaluation procedures for these flaws in the same spirit as Appendix A of Section XI for vessels. This Bulletin presents the technical basis for a pipe flaw evaluation procedure to determine the critical crack size, to predict the time required for the stress corrosion crack to reach this critical size, to assure that leakage and not pipe severance is the failure mechanism, to determine crack-opening areas, flow rates, and instrumentation to sense and measure leakage.

The flaw evaluation process is shown in Fig. 1. The steps are flaw characterization, flaw growth evaluation considering IGSCC and/or fatigue until the next inspection interval, determination of allowable flaw sizes based on applied stresses, flaw acceptance evaluation by comparing the end-of-

inspection period flaw size with the allowable value, and if the flaw is not acceptable, reduction of inspection interval or repair.

2.1 A Criterion for Evaluation of Circumferential Cracks

The critical crack size is calculated using a net-section plastic collapse criterion. The flawed pipe is at the point of incipient failure when the net section in the cracked plane forms a plastic hinge. Unrestrained plastic flow then occurs at a critical flow stress level σ_f (equal to the average of the yield and ultimate tensile strength) that is assumed to be a material property. In fact, Horn et al. [4] have shown that 3 S_m, the code allowable design stress used in the analysis below, is a reasonable approximation to the experimentally determined gross flow stress σ_f. We will show that the criterion is an accurate and simple way to predict failure of stainless steel pipes containing circumferential cracks.

The failure criterion (due to Ranganath and his coworkers [4,5] based on earlier work by Kanninen et al. [6]) is obtained by requiring force and moment equilibrium of the pipe section shown in Fig. 2. The crack depth and length at which plastic collapse is predicted is given by the following equations:

Case 1: Neutral axis located such that $\theta + \beta < \pi$

$$\beta = \frac{(\pi - \theta\, d/t) - (P_m/\sigma_f)\pi}{2} \qquad (1)$$

$$P_b = \frac{2\sigma_f}{\pi}\left(2 \sin\beta - d/t \sin\theta\right)$$

Case 2: Neutral axis located such that $\theta + \beta > \pi$ (assume crack takes compression

$$\beta = \frac{\pi\,(1 - d/t - P_m/\sigma_f)}{2 - d/t}$$

$$P_b = \frac{2\sigma_f}{\pi}\,(2 - d/t)\,\sin\beta \qquad (2)$$

where P_m and P_b are the membrane and bending stresses and the other variables are defined in Figure 2. Equations (1) and (2) define the combinations of β and d/t for which collapse failure is predicted for a given P_m and P_b.

The acceptance flaw size for the proposed criteria is found from the critical flaw size determined from Eqs (1) and (2) by application of appropriate safety factors on the stress levels at failure. The effect is to shift the collapse failure line (see Figure 3) to the lower left of the diagram, reducing the allowable crack length and depth. This curve is then modified by limiting the allowable crack depth to 75% of the wall thickness. This curve, and other similar curves for various load ratios $(P_m + P_b)/S_m$, is the basis of the criteria given in Tables 1 and 2.

The ASME Code design procedure for unflawed piping is based on providing a safety factor on the limit load of the pipe section. We use a similar procedure for the flawed pipe also and prescribe a safety factor on the collapse load of the flawed pipe section. This is justified since plastic collapse precedes or is coincident with crack growth instability in austenitic stainless steel pipe. Thus, our philosophy in setting the flaw acceptance

criteria is to preserve the minimum safety margin inherent in the ASME Code for uncracked piping.

For normal conditions the minimum margin on primary membrane stress is 3 since the code requires $P_m < S_m$. S_m is generally the lower of $S_u/3$ or $0.9\ S_y$ given in Appendix I of Section III. S_u and S_y are the code allowable ultimate and yield strength respectively. For pure bending the margin may be calculated from Eq. (9) of NB-3600 for straight piping, i.e., $P_m + P_b \leq 1.5\ S_m$ by setting $P_m = 0$. The safety margin for bending arises from the value of 2 coming from the ratio of the allowable limit of $1.5\ S_m$ to the flow stress of $3S_m$ and then the ratio of the fully plastic moment for a thin pipe ($4\ \sigma_f\ r^2\ t$) to the moment required to reach flow stress on the surface ($\pi\ \sigma_f\ r^2\ t$) giving a factor of $4/\pi$. Thus, for pipes in pure bending the overall safety margin is is $8/\pi = 2.55$. The required safety factor is the average of the Code minimum safety margins for P_m and $P_b = 1/2(3.0 + 2.55) = 2.77$.

For faulted conditions, the safety margin is one half of the value for normal conditions, i.e., 1/2 (2.77) = 1.39. This is also consistent with the Code design basis.

The allowable flaw sizes in Tables I and II were generated assuming $P_m = S_m/2$ and $\sigma_f = 3\ S_m$. Piping is designed such that the hoop stress is about equal to S_m and hence the axial stress (P_m) is about $S_m/2$. Results shown in Tables I and II are not sensitive to this assumption. Choosing the flow stress equal to $3\ S_m$ is consistent with experimental data discussed below and offers a convenient way of getting flow stresses from ASME Code minimum properties for different grades of material.

For a given value of d/t and angle θ (defining crack depth and length respectively), the angle β defining the neutral axis can be calculated from Equation (1) and the corresponding value of P_b at collapse can be found from

Equation (2). The allowable stress level for a given flaw size a and ℓ can be found by applying the safety factor on the value of $P_m + P_b$ at collapse. Using the allowable $P_m + P_b$ values corresponding to the different nondimensional crack parameters d/t and ℓ/2πr) assuming linear interpolation, a table specifying the allowable flaw parameters corresponding to different $P_m + P_b$ values can be constructed. Tables I and II show the allowable flaw parameters for normal and upset, and emergency and faulted conditions respectively.

Two modifications are included in Tables I and II. The maximum nondimension crack depth, d/t limited to 0.75 to provide additional conservatism. Also, for crack lengths greater than or equal to 50% of the circumference, the allowable flaw size was assumed to be constant, equal to the value for a 360° flaw. Since the variation in the allowable flaw size for flaw lengths exceeding 50% of the circumference was small, the simplified procedure is reasonable and conservative. The lower bound of the allowable values is fixed at allowable flaw standards of IWB-3514.3, Section XI, ASME Code. This is consistant with the code since flaws below the allowable flaw standards of IWB-3514.3 need not be evaluated.

2.2 Experimental Basis for the Circumferential Flaw Criteria

The procedures described above use traditional plastic limit design to analyze flawed austenitic piping. The assumption is made that the toughness of stainless steel is sufficiently high that failure is governed by the strength of the material and is not sensitive to material toughness. We present here the experimental data that justify this assumption.

Early experimental work at Battelle Columbus Laboratories by Broek and Marschall [6,7] used 12-inch wide, center-cracked Type 304 stainless steel panels tested in uniaxial tension to simulate circumferentially flawed 4-inch

diameter pipe. These panels were tested under a variety of loading conditions--monotonic, interrupted, cyclic, and seismic with cracks that included both saw-cut and fatigue initiators in sensitized and unsensitized material. The results of all these tests (see Fig. 4) show that stable crack initiation and maximum load correlate with unique values of the net-section stress.

Eighteen 4-point bending tests were performed by Wilkowski [7] on circumferentially flawed 2-, 4- and 16-inch diameter Type 304 stainless steel pipe. Eight experiments used through-the-wall cracks in all three diameters. Nine 4-inch pipes and one 16-inch diameter pipe were tested with internal surface flaws. Earlier work with pressurized pipe had shown the effect of internal pressure on maximum bending moment was negligible [6]. The results for through-wall cracks are compared with the net-section stress criterion in Fig. 5. Additional test data on 4-and 10-inch pipes in bending and tension are reported by Andrews [10].

Figure 6 compares results for part-through surface flaws in 4-inch diameter pipe. These data show that stable flaw growth started at 98 percent of maximum load associated with net-section collapse. Wilkowski [7] also tested a 16-inch diameter pipe with a circumferential flaw 66 percent of the wall thickness and 47.5 percent of the circumference. Stable radial flaw growth started at 76.5 percent of maximum load and continued until maximum load was reached at 86 percent of that predicted by the net-section collapse criterion.

2.3 Comparison With Theoretical Considerations

The net-section strength method assumes a unique value of the flow stress σ_f that is independent of pipe diameter, wall thickness, and flaw length. Smith [8] has considered this assumption for the center-cracked panel. Using

the estimation scheme of Kumar, German, and Shih [9], he calculated a net-section stress Y_{IC} for the onset of flaw extension. He found that Y_{IC} does not vary appreciably with flaw size for a fixed panel width (corresponding to a given pipe diameter) but is reduced as panel width increases. Although only one panel width was tested, this is consistent with the crack initiation result of the large pipe test discussed above. It is obvious that for a fixed flaw length-to-diameter ratio, flaws in large pipes will start to grow at scaled loads below those of small pipes since the crack-driving force J (or K^2) is proportional to crack length.

Crack-growth instability of the center-cracked panel was investigated by German et al. [10] who considered the additional load margin above crack initiation occurring with stable crack growth. They obtained crack-driving-force curves (J versus load) from which the loads at crack initiation could also be determined. This estimation procedure predicts the maximum load for stability that may be compared with the net-section stress criterion. The result for a plate 41-inches wide (modeling a 13-in. dia. pipe) shows that crack initiation (assuming J_{IC} = 4000 lb/in for stainless steel) starts at loads considerably below those for instability in contrast with the 12-inch wide plate (see Fig. 4) where initiation occurred at loads only a few percent below the collapse load. Final instability was computed to occur above the net-section collapse load. This result shows that the net-section stress criterion is conservative when stable crack growth is accounted for.

The elastic-plastic fracture mechanics estimation scheme [9] was also applied by German et al. [10] and Ranganath and Mehta [8] to flawed pipes and compared with results from the net-section stress criterion. Results for a through-wall crack with tension (from [8]) is shown in Fig. 7. One-half of the cylinder was modelled as a single-edge cracked plate with correction for

the curvature following German et al. [10]. The figure shows that cracks in large-diameter pipes initiate at lower stress values than small-diameter pipes but that the load for plastic collapse (and crack instability) is independent of pipe diameter for a given normalized crack size. There are no analogous calculations for surface flaws.

Experimental and analytical work [4,7] has shown additional margins of safety under dynamic loading as a result of material plastic energy absorption and time-of-application of the load. Static instability loads can be exceeded by large margins if the period of application of dynamic loads is sufficiently short. However, cyclic loading leading to fatigue or ratcheting damage plus moment reversal on circumferential cracks may lower such apparent dynamic margins.

2.4 A Criterion for Evaluation of Axial Flaws

An empirical formulation for axial through-wall flaws in pipes developed by Eiber et al. [11] for the hoop stress at failure is

$$\sigma_h = \frac{3S_m}{M} \tag{3}$$

where we have replaced σ_f with $3S_m$ as before and where M is a curvature correction factor

$$M = \left[1 + \frac{1.61L^2}{4Rt_m} \right]^{1/2} . \tag{4}$$

ℓ is the crack length, R is the mean radius of the pipe, and t_m is the minimum pipe-wall thickness. The data are compared with Eq. 3 in Fig. 8.

For part through axial cracks the hoop stress at failure is

$$\sigma_h = 3S_m \left[\frac{t_m/d - 1}{t_m/d - 1/M} \right] \qquad (5)$$

where d is the depth of crack. For a long axial part-through crack, 1/M and the criterion reduces to the requirement that the ligament stress corresponds to the flow stress. The data are compared with Eq. (5) in Fig. 9.

Piping designed by NB3641 of the Code has minimum thickness

$$t_m = \frac{PO_o}{2\,S_m} \qquad (6)$$

where P is the design pressure and O_o is the outside diameter of the pipe. The associated hoop stress σ_h is

$$\sigma_h = \frac{PO_o}{2t_m} = S_m , \qquad (7)$$

Since S_m is defined as the lower of 0.9 S_y and $S_u/3$, the minimum thickness requirements assure a safety margin of at least three for design conditions. Eq. (6) uses design pressure that is not less than the maximum pressure for normal conditions. This is somewhat higher than the pressure under normal operation. For faulted conditions the maximum pressure is two times the design pressure and the minimum safety margin is at least 1.5.

Although the code specifices the minimum required thickness, in practice the actual thickness of piping designed to the code is likely to be much higher. This allows the safety margin to be higher than the minimum value of 3.0 even when the pipe is degraded by the presence of a crack. This suggests establishing acceptance criteria for axial cracks in austenitic stainless steel piping such that a pipe with an axial crack is acceptable for continued operation if the minimum safety margins prescribed for uncracked piping can also be maintained with cracks.

Appropriate safety factors must be applied to Eqs. 6 and 8. If a safety factor of 3 is required, the allowable hoop stress is given by:

$$\frac{\sigma_h}{S_m} = \left[\frac{t/d - 1}{t/d - 1/M}\right] \qquad (8)$$

Knowing the "stress ratio" σ_h/S_m and the crack length ℓ, the allowable crack depth a can be calculated from Eqn. (8). Table III shows the nondimensional allowable flaw size as a function of stress ratio and nondimensional crack length $\ell/\sqrt{Rt_m}$. We disallow crack depths exceeding 75% of the wall thickness but from the viewpoint of structural margin, greater crack depth can be allowed. Table III limits the nondimensional flaw length $\ell/\sqrt{Rt_m}$ to the allowable length for a through-wall flaw calculated using Eq. 3. A flaw that exceeds this length is limited to that specified in IWB 3514.3. This flaw-length limit guarantees that surface flaws will remain below critical size (based on the plastic collapse condition) if they should grow through the wall.

Table IV shows the allowable axial flaw sizes for faulted conditions. These values were obtained by imposing a safety margin of 1.5 on Eq. (5). The minimum flaw size obtained from Tables III and IV is the critical end-of-inspection flaw size.

2.5 Experimental Basis for the Axial Flaw Criterion

In 1971 Eiber et al. [11] published the results of 24 experiments on representative nuclear reactor piping materials of Type 316 stainless steel and A106B carbon steel with diameters up to 24 inches. These data provided the basis for the axial flaw criterion discussed above.

Twenty eight of these tests were on carbon steel. Since stainless steel is more ductile than carbon steel, Eiber's conclusions on the validity of a limit load failure criterion are applicable also to stainless steel piping. The test results shown in Fig. 8 and 9 form the basis for Eqs. 3 and 5.

2.6 Materials

Materials applicable to the new criteria are wrought austenitic stainless steel, Inconel, and their associated weldments, and cast austenitic stainless steel with less than 20% (FN = 20) ferrite. Acceptable yield stress is less than or equal to 46 ksi at room temperature.

The sensitization of stainless steel caused by welding or furnace sensitization is an important contributor to environmental cracking. Kanninen et al. [6,7] investigated the effect of this sensitization on the net-section failure criteria and concluded that "the presence of the weld and the sensitization of the material surrounding the flaw do not significantly affect the applied stress at failure." Their conclusions were based on testing both furnace-sensitized plates and flawed pipes with welds made by manual gas

tungsten-arc and manual shielded metal-arc with 308L stainless steel weld rod according to procedures recommended by a prominent United States nuclear steam system supplier.

Inadequate data exist to assess the tearing stability (see Section 3.0) of sensitized material. However, the lower bound to crack growth instability is coincident with net-section collapse for which the data of reference [7] is applicable. The safety factor of three (based on this load) of the flaw evaluation criteria assures only stable crack growth and avoidance of guillotine pipe failure.

3.0 Leak-Before-Break

Prudent design requires that pipe with service-induced surface flaws fail by asymmetric radial growth to a local detectable leak condition rather than unstable circumferential growth leading to a guillotine pipe rupture. Two failure mechanisms must be considered: environmentally-aided stable crack growth (including fatigue), and unstable growth of an existing crack by loads associated with normal or faulted conditions.

The argument favoring the leak-before-break hypothesis for environmentally-aided crack growth relies on the asymmetry of the weld sensitization and bending loads. Table I, for example, shows that a complete circumferential crack can equal 63% of the wall thickness for loads double the design stress limit, S_m. Before the crack depth reaches this size, the azimuthal variations of welding residual stress and material susceptibility in the heat-affected zone, combined with the asymmetric bending loads, will lead to asymmetrical crack growth and the formation of a short through-wall crack. This hypothesis is verified by extensive field experience.

Unstable crack growth is avoided by adherence to the criteria of Tables I to IV since the basis of the criteria, plastic collapse of the flawed net-section, is coincident with the lower bound to crack-growth instability associated with load control.

3.1 Instability of Circumferential Flaws

Additional safety margins on flaw growth stability are available in piping systems if the loads are governed by prescribed displacement or rotation instead of the applied force or moment that forms the basis for the criteria discussed above. With prescribed displacement, for example, there is a relaxation of crack-tip stress with stable crack growth and the structure can sustain applied displacements beyond those associated with maximum load. For this class of loads, that probably includes seismic, additional safety margin is available over that predicted by the plastic collapse mechanisms discussed above. In fact, it is possible to show that in some piping systems it is impossible to have unstable circumferential crack growth at loads exceeding ASME Code Level D faulted conditions, and for these systems no guillotine pipe break will occur. Application of these criteria require the use of elastic-plastic fracture mechanics.

The basis for pipe tearing-instability analysis was given by Paris, Tada, and Gamble [12] who showed how added piping system compliance increases the potential for unstable crack growth. By increasing the unsupported pipe length, more stored elastic energy is available to feed into the plastic net-section containing a crack and drive it unstably. The added compliance makes the system loading mechanism appear to be closer to a force type of loading rather than a displacement load. They showed that if the ratio of pipe length to radius was less than a material property called the "tearing modulus," T_m,

instability was impossible. Taking T_m as 200 for stainless steel, the critical unsupported length of a 2-ft diameter pipe is 200 ft, a length that is unlikely in nuclear power plants. Circumferential flaw stability guarantees a leak-before-break condition. Extensive testing (see e.g. [7,10,12]) has verified the theory.

Cotter, Chang, and Zahoor [14] have recently applied this tearing instability theory to primary and secondary piping runs in existing BWR and PWR nuclear power plants. The analysis here is complicated by the three-dimensionality of the piping design and it is necessary to replace the straight pipe length L with an effective length equal to EI/K where EI is the pipe section modulus and K is taken to be the minimum bending stiffness of the pipe run computed at each assumed flaw location. This stiffness is obtained by an elastic, finite element piping computer program from which an effective L/R may be computed and compared with the material tearing modulus.

The results for some specific boiling water reactor piping are given in Table V. The analysis shows that it is impossible for Level D loads to cause guillotine pipe breaks in the austenitic piping runs considered. The description of the above analysis has been abbreviated for this summary paper and interested readers should refer to reference [14] for details (and assumptions) of the calculations. Additional information on the calculational procedure is given in the Appendix.

3.2 Growth of Surface Flaws

Zahoor [7] showed that the preferred growth direction of a semi-elliptical surface flaw is through the thickness. His calculations, for both bending and tension loading, gave the ratio J_c/J_a where J_c and J_a are crack driving forces (defined by the J-integral) in the circumferential and radial

directions respectively. Values less than one indicate preference for axial growth versus circumferential growth. The ratio is always less or equal to one as seen in Fig. 10. For bending loads, a 180° crack penetrating 40% of the wall has three times the driving force in the radial direction. This result strongly suggests leak-before-break behavior.

3.2 Instability of Axial Flaws

The criteria of Tables III and IV for axial flaws were based on the experiments of Eiber et al [11] and the critical net-section stress criterion. Flaw instability is precluded in these tables by maintaining a safety factor of three on the collapse load.

4.0 SUBCRITICAL FLAW GROWTH

The work above considered critical crack size with no discussion of subcritical growth. Fatigue crack growth for ferritic steel is treated in Appendix A, Section XI of the ASME Code, but the Code contains no guidance for intergranular stress corrosion cracking (IGSCC) or fatigue cracking in austenitic piping.

Considerable data is now available on crack growth rates due to IGSCC and fatigue as a function of the stress intensity factor. This stress intensity may be computed knowing the crack geometry and the primary and secondary stresses. In the work that follows, we summarize the crack growth-rate data and weld residual stress data to provide design recommendations and guidance in making crack-growth calculations. These calculations that provide the time required for a flaw to reach critical size may be useful in repair deferral decisions needed to develop a pipe replacement plan and to obtain replacement pipe.

4.1 Residual Stresses

We have reviewed the available data (see e.g. [4]) on weld residual stresses for use in crack-growth analyses. Typical through-wall distributions are given in Fig. 11 with more detailed results for large pipes shown in Fig. 12. The data show more benign distributions in both axial and circumferential directions as the pipe diameter increases because of the larger heat reservoir associated with the greater wall thickness. There is a transition in stress distribution at a pipe wall thickness of about one inch and we have chosen to separate the data at that pipe-wall thickness. The small pipe recommendations may be overly conservative for wall thickness approaching one inch.

The axial residual stress data (leading to circumferential cracking) are consistent and are conservatively represented by the simple distributions given in Fig. 11. The axial stress data base includes measurements on 4, 10, 12, 16, 24, and 28-inch diameter pipe.

There are fewer circumferential residual stress data and some of these are limited to measurements only on the inside and outside of the pipe. These data show much more variation but there is a trend to compressive stress on the inside wall as the pipe diameter increases as shown by Sasaki et al. [15] in Fig. 13.

4.2 Stress Corrosion Flaw Growth

Horn et al. [4] and Huet et al. [16] have compiled extensive crack-growth data on Type 304 stainless steel due to intergranular stress corrosion. Figure 14 shows crack growth rates obtained at 550°F in 8 and 0.2 ppm oxygenated water under constant load. The material was given isothermal heat

treatment to simulate furnace sensitized and weld sensitized stainless steel. The data fall into three broad classes; the lower line corresponds to weld sensitized material in 0.2 ppm oxygenated water at 550°F; the middle line represents the expected crack growth rate for furnace sensitized stainless steel[4] (FSSS) in 0.2 ppm water; the upper bound line represents highly furnace sensitized material in 8 ppm oxygenated water at 550°F.

Crack-growth data using CT and WOL specimens, pipe tests, and CERT tests have shown that furnace sensitized Type 304 stainless steel is more susceptible to IGSCC for both crack initiation and crack growth. Similarly, IGSCC crack growth rates in 8 ppm oxygenated water are significantly higher than in 0.2 ppm oxygenated water. For crack growth evaluation we therefore recommend the following:

- Use the line corresponding to furnace sensitized stainless steel (the middle design line in Figure 14) to calculate IGSCC crack growth for weld sensitized material in 0.2 ppm oxygenated water. The procedure is conservative since cracks grow more quickly in furnace sensitized material ~~is worse~~ than weld sensitized material.

- Use the upper bound line (corresponding to FSSS in 8 ppm water) to evaluate crack growth for furnace sensitized material in 0.2 ppm oxygenated water. Use of 8 ppm data is conservative because 0.2 ppm crack growth rates are lower.

[4] Heat 03580 was found to be severely sensitized based on CERT tests as well as ASTM A262E oxalic acid etch tests and is considered equivalent [17] to highly furnace sensitized material.

The conservatism in the above recommendations provide margin to account for fluctuations in water chemistry and higher oxygen during startup. Our calculations show that the presence of load fluctuations for normal operating conditions do not affect IGSCC crack growth rates significantly. Fatigue crack growth due to system transients is discussed in the next section.

We have elected not to extrapolate the existing data base beyond about 40 ksi $\sqrt{in.}$ and results from such high K tests are suspect. Classic IGSCC theories predict a plateau in crack growth rates above a specific value of K, however, the location of this plateau is uncertain. Unpublished data by Shack and his coworkers [18] suggest the upward trend may increase with increasing stress intensity. These crack growth rates at higher K may be needed for analysis of axial cracks, however, those axial cracks will grow out of the heat-affected zone into less sensitized material where the lower-bound (or zero) growth line is appropriate.

4.3 Fatigue Flaw Growth

Crack growth due to low-cycle fatigue may be computed by

$$\frac{da}{dN} = CK_{eff}^{n} \tag{9}$$

where $K_{eff} = K_{max}\,(1-R)^{0.5}$ and R is the stress intensity ratio K_{min}/K_{max}.

The data base [4,19] shown in Fig. 15 was obtained in simulated LWR environments for various R ratios. Reference [20] discusses problems in the definition of K_{eff} associated with high R values.

4.4 Flaw-Growth Calculations

Flaw-growth calculations may be done for a given flaw geometry by superposing the service and residual stresses from which the stress intensity factor may be easily computed (using e.g., the computer program of Dedhia and Harris [21]) for any flaw depth. Then, for a given time increment Δt, the growth increment Δa may be computed from the stress intensity factor at this flaw depth using the growth-rate curves and summed to obtain flaw depth versus time predictions. Computations should include the chronologic contributions from the steady and cyclic loads.

The calculational procedure has been verified by tension tests on flawed 16 and 24-inch diameter pipe [4,22] in simulated BWR environments. Calculated crack growth is compared with measured growth on a 24-inch diameter pipe in Fig. 16 for two crack growth-rate assumptions of Fig. 14. We elastically superposed the residual stress distribution of Fig. 11 with the 25 ksi test stress. Pipe yield stress was 36 ksi. Similar good correspondence has been obtained by Horn [4] in a (current test of a flawed 16-inch diameter pipe in a simulated BWR environment.

Crack growth predictions obtained in this way confirm that crack propagation in as-welded small-diameter lines is sufficiently fast that immediate repair is recommended if IGSCC is detected by in-service inspection. On the other hand, because welding residual stress distributions are more favorable in large-diameter pipes (say greater than 20-in. dia.), and the crack arrests in the compressive part of the residual stress field, periods of the order of years are predicted to be necessary for a small crack to grow to a point at which the remaining safety margin would be unacceptable. Consequently, it may be justifiable to defer repairs in large-diameter lines until scheduled refueling outages, in order to minimize plant downtime.

Crack growth calculations using the above procedures are based on LEFM; i.e., the stress intensity factor due to residual stress is added to that due to the applied stress. This is the procedure used in fatigue crack growth analysis. The LEFM approach is reasonable since the test specimens used for the crack-growth rate data are in the LEFM range. We believe that residual stresses and the crack-growth rates recommended here lead to conservative crack growth predictions.

5.0 Leak Rates and Detection

Prudent application of flaw repair deferral suggests that leak detection instrumentation may be desireable. This section discusses methods to predict crack-opening areas and resulting flow rates. Data is presented on the minimum flow rate detectable by acoustic sensors and the correlation of acoustic energy with flow rate.

5.1 Crack-Open Area

For normal loads, crack-opening area may be computed by formulas given by Tada and Paris [23]. For circumferential cracks subject to axial tension and bending

$$A = \frac{\sigma_t}{E}(\pi R^2) I_t(\theta)\left[1 + \frac{\sigma_b}{\sigma_t}\left(\frac{3 + \cos\theta}{4}\right)\right] \qquad (10a)$$

or

$$A = \frac{\sigma_b}{E}(\pi R^2) I_t(\theta)\left[\frac{\sigma_t}{\sigma_b} + \frac{3 + \cos\theta}{4}\right], \tag{10b}$$

where

$$I_t(\theta) = 2\theta^2\left[1 + \left(\frac{\theta}{\pi}\right)^{3/2}\left\{8.6 - 13.3\left(\frac{\theta}{\pi}\right) + 24\left(\frac{\theta}{\pi}\right)^2\right\}\right.$$

$$\left. + \left(\frac{\theta}{\pi}\right)^3\left\{22.5 - 75\left(\frac{\theta}{\pi}\right) + 205.7\left(\frac{\theta}{\pi}\right)^2\right.\right. \tag{11}$$

$$\left.\left. - 247.3\left(\frac{\theta}{\pi}\right)^3 + 242\left(\frac{\theta}{\pi}\right)^4\right\}\right] .$$

and θ ($0 < \theta < 100°$) is the one-half crack length in radians. A is the crack opening area, R the mean pipe radius, E is the elastic modulus, and the tension and bending stresses are

$$\sigma_t = \frac{P}{2\pi Rt}$$

and (12)

$$\sigma_b = \frac{M}{\pi R^2 t} .$$

P and M are the axial force and bending moment respectively and t is the nominal pipe thickness.

For internal pressure loading, the crack-opening area is found from

$$A = \frac{\sigma}{E}(2\pi Rt) \cdot G(\lambda) \tag{13}$$

where σ is the hoop or axial stress due to pressure and $\lambda = a/\sqrt{Rt}$. For circumferential through cracks

$$\begin{aligned} G(\lambda) &= \lambda^2 + 0.16\lambda^4 && (0 \leq \lambda \leq 1) \\ &= 0.02 + 0.81\lambda^2 + 0.30\lambda^3 + 0.03\lambda^4 && (1 \leq \lambda \leq 5) \end{aligned} \tag{14}$$

and for axial through cracks

$$\begin{aligned} G(\lambda) &= \lambda^2 + 0.625\lambda^4 && (0 \leq \lambda \leq 1) \\ &= 0.14 + 0.36\lambda^2 + 0.72\lambda^3 + 0.405\lambda^4 && (1 \leq \lambda \leq 5). \end{aligned} \tag{15}$$

Yielding near the crack tip may be modeled by a plastic zone correction

$$x_{eff} = x + \frac{K_{total}^2}{2\pi R\sigma_y^2} \tag{16}$$

where x may be θ or a in the above formulas.

Some crack-opening areas for faulted conditions where large-scale plasticity occurs are reported by German et al. [10] or may be computed by methods given by Zahoor [7].

5.2 Leak Rates

A computer program based on theory by Henry [24] is available for flow through cracks. The model accounts for water and steam phases, wall friction, flow area, area change, and bends in the flow path associated with IGSCC. Details of the work is given by Collier et al. [25] who describe the computer program that with the crack-opening areas of Section 5.1, allow calculations of leak rates.

Ranganath [4] used a simpler method to estimate crack-opening area and flow rate for circumferential through-wall cracks. Table VI shows results of a calculation to obtain the maximum crack length for three different pipe diameters such that the flow rate is limited to 5 gpm. The 5 gpm flow rate is the minimum undetected leakage rate allowed in nuclear power plants. The table assumes normal operating conditions with a pressure stress across the crack of $pr/2t = S_m/2$. The work used an internal pressure of 1000 psi, and temperature of 550°F.

5.3 Leak Detection

Collier et al. [25] have shown that it is possible to measure flow rates through actual intergranular stress corrosion cracks down to 5.8×10^{-5} Kg/sec (about 0.0003 gpm at 1000 psia and 500°F) with conventional acoustic sensors mounted on the pipe. The experiments used through cracks in 12 in.-diameter Schedule 100 pipe. The longest crack, 27.9 mm, leaked at 0.2 g/100 (about 1 gpm) for typical BWR conditions. Signals from circumferential cracks are three times stronger at a transducer station located at a given axial distance from the crack than at the same circumferential distance. Correlation of acoustic transducer signal with flow rate, discussed in the same

report, was shown to have potential. Resistive-tape sensors that are extremely sensitive to moisture have been used with repair deferral schemes.

6.0 Crack Detection and Sizing

Acceptance of a flawed pipe for continued service using the evaluation procedures discussed above requires flaw size determination by ultrasonic inspection (UT) or radiography (RT). The principal defects in stainless steel are axial and circumferential flaws caused by IGSCC in the heat-affected zone (HAZ) of the weldments.

These flaws are generally not clean cracks with high reflectivity. IGSCC is frequently a tree-like growth with branches extending into the intergranular medium. At any particular radial depth the branch or the trunk may be the predominant physical flaw and acoustic reflector. Under high stress intensity conditions the trunk section usually dominates; the crack being similar to a saw cut or notch with roughened sidewalls. At low stress intensity both trunk and branches may be extremely tight with small physical separation making signal interpretation difficult.

Signal interpretation is further complicated by geometric reflectors in or near the heat-affected zone, such as the weld crown, root, or by the counterbore and it is difficult to generalize quantitatively about our ability to detect and size stress corrosion cracks. Some guidance has been provided by Lapides [26] in Table VII that gives rough estimates on the probability of detection and sizing IGSCC. The basis for Table VII is judgment based on the current state of the art.

Recent utility response to increasing incidents of IGSCC has provided data on the ability of inspection teams to size IGSCC in 28-inch diameter piping removed from a BWR nuclear power plant. Some results, shown in

Table VIII, demonstrate that with proper equipment, training, and experience, adequate sizing capability is currently possible. An extensive size round robin is currently under way under EPRI sponsorship.

7.0 Summary and Conclusions

This Bulletin provides the technical basis for determining the acceptability for continued service of austenitic piping components containing flaws that exceed the allowable flaw standards of IWB-3514.3. Code Section IWB-3460 and the associated appendix allows this alternative analysis. The methodology is appropriate for normal and faulted loads in nuclear power systems of light-water reactor design.

The work addresses both margin of safety and the economic considerations required to plan a future outage for pipe repair. This requires determination of critical crack size, a prediction of the time required for the stress corrosion crack to reach this critical size, assurance that leakage and not pipe severance is the failure mechanism, determination of crack-opening areas and flow rates, and application of back-up instrumentation to sense and measure leakage.

The procedures addressed in this Bulletin to justify continued operation are not simple. They span a spectrum of engineering disciplines including materials, elastic plastic fracture mechanics, and thermal-hydraulic flow analysis. While the components of the analysis have a good technical basis, the actual calculations, documentation, and regulatory approval process have been shown to be sufficiently time consuming that utilities may find pipe repair or replacement a more economic choice. Piping engineers concerned with these repair-replace decisions should be familiar with the material in this Bulletin prior to nondestructive piping inspections, and should have stocked replacement piping to maintain maximum flexibility.

8.0 ACKNOWLEDGMENTS

We acknowledge the work of the ASME Section XI Pipe Flaw Evaluation Task Group in developing and reviewing the evaluation procedure. Members of the Task Group are T. U. Marston, W. H. Bamford, J. M. Bloom, R. C. Cipolla, E. DeBarba, T. J. Griesbach, J. P. Houstrup, R. E. Johnson, P. C. Paris, W. L. Server, F. A. Simonen, K. K. Yoon, S. Yukawa, S. Ranganath, and D. M. Norris. Part of the research reported here was sponsored by a Boiling Water Reactor Owner's Group formed to address intergranular stress corrosion cracking in austenitic piping managed by the Electric Power Research Institute. The individual research contributions are listed in the references for this summary paper. The authors acknowledge and thank these researchers for their important contributions. We appreciate the assistance and sponsorship of the Pressure Vessel Research Committee, Subcommittee on Piping, Pumps, and Valves.

Appendix A

Procedure for Computing Tearing Stability of Circumferential Through Flaws

Tada, Paris, and Gamble [13] used a fracture mechanics analysis to provide a criterion for stability of crack extension. The criterion is valid for materials whose failure is characterized by gross yielding of the cross section containing the crack, subsequent plastic instability, and guillotine pipe rupture. The method is applicable to piping systems of arbitrary stiffness loaded by static or dynamic boundary displacements. The methodology is used to evaluate leak-before-break behavior.

A tearing modulus, T, was developed using J-integral theory and the J-integral resistance curve. The nondimensional quantities T_{mat} and T_{appl} are defined as

$$T_{mat} = \frac{E}{\sigma_0^2} \frac{dJ_{mat}}{da} \qquad (1)$$

and

$$T_{appl} = \frac{E}{\sigma_0^2} \frac{dJ}{da}$$

where E is Young's modulus, σ_0 is the flow stress defined here as half the sum of the yield and ultimate material strength. a is the flaw depth in the

stability analysis, J_{mat} is the value of J following the material resistance curve, and J is the applied value of J. Stability of crack growth is given by

$$T_{mat} > T_{appl} \text{ stable}$$

and (2)

$$T_{mat} < T_{appl} \text{ unstable.}$$

T_{mat} is a material property measured in the laboratory; T_{appl} must be computed for a given geometry and load.

T_{appl} for a piping system is given by

$$T_{appl} = F_1 \frac{L}{R} + F_2 \frac{JE}{\sigma_0^2 R} \tag{3}$$

where

$$F_1 = \frac{2}{\pi} F_J^2$$

$$F_2 = \frac{1}{2F_J} (\cos \theta/2 - 2 \sin\theta) \tag{4}$$

and $F_J = \sin\theta/2 + \cos\theta$. L is taken to be the effective pipe length, discussed below; R is the mean radius; E is Young's modulus; σ_0 is the flow stress; J is the J-integral crack-driving force; θ is half the crack angle. Since the maximum value of F_1 is 0.81 and F_2 is negative for $2\theta < 60$ (the

second term in Eq. 3 contributes about 3% for $J = 3J_{IC}$), a conservative estimate for T_{app} is

$$T_{app} = L/R \quad . \tag{5}$$

An elastic piping computer program may be used to compute the effective pipe length by the procedure given by Cottar et al. [14]. A hinged section is used to model the plastic rotation at the flawed weld location. Equal moments applied on each side of the hinge (causing a kink angle) allow calculation of the corresponding in-plane and out-of-plane rotations. The process is repeated in the orthogonal bending direction from which a 2x2 flexibility matrix may be computed. The effective length is then chosen from the relation $L = EI/K_{min}$ where K_{min} is chosen as the lesser of the two principal stiffnesses.

J of Eq. (3) is computed from

$$J = \sigma_0 R F_J \phi \tag{6}$$

where ϕ is the kink angle due to plastic rotation at the cracked section. Cottar et al. conservatively chose ϕ equal to 1 degree. T_{appl} may then be calculated from Eq. (3) and used in Eq. (2) to evaluate stability. The calculation is repeated for each weld in the piping system.

REFERENCES

1. American Society of Mechanical Engineers Boiler and Pressure Vessel Code, 1980 Edition (and Addenda).

2. "Flaw Evaluation Procedures ASME Section XI," T. U. Marston, Ed., Electric Power Research Institute, EPRI NP-719-SR, Special Report, August 1978 (see Errata dated April 14, 1980).

3. "Nondestructive Examination Acceptance Standards, Technical Basis and Development of Boiler and Pressure Vessel Code, ASME Section XI, Division 1," edited by R. R. Maccary, Electric Power Research Institute, EPRI NP-1406-SR, Special Report, May 1980.

4. "The Growth and Stability of Stress Corrosion Cracks in Large-Diameter BWR Piping," R. M. Horn, Ed., Electric Power Research Institute Report NP-2472 (Vol. 1: Summary; Vol. 2: Appendices), July 1982.

5. "Engineering Methods for the Assessment of Ductile Fracture Margin in Nuclear Power Plant Piping," S. Ranganath and H. S. Mehta, Elastic-Plastic Fracture Second Symposium, Vol. 2, "Fracture Resistance Curves and Engineering Applications," ASTM STP 803, American Society for Testing and Materials, Philadelphia, Pa., 1983.

6. "Toward an Elastic-Plastic Fracture Mechanics Predictive Capability for Reactor Piping," M. F. Kanninen, et al., Nuclear Engineering and Design,

48, 117-134, 1978. More details are given in EPRI Report NP-192 on Project 585-1, 1978.

7. "Instability Predictions for Circumferentially Cracked Type-304 Stainless Steel Under Dynamic Loading," M. F. Kanninen, et al., Electric Power Research Institute Report NP-2347 (Volume 1: Summary; Volume 2: Appendices), April 1982.

8. "Theoretical Justification for the Association of a Critical Net-Section Stress with Fracture Initiation at a Crack Tip," E. Smith, Int. J. Pres. Ves. and Piping, 8 (1980) 303-311.

9. "An Engineering Approach for Elastic-Plastic Fracture Analysis," V. Kumar, M. D. German, and G. F. Shih, Electric Power Research Institute, EPRI NP-1931, Project 1237-1, Topical Report, July 1981.

10. "Elastic-Plastic Fracture Analysis of Flawed Stainless Steel Pipes," M. D. German, et al., Electric Power Research Institute, Report NP-2608-LD, Palo Alto, Ca., September 1982. See also, "Elastic-Plastic Analysis of Crack Opening, Stable Growth, and Instability Behavior in Flawed 304 Stainless Steel Piping," M. D. German and V. Kumar, presented at the ASME Pressure Vessel and Piping Conference, Orlando, Fla., June 1982.

11. "Investigation of the Initiation and Extent of Ductile Pipe Rupture," R. J. Eiber, et al., Battelle Columbus Laboratories, Report BMI-1908, June 1971.

12. "An Experimental Evaluation of Tearing Instability Using the Compact Specimen," J. A. Joyce and M. G. Vassilaros, in ASTM STP 743, R. Roberts, Ed., 1981, pp. 525-542.

13. "Stability Analysis of Circumferential Cracks in Reactor Piping Systems," H. Tada, P. C. Paris, and R. Gamble, Nuclear Regulatory Commission NUREG/CR-0838, June 1979.

14. "Application of Tearing Modulus Stability Concepts to Nuclear Piping," K. H. Cotter, H. Y. Chang, and A. Zahoor, Electric Power Research Institute Report NP-2261, February 1982.

15. "Mitigation of Inside Surface Residual Stress of Type 304 Stainless Steel Pipe Welds by Inside Water Cooling Method," R. Sasaki et al., Proceedings: Seminar on Countermeasures for Pipe Cracking in BWRs, Paper #9, Vol. 1, EPRI Report WS-79-174, May 1980.

16. "Stress Corrosion Cracking of Type-304 Stainless Steel in High-Purity Water: A Compilation of Crack Growth Rates," R. Huet, L. C. Hsu, D. A. Gerber, and P. C. Riccardella, EPRI Interim Report NP-2423-LD, Palo Alto, Ca., June 1982.

17. Personal Communication, R. M. Horn to S. Ranganath, "Comments on Crack Growth Data and Its Applicability to Welded Pipe Under Operation Conditions," June 1983.

18. Personal Communication, W. J. Shack to D. M. Norris, April 18, 1983. This letter contains unpublished crack growth data at stress intensity factors greater than 37.ksi√in.

19. W. H. Bamford, "Fatigue Crack Growth of Stainless Steel Piping in a Pressurized Water Reactor Environment, J. Pressure Vessel Technology, Vol 101, February 1979, pp. 73-79.

20. "Fatigue Crack Growth in Austenitic Stainless Steel," A. McMinn and P. M. Scott, United Kingdom Atomic Energy Authority Northern Division Report ND-R-802(S), June 1982.

21. "Stress Intensity Factors for Surface Cracks in Pipes: A Computer Code for Evaluation by Use of Influence Functions," D. D. Dedhia and D. O. Harris, EPRI Report NP-2425, Palo Alto, Ca., June 1982. Addenda Sept. 1982. Computer subroutine ORIVE is available from EPRI.

22. "Twenty-Six-Inch Pipe NDE Instrument Surveillance Test," R. L. Brickford, et al., Electric Power Research Institute Interim Report NP-2869, Research Project T104-1, February 1983.

23. "Estimation of Stress Intensity Factors and the Crack Opening Area of a Circumferential and Longitudinal Through-Crack in a Pipe," H. Tada and P. C. Paris, personal communication to the Section XI Task Group on Pipe Flaw Evaluation, San Diego, May 1982.

24. "The Two-Phase Critical Discharge of Initially Saturated or Sub-Cooled Liquid," R. E. Henry, Nuclear Science and Engineering, Vol. 41, 1970, pp. 336-342.

25. "Study of Critical Two-Phase Flow Through Intergranular Stress Corrosion Cracks," R. P. Collier, J. S. K. Liu, F. B. Stolen, and M. E. Mayfield, EPRI Report Project T118-2, January 1983 (in press). The LEAK computer program is available from EPRI.

26. Personal communication, M. E. Lapides to D. M. Norris, Electric Power Research Institute, May 1983.

27. "Radiographic Detection of IGSCC," M. E. Lapides, Electric Power Research Institute Report NP-3164SR, Palo Alto, California, May 1983.

LIST OF FIGURES

Fig. 9. Comparison of experimental critical axial surface flaw data [11] with calculated behavior for three pipe sizes.

Fig. 10. Ratio of crack-driving force in the circumferential to axial direction as a function of crack length [7].

Fig. 11. Design through-wall residual stress for use in crack-growth calculations.

Fig. 12. Through-wall weld residual axial stress measurements on large diameter pipes.

Fig. 13. Circumferential residual stress in HAZ (3 mm away from fusion line) on the inside surface of various diameter Schedule 80 pipe welds [15].

Fig. 14. Intergranular crack growth rates in sensitized Type 304 stainless steel in aqueous environments under constant load with recommended design curves [4].

Fig. 15. Type 304 and 304L stainless steel low-cycle fatigue crack-growth data obtained in simulated LWR environments.

Fig. 16. Comparison of predictions and observations of intergranular stress corrosion flaw growth in a 26 in. diameter Type 304 stainless steel pipe in a simulated BWR environment [22].

LIST OF TABLES

Table I

ALLOWABLE END-OF-EVALUATION PERIOD FLAW DEPTH[1]-TO-THICKNESS RATIO FOR CIRCUMFERENTIAL FLAWS, NORMAL OPERATING (INCLUDING UPSET AND TEST) CONDITIONS

$\frac{P_m + P_b}{S_m}$ [3]	Ratio of Flaw Length (ℓ) to Circumference[2]					
	0.0	0.1	0.2	0.3	0.4	0.5 or more
1.5	(4)	(4)	(4)	(4)	(4)	(4)
1.4	0.75	0.40	0.21	0.15	(4)	(4)
1.3	0.75	0.75	0.39	0.27	0.22	0.19
1.2	0.75	0.75	0.56	0.40	0.32	0.27
1.1	0.75	0.75	0.73	0.51	0.42	0.34
1.0	0.75	0.75	0.75	0.63	0.51	0.41
0.9	0.75	0.75	0.75	0.73	0.59	0.47
0.8	0.75	0.75	0.75	0.75	0.68	0.53
0.7	0.75	0.75	0.75	0.75	0.75	0.58
<0.6	0.75	0.75	0.75	0.75	0.75	0.63

Notes:

(1) Flaw depth = a_n for a surface flaw
= $2a_n$ for a subsurface flaw
t = nominal thickness
linear interpolation is permisible

(2) Circumference based on nominal pipe diameter

(3) P_m = Primary Membrane Stress
P_b = Primary Bending Stress
S_m = ASME Code Allowable Design Intensity

(4) IWB-3514.3 allowable flaw standards shall be used

Table II

ALLOWABLE END-OF-EVALUATION PERIOD FLAW DEPTH(1)-TO-THICKNESS RATIO FOR CIRCUMFERENTIAL FLAWS - EMERGENCY AND FAULTED CONDITIONS

$P_m + P_b$ (3) / S_m	Ratio of Length (2_ℓ) to Circumference(2)					
	0.0	0.1	0.2	0.3	0.4	0.5 or more
3.0	(4)	(4)	(4)	(4)	(4)	(4)
2.8	0.75	0.40	0.21	0.15	(4)	(4)
2.6	0.75	0.75	0.39	0.27	0.22	0.19
2.4	0.75	0.66	0.56	0.40	0.32	0.27
2.2	0.75	0.73	0.73	0.51	0.42	0.34
2.0	0.75	0.75	0.75	0.63	0.51	0.41
1.8	0.75	0.75	0.75	0.73	0.59	0.47
1.6	0.75	0.75	0.75	0.75	0.68	0.53
1.4	0.75	0.75	0.75	0.75	0.75	0.58
<1.2	0.75	0.75	0.75	0.75	0.75	0.63

Notes:

(1) Flaw depth = a_η for a surface flaw
= $2a_\eta$ for a subsurface flaw
t = nominal thickness
linear interpolation is permissible

(2) Circumference based on nominal pipe diameter

(3) P_m = Primary Membrane Stress
P_b = Primary Bending Stress
S_m = ASME Code Allowable Design Intensity

(4) IWB-3514.3 allowable flaw standards shall be used

Table III

ALLOWABLE END-OF-EVALUATION PERIOD FLAW DEPTH(1)-TO-THICKNESS RATIO FOR AXIAL FLAWS, NORMAL (INCLUDING UPSET AND TEST) CONDITIONS

Stress(3) Ratio	Nondimensional Flaw Length(2) ($\ell_f/\sqrt{Rt}$)													
	0.0	0.5	1.0	2.0	3.0	4.0	5.0	6.0	7.0	8.0	9.0	10.0	11.0	12.0 or greater
≤0.4	0.75	0.75	0.75	0.75	0.74	0.70	0.68	0.67	0.66	0.65	0.64	0.64	0.64	(4)
0.5	0.75	0.75	0.75	0.72	0.65	0.61	0.59	0.58	0.57	0.56	0.55	(4)	(4)	(4)
0.6	0.75	0.75	0.75	0.64	0.55	0.51	0.49	0.48	0.47	(4)	(4)	(4)	(4)	(4)
0.7	0.75	0.75	0.73	0.53	0.44	0.40	0.38	0.37	(4)	(4)	(4)	(4)	(4)	(4)
0.8	0.75	0.75	0.62	0.40	0.32	0.28	0.25	(4)	(4)	(4)	(4)	(4)	(4)	(4)
0.9	0.75	0.70	0.42	0.23	0.17	0.15	0.14	(4)	(4)	(4)	(4)	(4)	(4)	(4)
1.0	(4)	(4)	(4)	(4)	(4)	(4)	(4)	(4)	(4)	(4)	(4)	(4)	(4)	(4)

Notes:

(1) Flaw Depth = a_n for surface flaw
$2a_n$ for a subsurface flaw
Linear interpolation permissible

(2) ℓ_f = End-of-inspection period flaw length
r = Nominal pipe radius
t = Nominal pipe thickness

(3) Stress Ratio = $\frac{PD}{2t} / S_m$
Where P = Maximum pressure for normal operating conditions
D = Nominal outside diameter
t = Nominal thickness
S_m = ASME Code allowable design stress intensity

(4) IWB-3514.3 allowable flaw standard shall be used

Table IV

ALLOWABLE END-OF-INSPECTION PERIOD FLAW[1]
DEPTH-TO-THICKNESS RATIO FOR AXIAL FLAWS
EMERGENCY AND FAULTED CONDITIONS

Stress Ratio[3]	Nondimensional Flaw Length[2] ($\ell_e/\sqrt{Rt}$)							
	0.0	0.5	1.0	2.0	3.0	4.0	5.0	6.0 or greater
≤0.8	0.75	0.75	0.75	0.75	0.74	0.70	0.68	(4)
1.0	0.75	0.75	0.75	0.72	0.65	0.61	(4)	(4)
1.2	0.75	0.75	0.75	0.64	0.55	(4)	(4)	(4)
1.4	0.75	0.75	0.73	0.53	0.44	(4)	(4)	(4)
1.6	0.75	0.75	0.62	0.40	(4)	(4)	(4)	(4)
1.8	0.75	0.70	0.42	0.23	(4)	(4)	(4)	(4)
2.0	(4)	(4)	(4)	(4)	(4)	(4)	(4)	(4)

Notes:

(1) Stress Ratio = $\frac{PD}{2t} / S_m$

Where P = Maximum Pressure for Emergency and Faulted Conditions
D = Nominal Outside Diameter of the Pipe
t = Nominal Thickness
S_m = ASME Code Allowable Design Stress Intensity

(2) ℓ = End-of-Evaluation Period Flaw Length
r = Nominal Radius of the Pipe
t = Nominal Thickness

(3) Flaw Depth = a_o for a Surface Flaw
$2a_o$ for a Subsurface Flaw
Linear interpolation is permissible

(4) IWB-3514.3 allowable Flaw Standards Shall be Used

Table V

STABILITY OF BWR 304SS PIPING

System	Worst Location/ Number(1)	Pipe Size Outside Diameter Inch	Pipe Size Thick-ness Inch	L_{eff}/R	J_{app} lb/in (2)	T_{app}	T_{mat}	Crack Stability Criterion (3)
Iso-condenser								
Supply Line	70*	12.75	0.688	131	5352	105	230	T
"	70**	12.75	0.688	119	5352	96	230	T
Return Line	80*	8.63	0.500	203	4102	136	240	J
"	80**	8.63	0.500	194	4102	156	240	J
Core Spray	23*	10.75	0.594	150	4102	120	240	J
Recirc Line	46*	28.00	1.317	95	11944	75	210	T

Notes:

(1) "**" is system with hangers, supports and snubbers intact; "*" assumes hangers, supports, and snubbers failed. See Reference [14] for weld location.

(2) J_{app} assumes a crack plane rotation of 1 degree (see Appendix).

(3) Stability criterion: "T" means $J > J_{Ic}$ and if, $T_{app} > T_{mat}$ then unstable; "J" means $J < J_{Ic}$ and stability can be assumed. J_{Ic} for Type 304 stainless steel was 4300 lb/in.

Table VI

EFFECT OF PIPE SIZE ON THE RATIO OF THE CRACK LENGTH FOR 5 GPM LEAK RATE AND THE CRITICAL CRACK LENGTH[1]

Nominal Pipe Size[2] (in.)	Crack Length for 5 GPM Leak (in.)	Critical Crack Length ℓ_c (in.)[3]	ℓ/ℓ_c
4	4.50	6.54	0.688
10	4.86	15.95	0.305
24	4.97	35.79	0.139

Notes:

(1) See Reference [3], Appendix D
(2) Schedule 80
(3) Assumed Stress $\sigma = S_y/2$

Table VII

PROBABILITY[1] OF DETECTION AND SIZING OF INTERGRANULAR STRESS CORROSION CRACKS IN WROUGHT AUSTENITIC STAINLESS STEEL

UT - Circumferential[2] Flaws, a/t > 5%

Detection[3] (Flaws > 15mm in length)		90%
Sizing: Length Variance:	(Percent of nominal crack length)	±20 (±0.6 inch)[4]
Depth Variance:	(Percent of nominal crack depth) <6 mm	±70
	(Percent of nominal crack depth) >6 mm	±30 (±0.122 inch)[5]

RT-Axial and Circumferential Flaws, a/t > 15%[6]

Detection	85%
Sizing	Not defined

Notes:

[1]EPRI subjective best estimate
[2]Low reliability of UT for axial flaws.
[3]Detection probability varies with acceptable false alarm rate; some service access conditions will reduce probabilities shown.
[4]Length variation for a surface flaw (a/t=0.5, 2c/a=6) in a 24-inch diameter, Schedule 80 pipe with wall thickness t = 1.218 inches.
[5]Depth variation for a surface flaw (a/t=0.5, 2c/a=6) in a 24-inch diameter, Schedule 80 pipe with wall thickness t = 1.218 inches.
[6]Not generic, correct technology assumed (see Ref. [27]).

Table VIII

UT FLAW DEPTH MEASUREMENT COMPARED WITH DESTRUCTIVE TESTING[1]

Weld Number	Indication Number	Destructive Testing: Measured Max. Depth[2]	Destructive Testing: % Thru Wall	UT Measured Depth	UT Measured Depth: Error[2]
14S-SW-11	1	.215	16.5	.244	+0.029
	2	.275	21.1	(3)	(3)
	3	.205	15.7	.191	-0.014
12D-SW-19	1	.320	23.2	.407	+0.087
	2	.235	17.0	.306	+0.071
	3	.240	17.4	.408	+0.168
	4	.250	18.1	.260	+0.010

Notes:

[1] IGSCC Samples at Battelle Columbus Laboratories, December 1982
[2] All depth measurements in inches
[3] Team disagreed on result and did not submit data

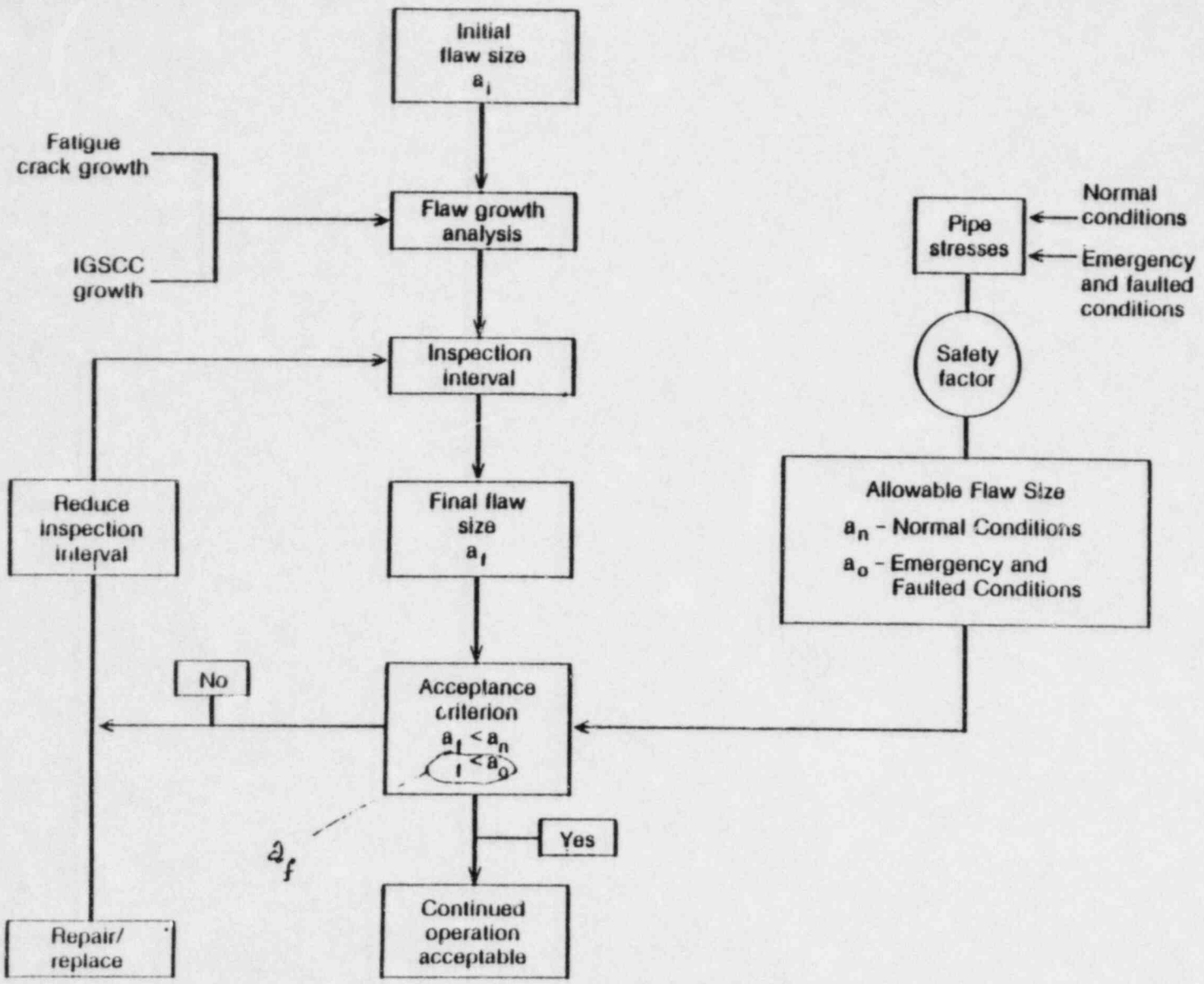
Initial flaw size a_i
Fatigue crack growth
IGSCC growth
Flaw growth analysis
Inspection interval
Reduce inspection interval
Final flaw size a_f
Pipe stresses
Normal conditions
Emergency and faulted conditions
Safety factor
Allowable Flaw Size
a_n - Normal Conditions
a_o - Emergency and Faulted Conditions
No
Acceptance criterion
$a_f < a_n$
$a_f < a_o$
a_f
Yes
Repair/ replace
Continued operation acceptable

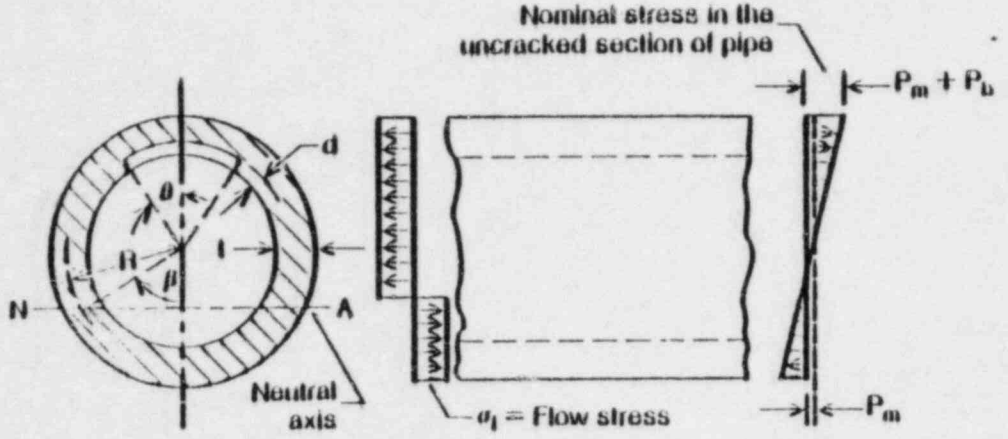
Nominal stress in the uncracked section of pipe
$P_m + P_b$
d
θ
R
β
t
N
A
Neutral axis
σ_f = Flow stress
P_m

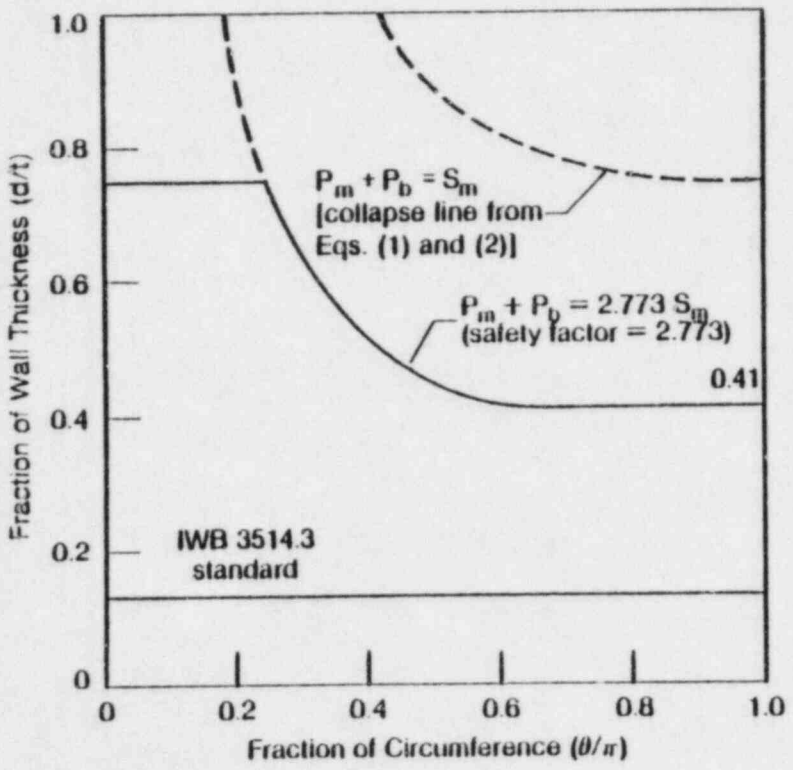
1.0
0.8
0.6
0.4
0.2
0
Fraction of Wall Thickness (d/t)
$P_m + P_b = S_m$
[collapse line from
Eqs. (1) and (2)]
$P_m + P_b = 2.773\ S_m$
(safety factor = 2.773)
0.41
IWB 3514.3
standard
0
0.2
0.4
0.6
0.8
1.0
Fraction of Circumference (θ/π)

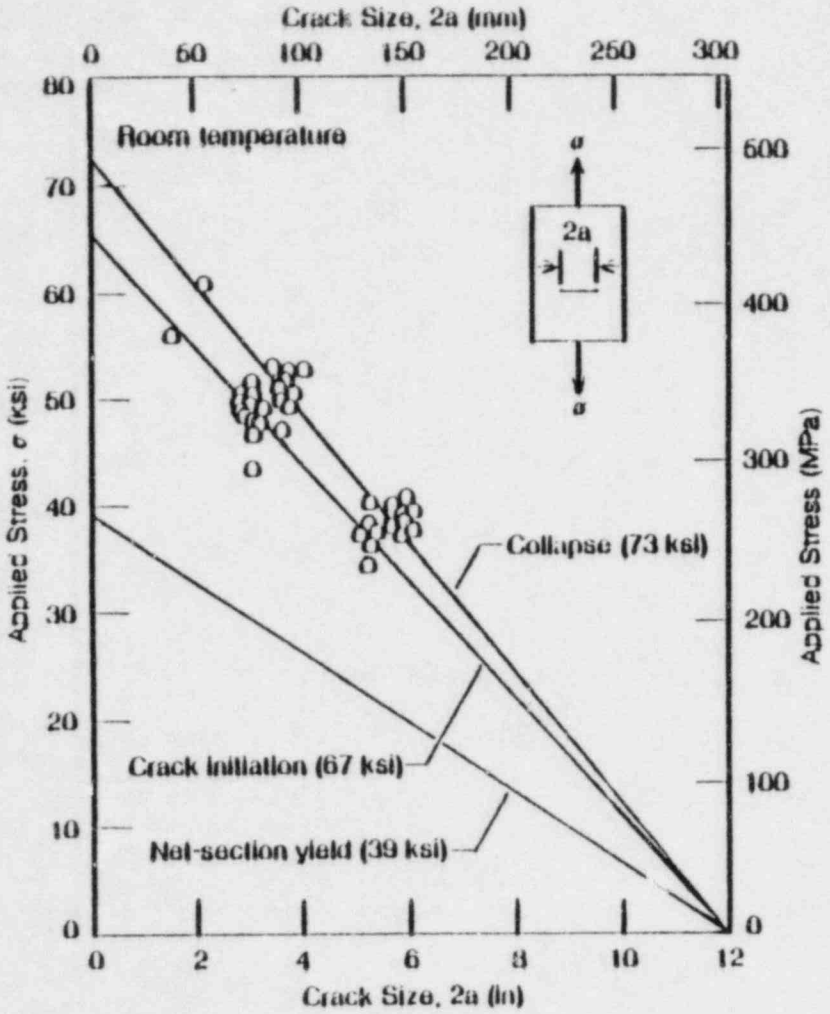
Crack Size, 2a (mm)
0
50
100
150
200
250
300
Room temperature
σ
2a
σ
Collapse (73 ksi)
Crack initiation (67 ksi)
Net-section yield (39 ksi)
Applied Stress, σ (ksi)
Applied Stress (MPa)
80
70
60
50
40
30
20
10
0
500
400
300
200
100
0
0
2
4
6
8
10
12
Crack Size, 2a (in)

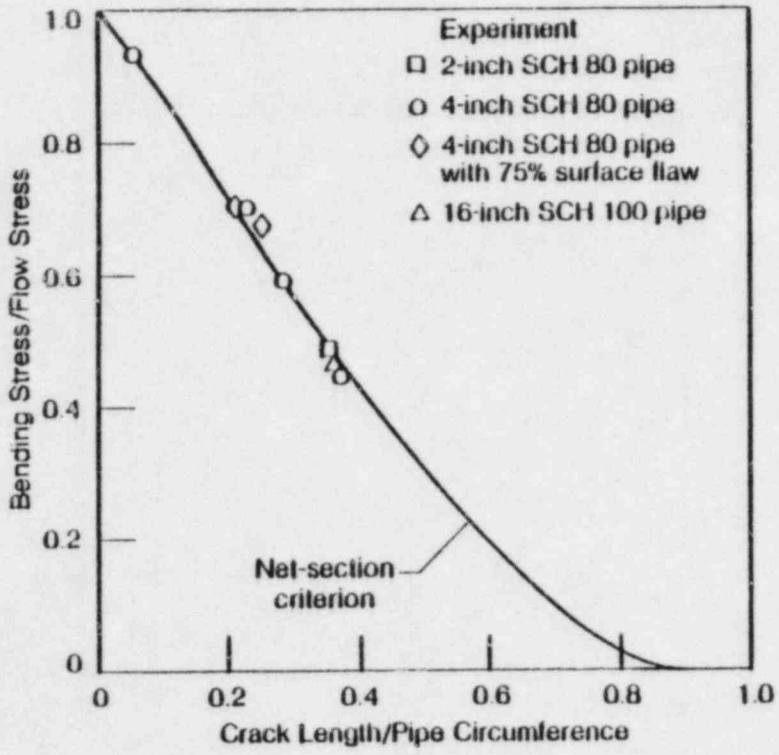
Experiment
2-inch SCH 80 pipe
4-inch SCH 80 pipe
4-inch SCH 80 pipe with 75% surface flaw
16-inch SCH 100 pipe
Net-section criterion
Bending Stress/Flow Stress
Crack Length/Pipe Circumference
1.0
0.8
0.6
0.4
0.2
0
0
0.2
0.4
0.6
0.8
1.0

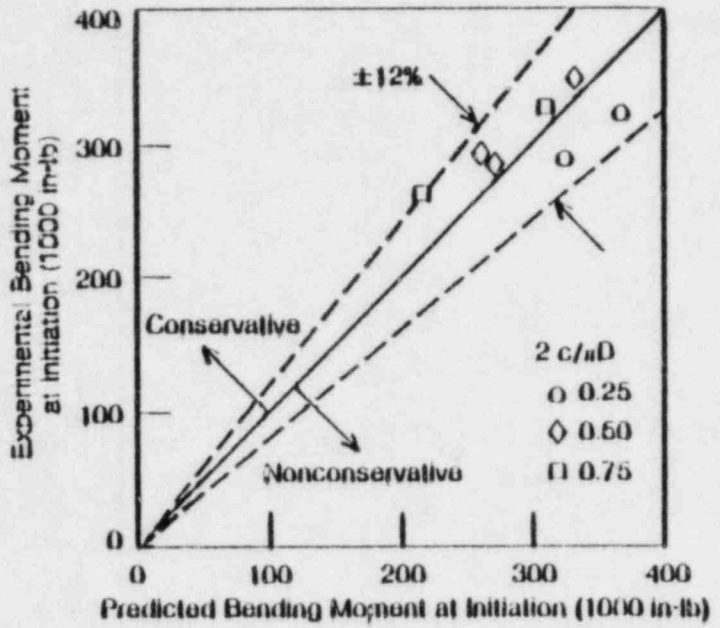
400
300
200
100
0
±12%
Conservative
Nonconservative
2 c/πD
0 0.25
◊ 0.50
□ 0.75
0
100
200
300
400
Predicted Bending Moment at Initiation (1000 in-lb)
Experimental Bending Moment at Initiation (1000 in-lb)

ac
br

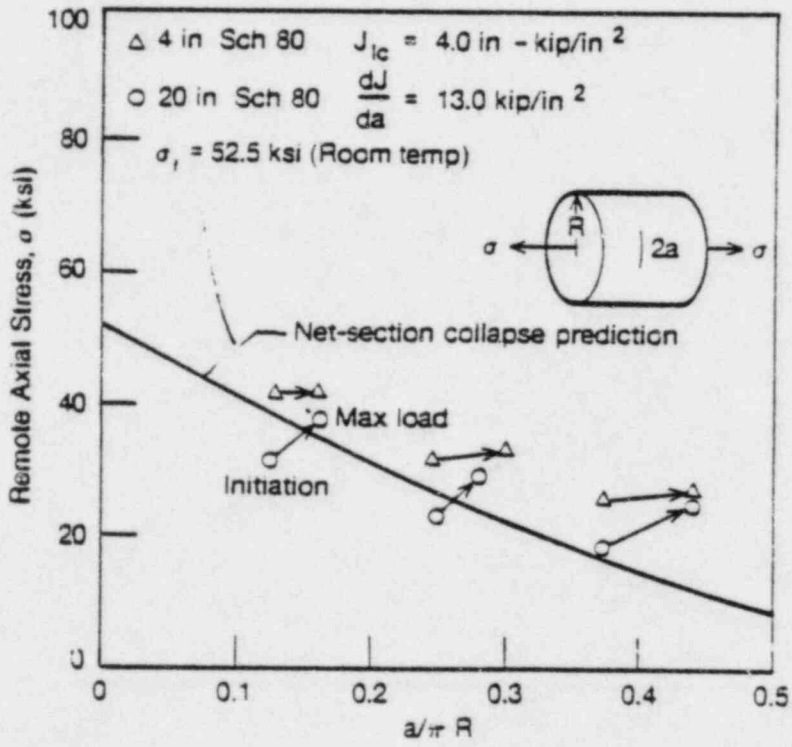
△ 4 in Sch 80 J_{Ic} = 4.0 in - kip/in²
○ 20 in Sch 80 $\frac{dJ}{da}$ = 13.0 kip/in²
σ_f = 52.5 ksi (Room temp)
R
2a
σ
σ
Net-section collapse prediction
Max load
Initiation
Remote Axial Stress, σ (ksi)
100
80
60
40
20
0
0
0.1
0.2
0.3
0.4
0.5
a/π R

S

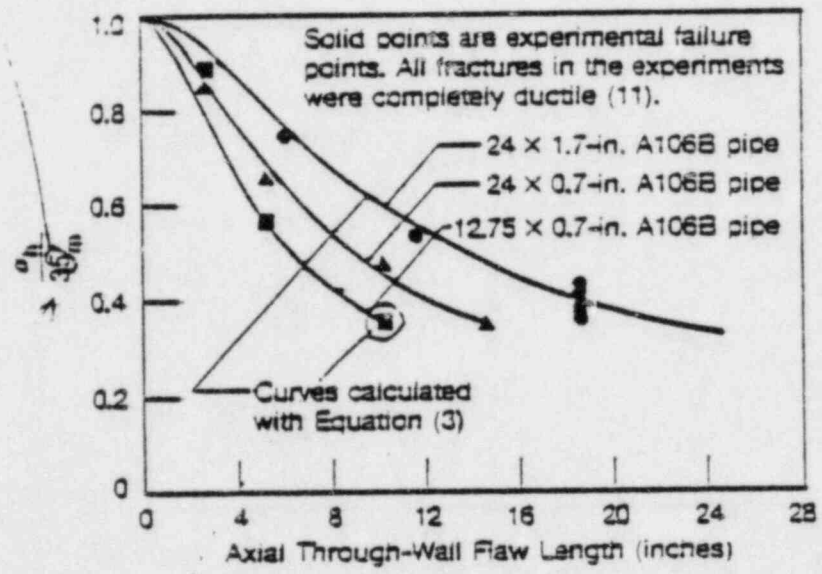

3 Sm

point incorrectly located relative to line see original

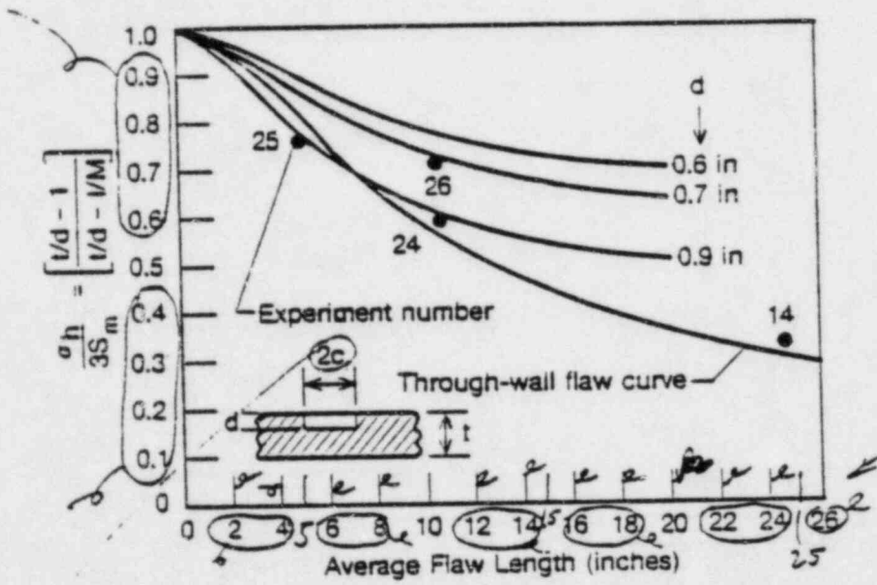

Figure 11. Comparison of analytical predictions and data for failure of axial cracks in 24 × 1.5-in. type 316 pipe.

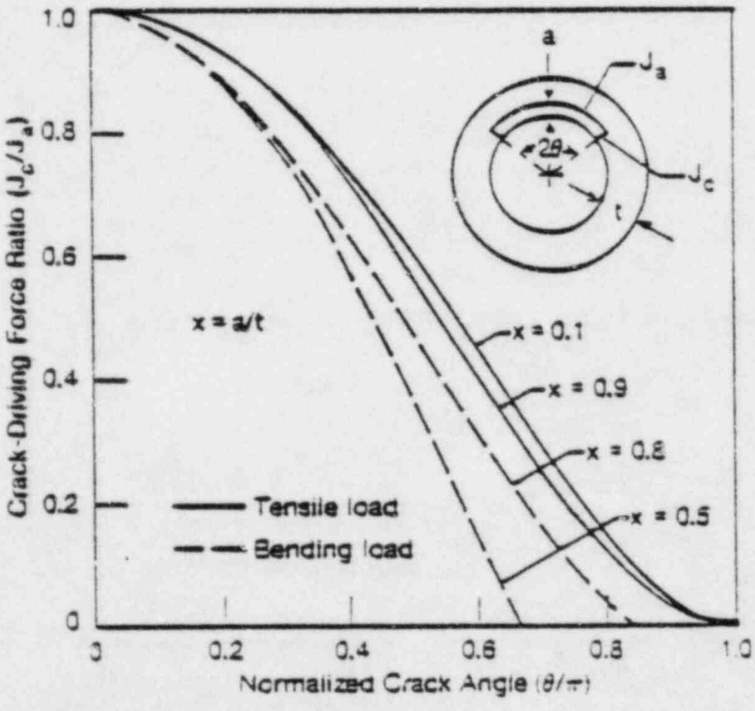
1.0
0.8
0.6
0.4
0.2
0
0
0.2
0.4
0.6
0.8
1.0
Crack-Driving Force Ratio (J_c/J_a)
Normalized Crack Angle (θ/π)
a
J_a
2θ
J_c
t
x = a/t
x = 0.1
x = 0.9
x = 0.8
x = 0.5
Tensile load
Bending load

Wall Thickness	Through-Wall Residual Stress[1]	
	Axial	Circumferential[2]
<1 inch	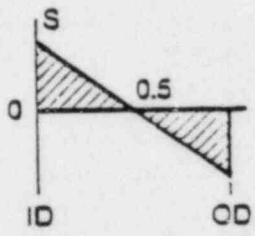	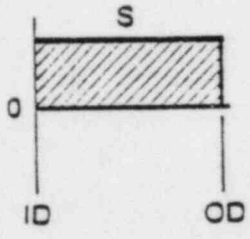
>1 inch	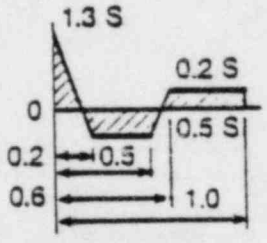	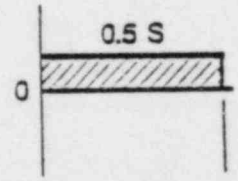

≥ 1 inch

[1] S = 30 ksi

[2] Considerable variation with weld heat input.

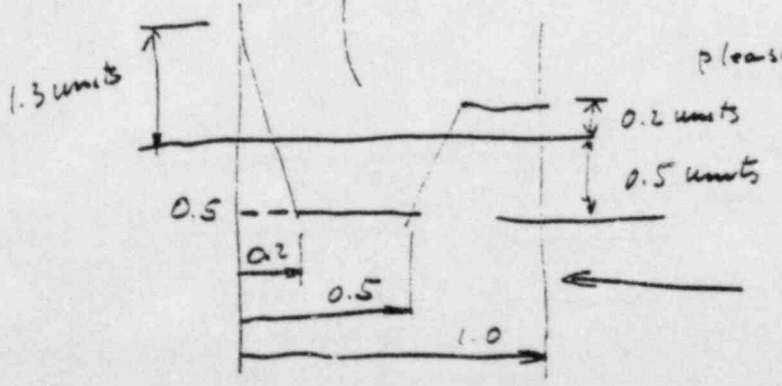

please draw this to scale -

Illustrator has confused horizontal and vertical dimension labels

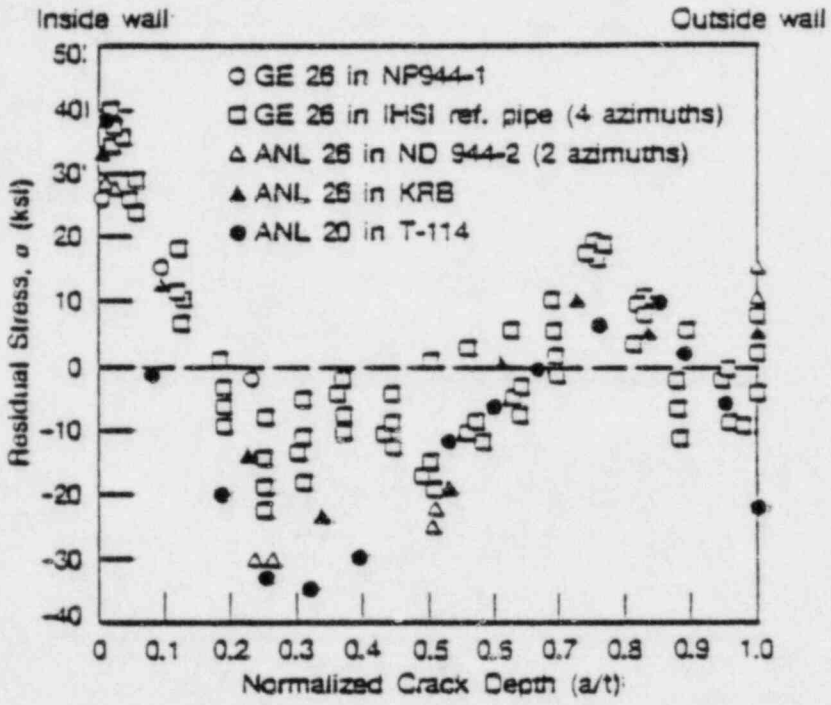
Inside wall
Outside wall
GE 26 in NP944-1
GE 26 in IHSI ref. pipe (4 azimuths)
ANL 26 in ND 944-2 (2 azimuths)
ANL 26 in KRB
ANL 26 in T-114
Residual Stress, σ (ksi)
50
40
30
20
10
0
-10
-20
-30
-40
0
0.1
0.2
0.3
0.4
0.5
0.6
0.7
0.8
0.9
1.0
Normalized Crack Depth (a/t)

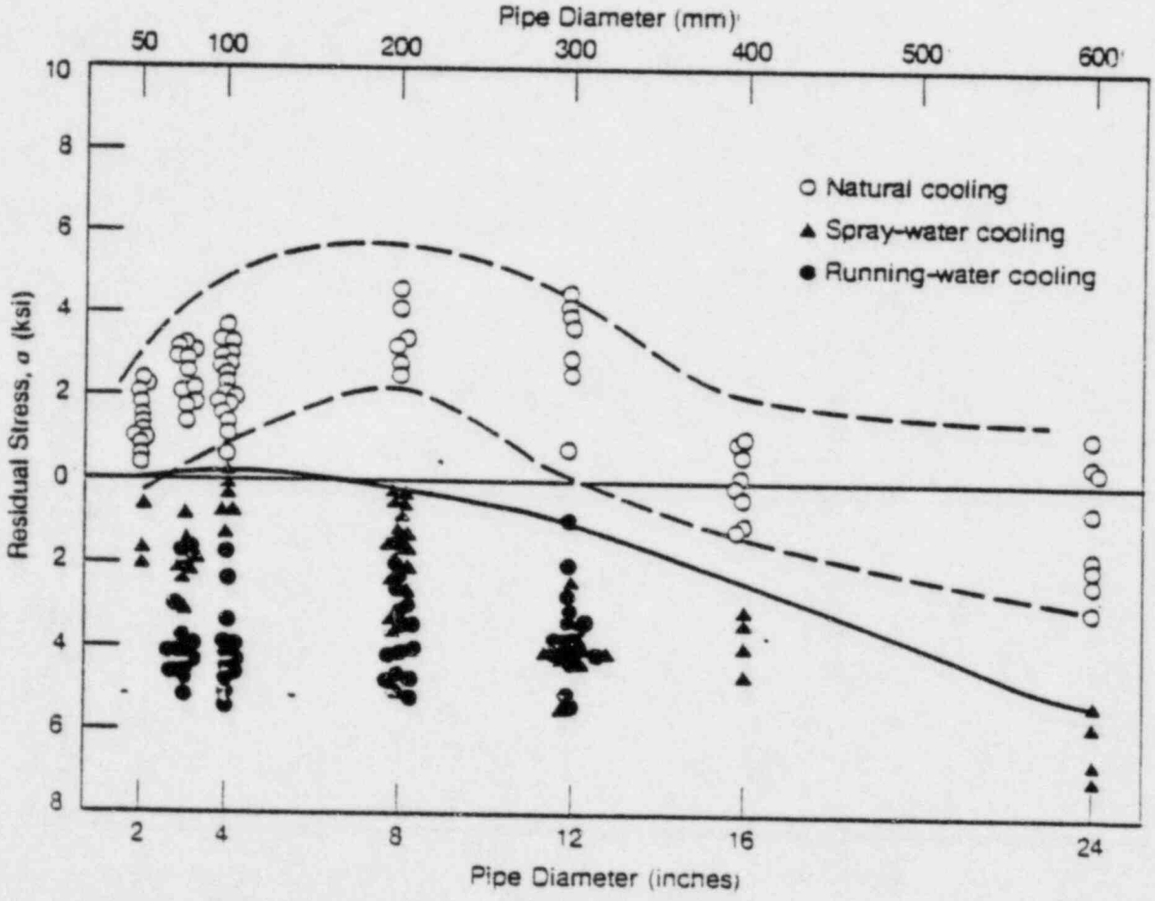
Pipe Diameter (mm)
50
100
200
300
400
500
600
10
8
6
4
2
0
2
4
6
8
Residual Stress, σ (ksi)
Natural cooling
Spray-water cooling
Running-water cooling
2
4
8
12
16
24
Pipe Diameter (inches)

- add tics at logarithmic positions 2, 4, 6, 8 as per original copy

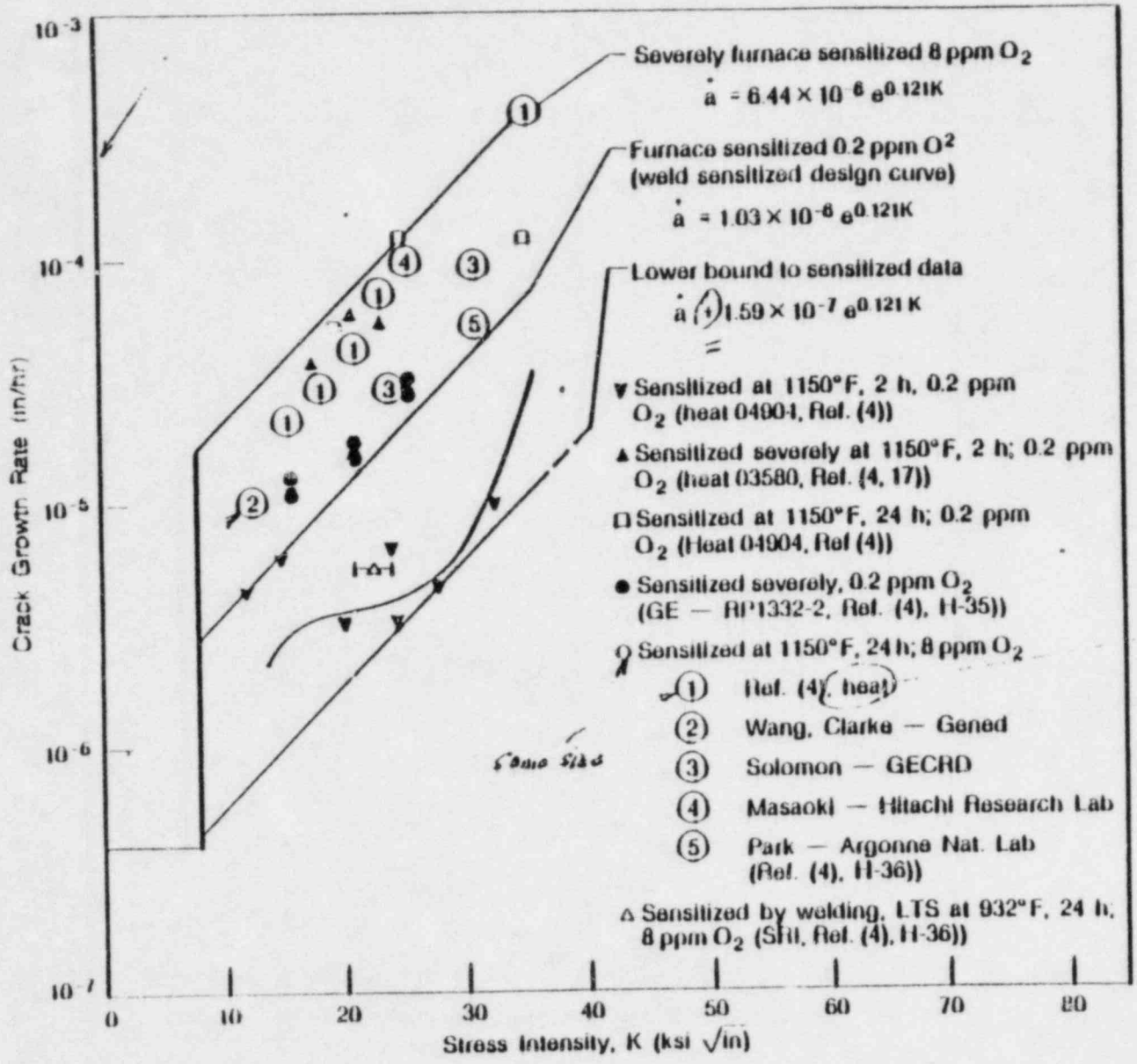

2nd pt (2) missing

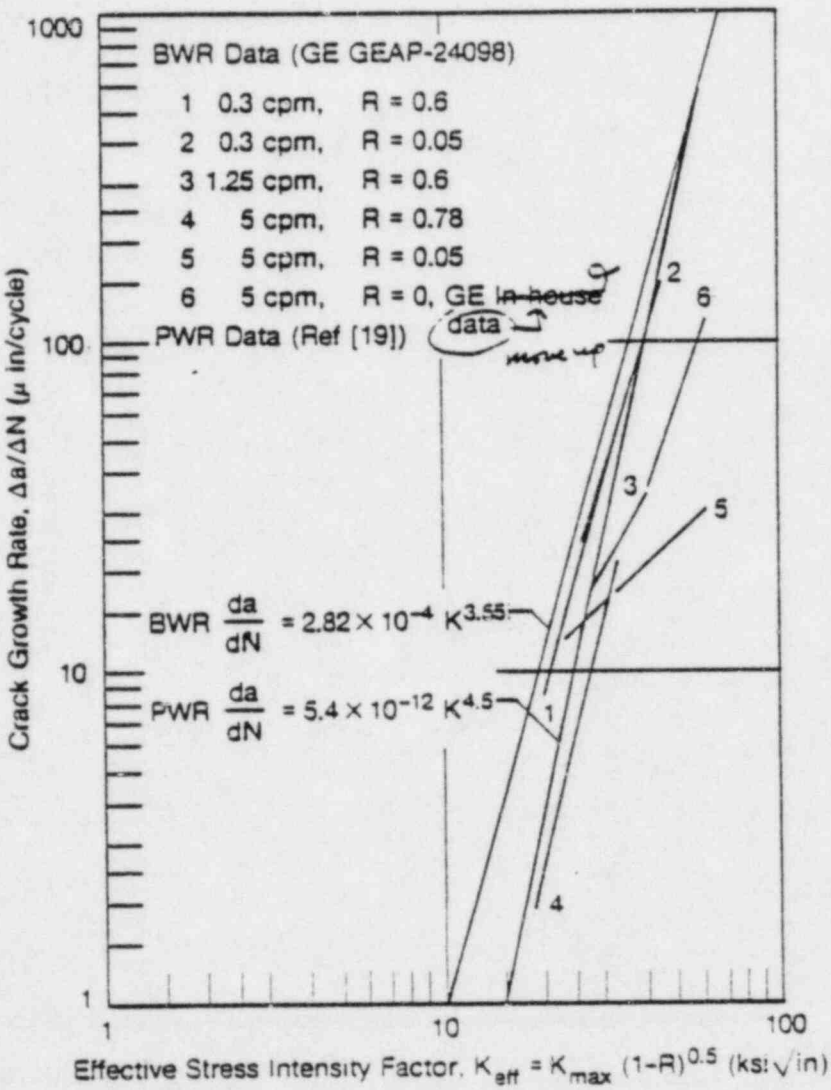
BWR Data (GE GEAP-24098)
1 0.3 cpm, R = 0.6
2 0.3 cpm, R = 0.05
3 1.25 cpm, R = 0.6
4 5 cpm, R = 0.78
5 5 cpm, R = 0.05
6 5 cpm, R = 0, GE in-house data
PWR Data (Ref [19])
BWR da/dN = 2.82 × 10⁻⁴ K^3.55
PWR da/dN = 5.4 × 10⁻¹² K^4.5
Crack Growth Rate, Δa/ΔN (μ in/cycle)
Effective Stress Intensity Factor, K_eff = K_max (1-R)^0.5 (ksi√in)
1000
100
10
1
1
10
100

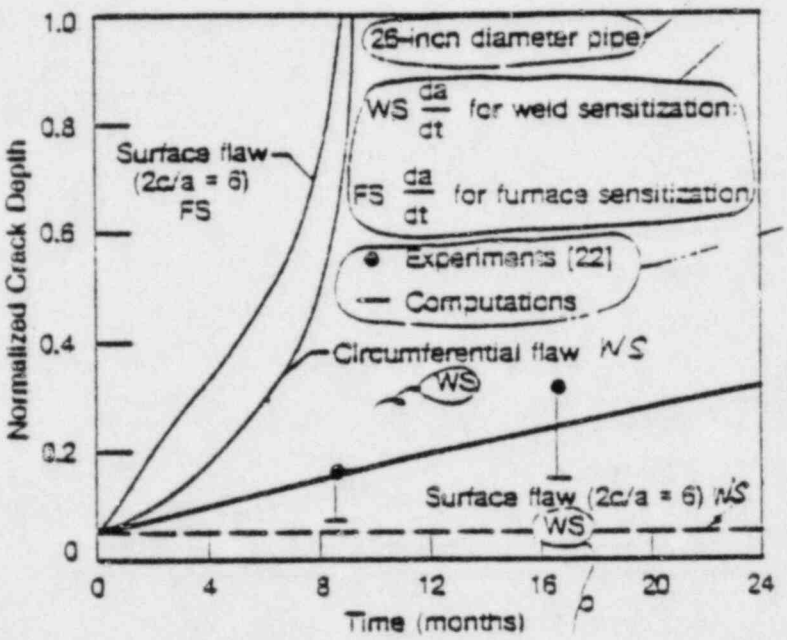
26-inch diameter pipe
WS da/dt for weld sensitization
FS da/dt for furnace sensitization
Experiments [22]
Computations
Surface flaw (2c/a = 6) FS
Circumferential flaw WS
Surface flaw (2c/a = 6) WS
Normalized Crack Depth
Time (months)
1.0
0.8
0.6
0.4
0.2
0
0
4
8
12
16
20
24